INVESTIGATION OF THE INTERACTION AND OLIGOMERIZATION OF HIV CAPSID AND SINGLE DOMAIN ANTIBODY AS A BIOTECHNOLOGICAL DRUG AGAINST HIV

A Thesis Submitted to
the Graduate School of Engineering and Sciences of
İzmir Institute of Technology
in Partial Fulfillment of the Requirements for the Degree of

MASTER OF SCIENCE

in Bioengineering

by
Seniha GÜNEY

July 2022
İZMİR

ACKNOWLEDGMENTS

First of all, I would like to thank my supervisor Asst. Prof. Hümeyra TAŞKENT SEZGIN for supporting, guiding and teaching me throughout my graduate education.

I would like to thank Prof. Dr. Erdal BEDİR, Assoc. Prof. Dr. Nur Başak SÜRMELI ERALTUĞ, Assoc. Prof. Dr. Cumhur TEKIN, Prof. Dr. Volga BULMUŞ ZAREIE, Asst. Prof. Ceyda ÖKSEL, Prof. Dr. Bünyamin AKGÜL, Prof. Dr. Sami DOĞANLAR and Prof. Dr. Hüseyin Çağlar KARAKAYA for allowing me to use their laboratory and equipments throughout this thesis.

I would like to thank "TÜBİTAK 2210-C Öncelikli Alanlara Yönelik Yurt İçi Yüksek Lisans Burs Programı 2020/2" for supporting me during my thesis studies.

I would like to thank Biotechnology and Bioengineering Applications and Research Centre (BİYOMER) for their contribution to this thesis.

I would also like to thank my laboratory mates; Selcen ÜSTÜN, Sanem AYAZ and Berk ATIK for their support and friendship. I would also like to thank my friends from the department; Alper ŞAHIN and Melis KÜÇÜKSOLAK, for their help in this study process.

Furthermore, I would like to thank Baran ABBAN, who always believed and supported to me, and did not spare me his technical knowledge during the writing process of this thesis.

Finally, I would like to thank my family who have always been there for me and supporting me.

ABSTRACT

INVESTIGATION OF THE INTERACTION AND OLIGOMERIZATION OF HIV CAPSID AND SINGLE DOMAIN ANTIBODY AS A BIOTECHNOLOGICAL DRUG AGAINST HIV

Human immunodeficiency virus (HIV) causes AIDS which is still a global public health threat. Current drugs against HIV infection cannot eradicate the virus therefore, research on new drug targets continues. HIV capsid protein, which has a highly conserved sequence and is sensitive to mutations, has critical roles in the virus lifecycle, making it a high-potential drug target. A nanobody is the antigen-binding domain of heavy-chain only antibodies of camelids. Small size, thermal stability and ease of production makes nanobodies ideal antibody fragments for therapeutic and diagnostic purposes. In the literature, a nanobody binding to the HIV-1 capsid-N terminal domain (NTD) has been reported. The aim of this thesis is to examine the potential of this nanobody as a biotechnological drug candidate against the HIV-1 and HIV-2 capsid proteins. In the study, HIV-1 capsid was expressed, purified and biophysically characterized. Thermal and chemical denaturation of the protein were done, the melting temperature and unfolding free-energy values of the protein were determined. In-vitro oligomerization of the HIV-1 capsid was performed and observed that the protein self-oligomerized over time. Pure HIV-2 capsid protein could not be produced recombinantly. Thereupon, HIV-1 capsid-NTD and HIV-2 capsid-NTD proteins were expressed and purified. Secondary structure of HIV-1 capsid, HIV-1 capsid-NTD and nanobody were analyzed with circular dichroism (CD) spectroscopy and the results matched with the literature. Isothermal titration calorimetry (ITC) experiments were done to examine the HIV-1 capsid-nanobody interaction, but good binding was not observed between the two proteins. Future work requires repeating ITC experiments.

ÖZET

HİV'E KARŞI BİYOTEKNOLOJİK İLAÇ OLMAK ÜZERE HİV KAPSİT VE TEK BÖLGELİ ANTİKORUN ETKİLEŞİMİ VE OLİGOMERİZASYONUN İNCELENMESİ

İnsan immün yetmezlik virüsünün sebep olduğu AIDS, halen küresel bir halk sağlığı tehdidir. Virüsün mevcut ilaçlarla yok edilememesi ve ilaçlara direnç geliştirmesi, yeni ilaç hedefleri ihtiyacı oluşturmaktadır. Virüsün kapsit proteini; mutasyonlara karşı duyarlı oluşu, dizisinin yüksek korunumu ve yaşam döngüsündeki rolleriyle yüksek potansiyelli bir ilaç hedefidir. Literatürde, kapsit proteinine bağlanan ve inhibitor etki gösteren birçok molekül bildirilmiştir. Nanokor, devegillerdeki sadece ağır zincirden oluşan antikorların antijen bağlanma bölgesidir. Nanokorlar sahip oldukları özellikler sayesinde hedefledikleri moleküller için uygun ajanlardır. Literatürde HIV-1 kapsit-N terminal alanına (NTD) bağlanan bir nanokor rapor edilmiştir. Bu tez çalışmasında, bu nanokorun HIV-1 ve HIV-2 kapsit proteinleri hedefine karşı ilaç olma potansiyelinin incelenmesi amaçlanmıştır. Çalışmada HIV-1 kapsitin üretimi ve saflaştırması başarıyla gerçekleştirilmiş, ilaç geliştirme teknolojileri için önemli olan biyofiziksel karakterizasyon deneyleri yapılmıştır. Proteinin termal, kimyasal denatürasyonu incelenmiş, deneylerde proteinin erime sıcaklığı ve açılma serbest enerjisi değerleri elde edilmiştir. Virüs yaşam döngüsünün geç aşamasında HIV-1 kapsit, viral genomu da içinde konik kapsit kafesi oluşturur. Viral enfeksiyon, büyük ölçüde kapsit kafes oluşumuna bağlıdır. Bu nedenle çalışmada, HIV-1 kapsitin in-vitro oligomerizasyonu incelenmiş, proteinin kendi kendine oligorimerize olduğu gözlenmiştir. Çalışmada, HIV-2 kapsitin üretimi ve saflaştırılmasında başarılı sonuç alınamamıştır. Bunun üzerine HIV-1 kapsit-NTD, HIV-2 kapsit-NTD proteinleri rekombinant yöntemlerle üretilip saflaştırılmıştır. HIV-1 kapsit, HIV-1 kapsit-NTD ve nanokor proteinlerinin yapısal karakterizasyonu CD ile incelenmiş, proteinlerin literatürdeki ikincil yapı özellikleriyle uyuşan sonuçlar gözlenmiştir. Kapsit-nanokor etkileşimini incelemek için yapılan ITC başlangıç deneylerinde nanokor, HIV-1 kapsit ile iyi bir bağlanma göstermemiştir. Gelecek çalışmalar daha fazla nanokorun üretilmesiyle ITC deneylerinin tekrarını gerektirmektedir. Böylece proteinlerin etkileşimi hakkında daha iyi yorum yapılabilir.

TABLE OF CONTENTS

LIST OF FIGURES

Figure **Page**

Figure **Page**

Figure **Page**

Figure **Page**

Figure **Page**

Figure **Page**

LIST OF TABLES

Table **Page**

CHAPTER 1

INTRODUCTION

1.1. Human Immunodeficiency Virus (HIV)

Human immunodeficiency virus (HIV) is an enveloped retrovirus. It belongs to the *Lentivirus* genus of the *Retroviridae* family. There are two types of HIV which are HIV-1 and HIV-2, based on genetic characteristics and differences. HIV-2 virulence is lower than HIV-1, and HIV-1 infection progresses much more quickly to AIDS than HIV-2 (Fanales-Belasio et al., 2010). HIV genetic material consists of single-stranded RNA (ssRNA) and it exists as two identical copies in the virus core (Figure 1.1). The virus genome is reverse transcribed into double-stranded DNA by the reverse transcriptase (RNA-dependent DNA polymerase). Viral double-stranded DNA is integrated into the host cell DNA with the help of integrase (German Advisory Committee Blood (Arbeitskreis Blut), 2016).

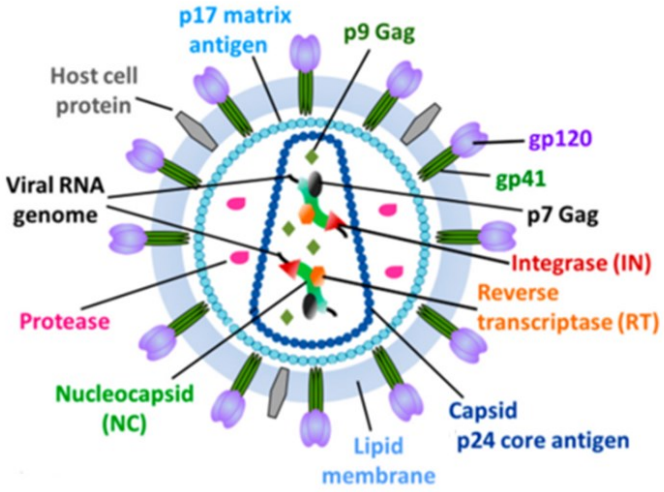

Figure 1.1. Structure of a HIV virion particle
(Source: Musumeci et al., 2015).

HIV genome contains Gag, Pol, Env genes and 6 regulatory genes from 5' to 3' end, respectively (Figure 1.2). The genomic RNA encodes three polyprotein which are

Gag, Pol, and Env. The Gag polyprotein is processed to three structural proteins, which are conserved in the retrovirus family. These are; matrix protein (MA), capsid protein (CA), and nucleocapsid protein (NC). The Pol polyprotein is processed to viral enzymes. These are protease (PR), reverse transcriptase (RT), and integrase (IN). The Env polyprotein is processed to the envelope glycoproteins gp120 and gp41. The other six accessory genes encode Tat, Rev, Nef, Vif, Vpr, and Vpu regulatory proteins, which have different effects on the virus life cycle (German Advisory Committee Blood (Arbeitskreis Blut), 2016; Mattei et al., 2016).

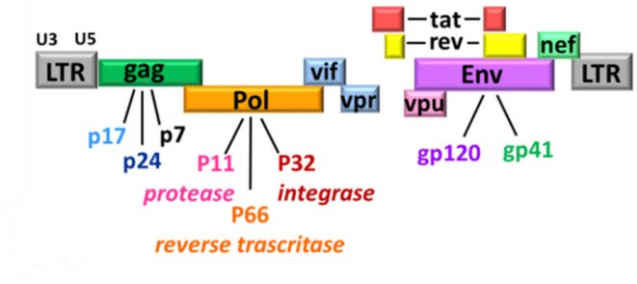

Figure 1.2. Organization of the HIV genome
(Source: Musumeci et al., 2015).

1.2. HIV Infection and AIDS

Human immunodeficiency virus (HIV) directly attacks the immune system. After HIV enters the body, it destroys $CD4^+$ T white blood cells over time. This weakens the person's immunity against other infections and cancer, leading to AIDS (Acquired-Immunodeficiency Syndrome) (World Health Organization, 2020). AIDS was first identified in 1981 in formerly healthy, young homosexual men in the United States. HIV was identified in 1983 as the agent causing AIDS by being isolated from the blood samples of people with AIDS-related clinical picture (Deeks et al., 2015; T.C. Sağlık Bakanlığı Halk Sağlığı Genel Müdürlüğü, 2018; Turner & Summers, n.d.).

According to UNAIDS (The Joint United Nations Program on HIV/AIDS) data; As of 2021, 79.3 million people in the world have been infected with HIV since the beginning of the epidemic, and 36.3 million people have died from AIDS-related diseases. Currently, 37.7 million people worldwide are infected with HIV (Joint United

Nations Programme on HIV/AIDS, 2021). AIDS continues to be a global public health threat and is at the forefront of active outbreaks in the world (Carnes et al., 2018).

1.3. Current HIV Treatment and Medicines

Treatment of the infection with the use of HIV drugs is called antiretroviral therapy (ART). Daily use of a combination of multiple HIV drugs is called the HIV regimen. A typical initial HIV regimen for patients includes the use of three drugs from at least two drug classes. The purpose of these drugs is to prevent HIV from multiplying and to make the patient live longer (Kemnic & Gulick, 2018). Although current antiretroviral therapy (ART) drugs against HIV infection are successful in reducing the spread and severity of the infection, they are not curative. Since the virus cannot be completely eradicated with current treatments, these drugs increase the quality of life of individuals, but require continuous use (Carnes et al., 2018; Pawar et al., 2019).

Currently, there are twenty-three FDA (U.S. Food and Drug Administration) approved drugs belonging to seven different antiretroviral classes for treatment. HIV drug classes are created based on how each drug affects the HIV life cycle. The seven classes available are nucleoside reverse transcriptase inhibitors (NRTIs), non-nucleoside reverse transcriptase inhibitors (NNRTIs), protease inhibitors (PIs), fusion inhibitors, CCR5 antagonists, post-attachment inhibitors, and integrase strand transfer inhibitors (INSTIs) (HIVinfo, 2020).

However, since the virus can develop resistance to these currently applied drugs and the drugs require daily use, the search for new drug targets and the development of new therapeutics continues (Carnes et al., 2018; Prevelige, 2011). In recent years, long-acting antiretroviral drugs (LA-ARTs) that can be applied on a monthly basis have been developed. LA-ARTs show great promise in the treatment and prevention of HIV. Currently, these drug molecules are at different clinical or preclinical levels (Jing & Heine, 2020; Margolis & Boffito, 2015). There are sixteen drug molecules belonging to five different classes in current LA-ART studies. These antiretroviral classes are NRTIs, NNRTIs, PIs, INSTIs, entry inhibitors, and capsid inhibitors. In the capsid inhibitor class, there is molecule GS-6207 (Lenacapavir), which is a highly potent inhibitor on HIV-1 capsid assembly. HIV capsid inhibitor class is novel and it has a great potential as an antiviral target for which no antiretroviral has yet been approved (Flexner et al., 2021;

Gulick & Flexner, 2019). HIV-1 capsid is being actively studied as a drug target (Blair et al., 2010; James, 2019; Tang et al., 2003).

1.4. HIV Capsid Protein

The capsid protein is a structural protein of the HIV. The monomer capsid protein consists of two domains as the N-terminal domain (NTD) and the C-terminal domain (CTD). They are linked by a flexible linker of 5 amino acids (Curreli et al., 2011; Mcarthur et al., 2019). The capsid monomers come together to form a lattice structure seen in Figure 1.3. It hosts the viral RNA genome, reverse transcriptase and integrase enzymes in its lattice structure. The conical capsid lattice is arranged as hexameric and pentameric rings of capsid monomers and stabilized by interactions between monomers and multimers (Figure 1.3) (Carnes et al., 2018; Mcarthur et al., 2019).

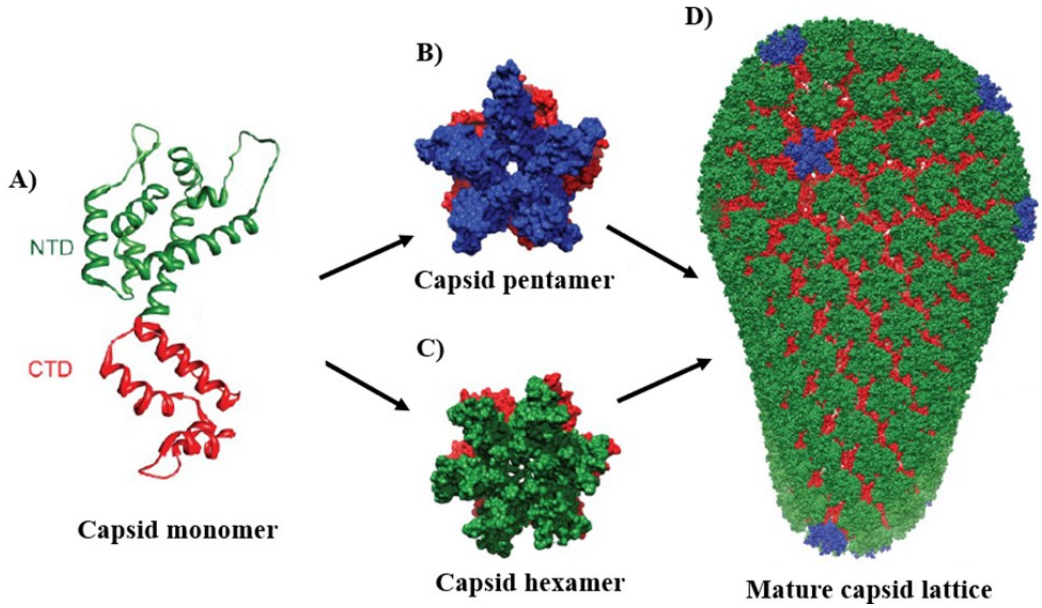

Figure 1.3. Structure of HIV capsid. A) Capsid monomer. NTD: N-terminal domain. CTD: C-terminal domain. B) Hexamer capsid structure formed from the capsid monomer. C) Pentamer capsid structure formed from the capsid monomer. D) Conical capsid lattice structure formed by approximately 250 hexamers and 12 pentamers (Source: Deshmukh et al., 2013).

In the capsid lattice structure, the interactions of NTDs with each other form the hexamer ring, providing intra-hexamer stability. CTDs are located below the hexamer ring formed by NTDs, they formed CTD-CTD interactions and it provides inter-hexamer stability by interacting between hexamers. Also, there are an interface between each CTD and the NTD of the neighboring capsid molecule in the hexameric ring. The majority of the capsid lattice consists of about 250 hexamers, but the lattice structure is closed with the inclusion of 12 pentamers in the structure and formed conical structure (Carnes et al., 2018; Lemke et al., 2012; Mattei et al., 2016). The HIV capsid lattice is metastable, and mutations that increase or decrease the stability of this structure reduce the infection success of the virus (Carnes et al., 2018; Tang et al., 2003). The sequence of the capsid protein is highly conserved and sensitive to mutations. Therefore, HIV resistance is less likely to develop in capsid-targeted drugs (Carnes et al., 2018; Rihn et al., 2013)

1.4.1. Function of the HIV Capsid Protein in the Virus Life Cycle

The capsid protein has important effects on the HIV life cycle. After the virus binds to the host cell receptor, it enters the cell by fusion. Once the virus enters the host cell, the capsid lattice is dissembled in a coordinated manner to allow binding of the viral genome to the host DNA by reverse transcription and integration reactions. This stage is called uncoating. Capsid stability and capsid disassembly rate are important to form infectious virus (Carnes et al., 2018; Hung et al., 2013; Mcarthur et al., 2019).

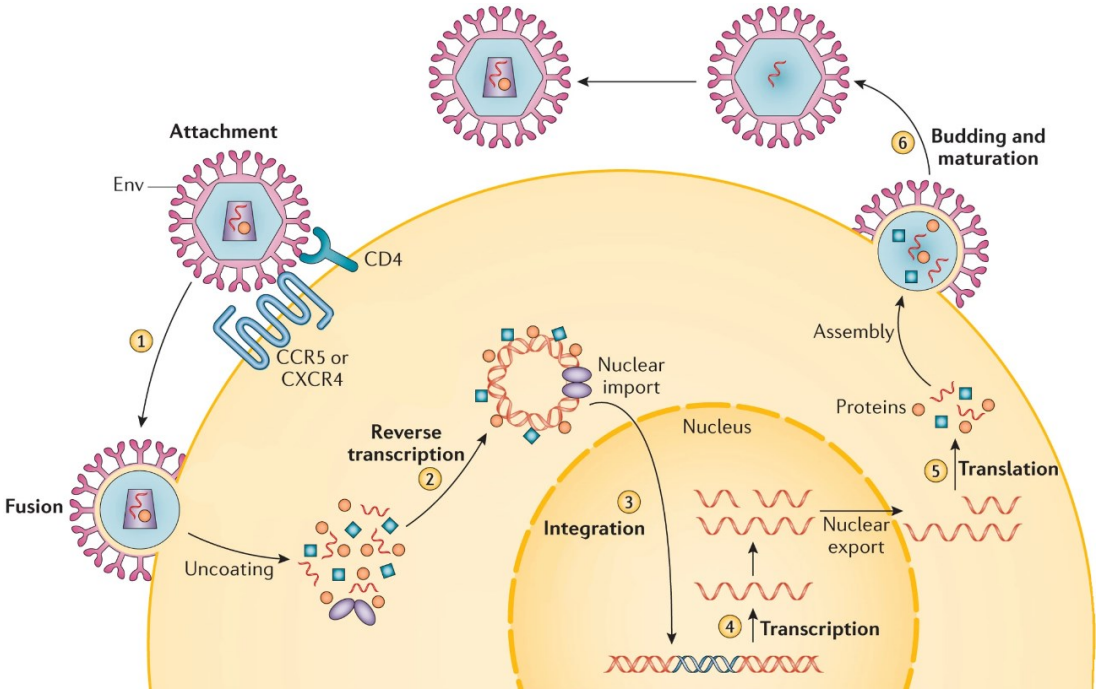

Figure 1.4. Life cycle of the HIV
(Source: Deeks et al., 2015).

On its way to the nucleus, the capsid protein interacts with different host cell proteins effective in nuclear entry and determining integration sites in the host (Carnes et al., 2018; Mcarthur et al., 2019). After uncoating, the viral RNA is reverse transcribed into DNA which is integrated into the host DNA. Integration of the virus genome makes the infection permanent. Therefore, the infection cannot be cured. In the cell nucleus, viral DNA is transcribed into viral RNAs and these RNAs are translated into viral proteins in the cytoplasm. Then, new viral RNA and proteins move to the cell surface and are collected at the plasma membrane. In the late phase of the virus life cycle, the Gag polyprotein buds through the cell membrane forming a new non-infectious virion. During virus maturation, capsid is formed as a result of cleavage of the Gag polyprotein by viral protease enzyme. The viral genome and enzymes necessary for infectivity are packaged inside the conical capsid lattice, and a mature, infectious virus particle is formed. Viral infection is highly dependent on capsid lattice formation and stability, making the capsid protein a potentially attractive antiviral target (Carnes et al., 2018; Lemke et al., 2012; Mcarthur et al., 2019; Tang et al., 2003).

1.4.2. HIV Capsid Targeted Inhibitors in the Literature

Numerous studies have reported various compounds that bind to the capsid protein. These compounds interfere with different stages of the HIV life cycle that are important for infection. Some of these molecules, which bind to the capsid protein at different positions, inhibit events in the early phase of the virus life cycle, while some disrupt capsid formation in the late phase, resulting in non-infectious virions (Blair et al., 2010; Carnes et al., 2018; Lamorte et al., 2013; Singh et al., 2019; Tang et al., 2003; Ternois et al., 2005).

The first capsid-targeted inhibitors (CAP-1 and CAP-2) were reported in 2003 by Tang et al. Molecules that bind to the NTD region of the capsid interfere with NTD-CTD interactions and inhibit capsid assembly during virus maturation. The resulting defective capsid core structure leads to viral particles with low infectivity. CAP-1 showed a 95% reducing effect on HIV-1 replication (Tang et al., 2003). Another small molecule PF-74, identified in 2010, binds to intersubunit NTD-CTD interface in the capsid hexamer. PF74 shows activity against many different HIV isolates (Blair et al., 2010). PF74 shows a dual antiviral activity by acting on both early and late events in the virus life cycle (Novikova et al., 2019). In the early stages, the compound competes with host proteins that bind to the capsid, and inhibits reverse transcription, causing early uncoating (Bhattacharya et al., 2014). PF74 destabilizes the HIV-1 core structure (Fricke et al., 2014). However, its main mechanism is to inhibit the binding of host factors that bind to the capsid (Price et al., 2014; Shi et al., 2011). BI-1 and BI-2 small molecules, identified in 2013, inhibit HIV-1 replication by binding to the NTD region of the capsid. BI-2 shows stronger inhibitory effect. It binds to the same site as PF74 and exhibits a similar mechanism of action to PF74 by interfering with the binding of host factors that bind to the capsid (Fricke et al., 2014; Lamorte et al., 2013). In 2013, the C1 compound that is a benzimidazole-based compound, was shown to interfere with capsid assembly. Unlike other inhibitors, this molecule binds near the CypA-binding loop in the NTD region of the capsid. C1 compound does not affect the early stage of the virus lifecycle; in the late stage, it inhibits HIV-1 replication by disrupting capsid assembly (Goudreau et al., 2013; Lemke et al., 2013). In 2012, two small molecules named CK026 and I-XW-053 were identified. The CK026 molecule showed a moderate antiviral effect. The smaller I-XW-053 fragment synthesized from CK026 was found to bind to the capsid and inhibit the

reverse transcription (Kortagere et al., 2012). In a related study conducted 2 years later, I-XW-053 molecule was optimized and Compound 34, which showed 11 times higher activity, was reported (Kortagere et al., 2014).

In addition to the compounds mentioned above, capsid-targeted peptide inhibitors have also been reported. CAI peptide, which was first reported in 2005, prevents capsid assembly by affecting capsid stabilization and causes a decrease infectivity (Sticht et al., 2005). The peptide nature of CAI prevents it from being used as an antiviral agent since it cannot penetrate cell membranes. The CAI peptide was modified to improve cell penetration and the NYAD-1 peptide was identified. NYAD-1 can prevent infection by inhibiting HIV-1 maturation (Zhang et al., 2008).

Among the recently reported small molecule inhibitors, GS-CA1 and GS-6207 (an analogue of GS-CA1) are the first compounds in their class with long-acting potency. Both compounds have been reported to have greater efficacy than approved antiretroviral HIV drugs and exhibit high levels of antiviral activity (Singh et al., 2019). GS-CA1 binds to the intersubunit NTD-CTD interface in the capsid hexamer and acts on nuclear import of viral DNA and ordered capsid assembly events. It was observed that GS-CA1 increased the rate and extent of capsid oligomerization in vitro, but as a result, irregular structures differentiated from normal (Yant et al., 2019). After studies with GS-CA1, GS-6207 was developed as an analogue of GA-CA1. Phase-2 studies of this molecule are being carried out under the name Lenacapavir. GS-6207 is the first inhibitor to enter clinical trials in capsid targeted drug molecule studies. GS-6207 shows a similar pharmacological profile with GS-CA1 and acts to different stages in the virus life cycle (Bester et al., n.d.; Gulick & Flexner, 2019; Yant et al., 2019).

Also, nanobodies binding to the HIV-1 capsid have been reported in the literature. Two of these (59H10, VHH9) binds to different sites in the CTD of the HIV-1 capsid (Alfadhli et al., 2021). Another nanobody (CANTDcb1) binds to the NTD of the HIV-1 capsid (Alfadhli et al., 2021; Helma et al., 2012). This HIV-1 CA NTD-specific nanobody is also the nanobody protein working in this thesis.

1.5. Nanobody Protein

Nanobody is a kind of antibody. Antibodies or immunoglobulins (Ig) are immunological proteins that are main proteins of the immune system. Most common

antibody is IgG1 (Salvador et al., 2019; Schumacher et al., 2018) Nanobodies are small-sized antigen binding sites that are consisting of single domain, isolated from antibodies in camelids (camel, llama, alpaca) or cartilaginous fish (shark). Their sizes are approximately 15 kDa. There are three types of IgG in the camelid family (Figure 1.4). One of them is the conventional antibody, IgG1; the other two are IgG2 and IgG3 antibodies called HCAb (Heavy-Chain Antibody) (Muyldermans, 2013).

The conventional antibody, IgG1, contains two identical heavy (H) chains and two light (L) chains (Figure 1.4, A). The heavy and light chains consist constant (C) and variable (V) domains. Heavy chain contains three constant domains, these are CH1, CH2, CH3 and one variable (VH) domain. Light chain contains one constant (CL) and one variable (VL) domain. The variable domains (VH, VL) represent the antigen recognizing site (Variable Fragment - Fv) and are different in each antibody. The variable domain (VH) of the heavy chain and the first constant domain (CH1) combine with the light chain to form the antigen binding site (Antigen Binding Fragment - Fab) (Li et al., 2018; Muyldermans, 2013).

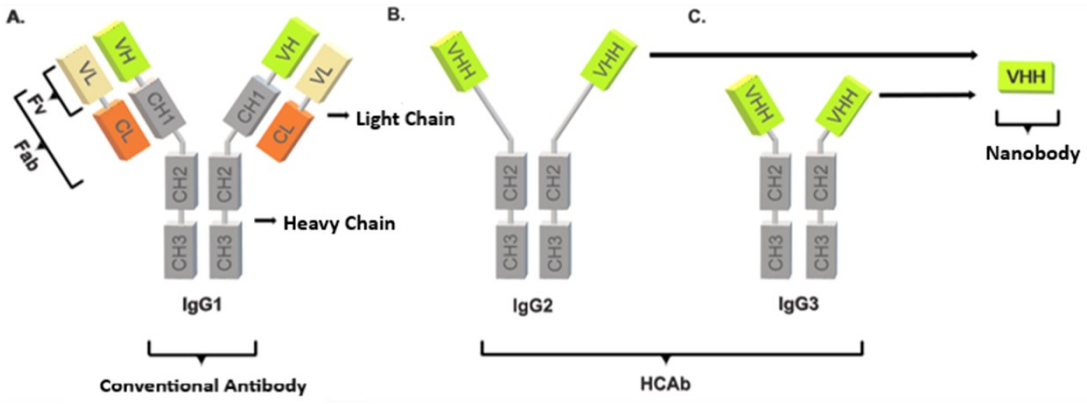

Figure 1.5. Naturally occurring IgGs in Camelids. A) Conventional antibody; IgG1. (B, C) Heavy chain antibodies (HCAb); IgG2 and IgG3 (Source: Muyldermans, 2013).

The most important feature of IgG2 and IgG3 antibodies is that, unlike the conventional antibody, IgG1, they lack the light chain and the first constant domain of the heavy chain (CH1). Thus, HCBs have smaller size and more compact structure than IgG1. While IgG1 molecular weight is around 150 kDa, IgG2 and IgG3 are around 90 kDa (Wang et al., 2016).

By isolating the VHH region at the N-terminal end of IgG2 and IgG3 antibodies, a nanobody, also known as a single-domain antibody, is obtained. This region is functionally equivalent to the antigen binding site (Fab) in conventional antibodies (Muyldermans, 2013). Location of the antigen binding site (VHH) apart from constant domains and some of its structural differences allow for the production of strong recombinant VHHs by providing an easy isolation process (Muyldermans & Lauwereys, n.d.; Schumacher et al., 2018). The fact that the antigen binding site (VHH) naturally consists of a single protein structure ensures correct folding of the protein. VHHs produced in this way are expected to have higher protein stability and antigen binding capacity (Muyldermans & Lauwereys, n.d.; Schumacher et al., 2018).

1.6. Applications of Nanobodies in Diagnosis and Treatment

Nanobodies are used in the fields of diagnosis and treatment, thanks to their biophysical and biochemical properties (Hoey et al., 2019; Salvador et al., 2019). They have advantages and great potential compared to monoclonal antibodies (mAbs). The large size of monoclonal antibodies prevents effective tissue penetration (Salvador et al., 2019). Nanobodies, have a strong and rapid tissue penetration and can be quickly eliminated from the body thanks to their rapid circulation in the blood (Hoey et al., 2019; Li et al., 2018). On the other hand, since monoclonal antibodies involve mammalian cell culture production techniques their production takes a long time and their cost is high. However, nanobody can be produced in the bacterial cells, which greatly reduces the cost (Salvador et al., 2019).

Their high specificity and affinity make nanobodies suitable for target molecules. Nanobodies can easily access to hidden epitopes thanks to their small size (~15kDa), and can bind to wide range of epitopes with high affinities. With these properties, nanobodies can be used in the field of diagnosis (Hoey et al., 2019; Li et al., 2018).

In therapeutic applications, they are investigated in many areas such as oncology, inflammation, viral infection and neurology. Currently, the Therapeutic Antibody Database lists 43 nanobodies under development in phases ranging from preclinical to clinical development (https://tabs.craic.com). There are two approved nanobody-based drugs. Caplacizumab is a humanized single domain antibody which was developed for use in the treatment of acquired thrombotic thrombocytopenic purpura. It is the first

nanobody-based drug that was approved and started to be used in 2019 (Tillib, 2020). Envafolimab is a humanized single domain antibody which was developed for the treatment of breast cancer, was also approved and started to be used in 2021 (https://tabs.craic.com).

1.7. Aim of This Study

The target proteins HIV-1 and HIV-2 capsid have high sequence conservation among the observed strains. Capsid is known to interact with many host cell proteins so it does not tolerate mutations well. This makes capsid a good target for HIV therapy. In a study conducted by (Helma et al., 2012), a nanobody protein was created that specifically binds to the NTD of the HIV-1 capsid protein at sub nanomolar affinity. The aim of this thesis is to examine the potential of this nanobody as a biotechnological drug candidate against HIV-1 and HIV-2 capsid proteins. Before investigating the binding interaction of capsid and nanobody, the proteins were characterized with biophysical methods individually. Protein-protein interaction studies with isothermal titration calorimetry started.

CHAPTER 2

MATERIALS AND METHODS

2.1. Confirmation of the Sequences of HIV Capsid Genes

2.1.1. Transformation of HIV-1 CA and HIV-2 CA Genes to E. *coli* DH5α

The gene sequences of the HIV-1 CA and HIV-2 CA proteins were in the pET-11a expression plasmid. Plasmids that containing HIV-1 CA and HIV-2 CA gene were transformed to E. *coli* DH5α competent cells. For transformation method, standard bacterial transformation protocol was followed. Competent cells were thawed on the ice for 20 minutes. Also, plasmid tubes were removed from -20˚C and incubated on the ice. Plasmids (2 µl) was added to the cells (50 µl) for each plasmid. Cells and plasmid mixtures were mixed by flicking of the tube with finger. Mixture tubes were incubated on the ice for 20 min. Then, tubes were incubated at 42˚C for 45 sec for heat shock treatment in water bath. After that they was quickly put to the ice for 2 min. LB media (950 µl) was added to each mixture tube and incubated at 37˚C for 1 hour by shaking at 220 RPM. After incubation of the cells, 70 µl of the cultures were spread to LB agar plate with 0.1 mg/ml ampicillin for both cultures. Remaining cultures were centrifuged at 7000 RPM for 1 min to concentrate the cells. 800 µl of media was discarded, cell pellets were resuspended by pipetting and 70 µl cells were spread to other LB agar plate with 0.1 mg/ml ampicillin for both cultures. Then plates were incubated at 37˚C for overnight.

2.1.2. Plasmid Isolation

The plasmids containing HIV-1 CA and HIV-2 CA genes were isolated from E. *coli* DH5α cell to confirmation of the sequence. For plasmid isolation, a single colony from the transformation plates was selected randomly and inoculated to 7.5 ml LB media with 0.1 mg/ml ampicillin and incubated at 37˚C for overnight by shaking at 220 RPM

for both cultures. The cultures that grown in LB media for overnight used for plasmid isolation. Also, glycerol stocks were prepared by adding 500 µl of these cultures into 500 µl 50% sterile glycerol and stored at -80˚C for next plasmid isolation experiments.

Plasmid isolation was done by alkaline lysis method using the Presto™ Mini Plasmid Kit (PDH300). 3200 µl cell culture was used for each plasmid isolation. In the process, cells are harvested and lysed, plasmid DNA in the cell lysate is eluted from bacterial DNA, contaminants are removed and plasmid DNA are obtained. Desired plasmid DNA was collected in the eppendorf tube as 35 µl. Plasmids were stored at -20˚C.

2.1.3. Sequence Analysis

Isolated pET-11a-HIV-1 CA and pET-11a-HIV-2 CA plasmids were analyzed on 1% agarose gel before sequencing analysis. After gene sizes were confirmed in the agarose gel, sequence analysis was performed by Sanger sequencing. Samples were sequenced and analyzed to ensure that the plasmids contained the gene of interest. DNA concentrations of isolated HIV-1 CA and HIV-2 CA plasmids were measured with Nanodrop Spectrophotometer device. Then, samples were sent to sequencing analysis together with T7 Promoter primer. Sequence analyzing was done by Genometri Biyoteknoloji. Results of sequences were analyzed by SnapGene Viewer Software.

2.2. Production of HIV Capsid Proteins

2.2.1. Transformation HIV-1 CA and HIV-2 CA Genes to E. *coli* BL21(DE3)

pET-11a vectors containing the genes which sequences were confirmed, to produce recombinant HIV-1 CA and HIV-2 CA proteins were transformed into E. *coli* BL21(DE3) competent cells designed for expression. The same steps of the transformation protocol applied to E. *coli* DH5a competent cells were followed. Both cultures were spread to LB agar plate with 0.1 mg/ml ampicillin. Then plates were incubated at 37˚C for overnight. Next day, a single colony was randomly selected from

the overnight grown colonies on the plate and inoculated into falcon tube that containing 10 ml LB media with 0.1 mg/ml ampicillin. Then, cultures were incubated at 37˚C for overnight by shaking at 220 RPM. Next morning, glycerol stocks were prepared by adding 500 µl of these cultures into 500 µl 50% sterile glycerol and stored at -80˚C for next protein expression experiments.

2.2.2. Expression Test of HIV-1 CA and HIV-2 CA Proteins

A single colony was selected from E. *coli* BL21(DE3) transformation plates that are containing pET-11a plasmids with HIV-1 CA and HIV-2 CA. Randomly selected colony was inoculated to 10 ml LB media with 0.1 mg/ml ampicillin for both cultures. Then, cultures were grown at 37˚C for overnight by shaking at 220 RPM. Expression tests were carried out at 37°C in 25 ml LB media with ampicillin by inoculating a propagated single colony culture. 500 µl of overnight culture (2% of media volume) was inoculated to fresh 25 ml LB media with 0.1 mg/ml ampicillin for both cultures. Optical density (OD) of cultures was followed at 600 nm. These cultures were grown at 37˚C and 220 RPM, until OD_{600nm} reached ~0,8. When the OD value reached around 0.8, the production of HIV CA proteins in bacteria was induced by adding 0.5 mM or 1 mM IPTG (Isopropyl ß-D-1-thiogalactopyranoside) into the cultures. After IPTG addition, cultures were incubated at 25˚C and 220 RPM. Optical density of cultures was followed at 600 nm by taken samples from the culture at certain interval. Afterwards, protein expression level was examined by Sodium Dodecyl Sulfate-Polyacrylamide Gel Electrophoresis (SDS-PAGE).

2.2.3. SDS-PAGE Analysis

Protein expressions of HIV-1 CA and HIV-2 CA proteins were analyzed in SDS-PAGE. During the expression test, samples taken before and after induction with IPTG were analyzed in 12% SDS-PAGE gel. In the samples taken after induction, a band was expected at the molecular weight level of the proteins. HIV-1 CA has a molecular weight of 25.6 kDa. HIV-2 CA has a molecular weight of 25.7 kDa. Samples were run on a 12% SDS-PAGE gel. Cell pellets were resuspended with 1X SDS Running Buffer (25 mM Tris Base, 192 mM Glycine, 0.1% w/v SDS) and diluted according to their OD values.

5X SDS Loading Dye (100 mM DTT, 1% w/v Bromophenol blue, 50% v/v Glycerol, 8% w/v SDS, 250 mM Tris-HCl pH 6.8) was added to the resuspended cell pellets at a final concentration of 1X. Then, these samples and ladder were heated in block heater at 95˚C for 7 min. Samples and ladder were loaded into the gel wells and run at 60V with 1X SDS Running Buffer. After run was finished, gel was carefully removed and rinsed with dH2O. Then, gel was transferred to staining box with 25 ml Solution 1 (50% Ethanol, 10% Acetic Acid) and heated in microwave for 30 sec and cooled for 5 min in the shaker at 25˚C. Then Solution 1 was discarded and 25 ml Solution 2 (5% Ethanol, 7.5% Acetic Acid) was added. Also, 350 µl Staining Dye (0.25% Coomassie Brilliant Blue R-250 in %95 Ethanol) was added. Gel was heated in microwave for 30 sec again and incubated in the shaker at 25˚C for 1 hour. After 1 hour, Solution 2 was removed and dH2O was used to destain the gel.

2.2.4. Large-Scale Production of HIV Capsid Proteins

Both HIV-1 and HIV-2 capsid proteins were produced in E. *coli* BL21(DE3) and E. *coli* BL21(DE3) pLysS cells in both LB and TB media.

2.2.4.1. Large-Scale Production of the HIV-1 CA

For large-scale production of recombinant HIV-1 CA protein, pET-11a vector containing HIV-1 CA, was transformed into E. *coli* BL21(DE3) pLysS competent cells designed for expression. After transformation, culture was spread to TB agar plate with 0.1 mg/ml ampicillin and 0.025 mg/ml chloramphenicol. Then plate incubated at 37˚C for overnight in the incubator. Next day, a single colony was randomly selected from the overnight grown colony on the plate and inoculated into 25 ml TB media with 0.1 mg/ml ampicillin and 0.025 mg/ml chloramphenicol. Then, culture was incubated at 37˚C for overnight by shaking at 220 RPM. Next morning, glycerol stock was prepared by adding 500 µl of this culture into 500 µl 50% sterile glycerol and stored at -80˚C for next protein expression experiments. Then 20 ml (2% of media volume) of overnight culture was inoculated to fresh 1000 ml TB media with 0.1 mg/ml ampicillin and 0.025 mg/ml chloramphenicol and grown at 37˚C and 220 RPM until $OD_{600_{nm}}$ reached ~0,8. When the OD value reached around 0.8, 0,5 mM IPTG (Isopropyl ß-D-1-thiogalactopyranoside)

was added into the culture for induction of expression. After IPTG addition, culture was incubated at 25˚C and 220 RPM for overnight. Next morning, all culture was centrifuged at 3200 RPM, 4˚C for 40 min for harvesting of cells and obtained cell pellet were stored at -20˚C. Also, protein expression level was examined by SDS-PAGE with samples taken from the culture.

2.2.4.2. Large-Scale Production of the HIV-2 CA

HIV-2 CA large-scale production was performed with E. *coli* BL21(DE3) cells. A single colony was selected from E. *coli* BL21(DE3) plate that are containing pET-11a plasmid with HIV-2 CA and inoculated to 10 ml LB media with 0.1 mg/ml ampicillin. Then, culture was grown at 37˚C for overnight by shaking at 220 RPM. Next morning, 8 ml of overnight culture (2% of media volume) was inoculated to fresh 400 ml LB media with 0.1 mg/ml ampicillin. Then incubated at 37˚C and 220 RPM until OD_{600nm} reached ~0,8. When the OD value reached around 0.8, 0,5 mM IPTG (Isopropyl ß-D-1-thiogalactopyranoside) was added into the culture for induction of expression. After IPTG addition, culture was incubated at 25˚C and 220 RPM for overnight. Next morning, all culture was centrifuged at 3200 RPM, 4˚C for 40 min for harvesting of cells and obtained cell pellet were stored at -20˚C. Also, protein expression level was examined by SDS-PAGE with samples taken from the culture.

2.3. Isolation and Purification of HIV Capsid Proteins

The protein purification protocol adapted from (Pornillos et al., 2010) was applied to both HIV-1 and HIV-2 capsid proteins. All purification processes were carried out at +4°C.

The cell pellet that was stored at -20˚C was dissolved in Lysis Buffer (50 mM Tris pH 8.0, 50 mM NaCl, 0.2% Deoxycholate, 20 mM BME). Additionally, PMSF (1mM), a protease inhibitor, was added to the solution to stop bacterial protease enzymes from working. Cells were lysed by sonication. After sonication, centrifugation was applied at 5000 RPM, 4˚C for 90 min to get rid of the cell debris. At this step, HIV-1 CA and HIV-2 CA proteins are soluble in the supernatant. The supernatant was taken, put into the beaker and subjected to 25% ammonium sulfate precipitation. The required amount of

ammonium sulfate was slowly added to the supernatant while it was mixing on stirrer in the ice. After the solution was thoroughly mixed, protein was separated as pellet from the solution by centrifugation at 4000 RPM, 4˚C for 40 min. The pellet was resuspended by adding SP-Binding Buffer (25 mM MOPS pH 6.8, 20 mM βME) and stirred for overnight at 4˚C. Next morning, the resuspended pellet centrifuged again at 4000 RPM, 4˚C for 40 min to remove ammonium sulfate. Supernatant was taken and filtered with 0.45 µm membrane filter. Filtered solution was dialyzed against to the same buffer (SP-Binding Buffer) at 4˚C for overnight by using 3.5 kDa MWCO dialysis membrane to remove remaining ammonium sulfate. Next morning, dialyzed solution was filtered again with 0.45 µm syringe filter. Thus, the pre-purification process was completed. As the main purification process, ion exchange chromatography method was used.

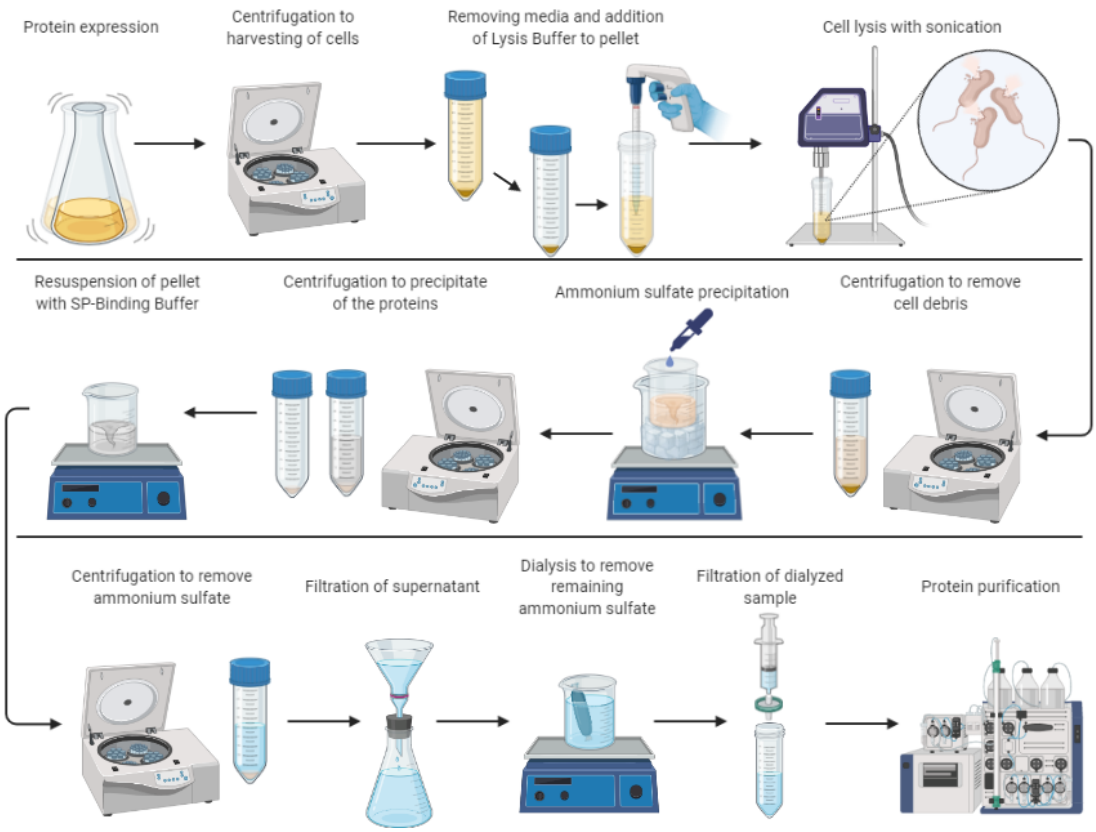

Figure 2.1. Illustration of pre-purification process of proteins.

SP (Sulphopropyl) Sepharose cation exchange column (GE Healthcare) was used for the purification of HIV-1 CA and HIV-2 CA proteins. So, filtered sample was loaded to SP cation exchange column in the GE Healthcare AKTA Prime Plus FPLC (Fast

Protein Liquid Chromatography) system. Samples were collected in two steps during the process. To prepare the device for use, the system was washed with SP-Binding Buffer (25 mM MOPS pH 6.8, 20 mM βME). Then the SP cation exchange column was placed in the system. Filtered sample containing the protein of interest was injected into the system and washed with Binding Buffer. At this step, the relevant protein binds to the column and other molecules that do not bind to the column are separated from the system. The fractions were collected at this step for control in case the relevant protein did not bind to the column either. These fractions are flowthrough samples. Then, the SP-Elution Buffer (25 mM MOPS pH 6.8, 20 mM βME, 1M NaCl) was given to the system by increasing its concentration in a gradient manner. The high salt concentration in the SP-Elution Buffer allows the protein of interest to be separated from the column. At this step the second group of fractions were collected, these fractions are gradient samples.

Q (Quaternary Ammonium) Sepharose anion exchange column (GE Healthcare) was used as an additional purification step for HIV-1 CA protein. For this, gradients samples collected from first chromatography were put together and dialyzed against to Q-Binding Buffer (20 mM Tris pH 8.0, 40 mM NaCl, 10 mM βME) at 4˚C for overnight by using 3.5 kDa MWCO dialysis membrane to exchange the buffer system. Next morning, dialyzed solution was filtered again with 0.45 µm membrane filter. Then filtered sample was loaded to Q anion exchange column in the GE Healthcare AKTA Prime Plus FPLC system. In the process, the procedures applied for the SP cation exchange column were applied using Q-Binding Buffer (20 mM Tris pH 8.0, 40 mM NaCl, 10 mM βME) and Q-Elution Buffer (20 mM Tris pH 8.0, 1 M NaCl, 10 mM βME) in the same order. Flowthrough samples containing the purified protein were put together and concentrated with Pall Macrosep Advance Centrifugal Device 10 kDa MWCO and stored at -80˚C. Absorbance signal of concentrated sample was measured at 280 nm. Protein concentration was measured based on extinction coefficient of protein. Samples taken at certain steps during the purification process, were taken for examination in SDS-PAGE gel. Then, the presence of relevant protein and the degree of purity were examined on the SDS-PAGE gel.

2.4. Cloning of the HIV Capsid NTD Genes

HIV-1 CA NTD and HIV-2 CA NTD genes were cloned into pET-21a plasmid

that is containing His-Tag, by PCR (Polymerase Chain Reaction). pET-11a-HIV-1 CA plasmid and pET-11a-HIV-2 CA plasmid were used as template. The desired target region is NTD domains of HIV-CA genes in pET-11a plasmid. The forward and reverse primers (Table 2.1) were designed and synthesized by Sentebiolab Biyoteknoloji (Ankara, Turkey). HIV-CA NTD inserts contain NdeI restriction cut site at the 5' end, and XhoI restriction cut site at the 3' end. Then, both the inserts and the empty pET-21a vector were digested with NdeI and XhoI restriction enzymes and ligated together.

Table 2.1. Designed primers to clone NTD domains of HIV-CA genes to pET-21a plasmid.

Template	**Target Region**	**Primers**	
pET-11a-HIV-2 CA	NTD domain of HIV-2 CA	Forward	5'-CAGACTACATATGCCGGTTCAGCAG3'
		Reverse	5'-TATCTCGAGAAGGATGTTGGTCGGGTTAT-3'
pET-11a-HIV-1 CA	NTD domain of HIV-1 CA	Forward	5'-TAGAATACATATGCCTATAGTGCAGAACC-3'
		Reverse	5'-TAACTCGAGAAGAATGCTGGTAGGGCTATAC-3'

2.4.1. Amplification of the HIV-1 CA NTD and HIV-2 CA NTD Genes by PCR

PCR was performed to obtain the HIV-1 CA NTD sequence from pET-11a-HIV-1 CA template and HIV-2 CA NTD sequence from pET-11a-HIV-2 CA template. The PCR reactions was performed in 50 µl volume. Phusion High-Fidelity PCR Kit (Thermo Fisher Scientific, F553L) was used for PCR reaction. HIV-1 CA NTD PCR reaction ingredients and conditions are given Table 2.2 and Table 2.3, respectively. HIV-2 CA NTD PCR reaction ingredients and conditions are given Table 2.4 and Table 2.5, respectively. Also, negative control reactions were prepared without enzyme for both PCR reactions. Annealing temperatures of primers were calculated by Thermo Fisher Scientific Tm Calculator.

Table 2.2. HIV-1 CA NTD PCR ingredients.

Components	**Amount in 50 µl Reaction**	**Final Concentration**
dH2O	31.67 µl	-
5X HF Buffer	10 µl	1x
10 mM dNTP Mix	1 µl	200 mM
Forward	2.5 µl	0.5 µM
Reverse	2.5 µl	0.5 µM
Template DNA	1.83 µl	5 ng/50 µl
PFU enzyme	0.5 µl	0.02 U/µl

Table 2.3. HIV-1 CA NTD PCR conditions.

Step	**Temperature**	**Time**	**Cycles**
Initial Denaturation	98˚C	30 sec	1
Denaturation	98˚C	10 sec	30
Annealing	65˚C	15 sec	
Extension	72˚C	10 sec	
Final Extension	72˚C	10 min	1
Hold	4˚C	-	-

Table 2.4. HIV-2 CA NTD PCR ingredients.

Components	**Amount in 50 µl Reaction**	**Final Concentration**
dH2O	31.62 µl	-
5X HF Buffer	10 µl	1x
10 mM dNTP Mix	1 µl	200 mM
Forward	2.5 µl	0.5 µM
Reverse	2.5 µl	0.5 µM
Template DNA	1.88 µl	5 ng/50 µl
PFU enzyme	0.5 µl	0.02 U/µl

Table 2.5. HIV-2 CA NTD PCR conditions.

Step	**Temperature**	**Time**	**Cycles**
Initial Denaturation	98˚C	30 sec	1
Denaturation	98˚C	10 sec	30
Annealing	64.5˚C	15 sec	
Extension	72˚C	10 sec	
Final Extension	72˚C	10 min	1
Hold	4˚C	-	-

PCR products were confirmed by 1.5% Agarose gel electrophoresis. Then all PCR products were purified from the agarose gel with Gel/PCR DNA Fragments Kit (Geneaid, DF100). The kit protocol was followed.

2.4.2. Single Digesting of the PCR Products and pET-21a Plasmid

After, PCR products were confirmed by 1.5% Agarose gel electrophoresis, each purified PCR products (25 µl) and empty pET-21a vector were digested with NdeI restriction enzyme. The NdeI restriction reactions were performed in 25 µl volume. The reactions mix were incubated at 37˚C for 16 hours then, enzyme was inactivated at 65˚C for 20 min. The NdeI reactions ingredients are given at Table 2.6.

Table 2.6. NdeI digesting reactions ingredients.

Components	**Amounts in 25 µl reaction**
Purified PCR Product	22 µl
10x Buffer O	2.5 µl
NdeI Enzyme	0.5 µl

The NdeI digested PCR products and pET-21a plasmid were confirmed by Agarose gel electrophoresis (%1.5 for inserts, %1 for vectors). Then all samples were purified from the agarose gel again with Gel/PCR DNA Fragments Kit (Geneaid, DF100). The kit protocol was followed. Then, each purified PCR products (25 µl) and pET-21a

vector were digested with XhoI restriction enzyme. The XhoI restriction reactions were performed in 25 µl volume. The reactions mix were incubated at 37˚C for 1 hours then, enzyme was inactivated at 80˚C for 5 min. The XhoI reactions ingredients are given at Table 2.7.

Table 2.7. XhoI digesting reactions ingredients.

Components	**Amounts in 25 µl reaction**
Purified PCR Product	21.5 µl
10x Fast Digest Buffer Green	2.5 µl
XhoI Fast Digest Enzyme	1 µl

The XhoI digested PCR products and pET21-a vector were confirmed by Agarose gel electrophoresis (%1.5 for inserts, %1 for vectors). Then all samples were purified from the agarose gel again with Gel/PCR DNA Fragments Kit (Geneaid, DF100). The kit protocol was followed. Thus, HIV-1 CA NTD gene, HIV-2 CA NTD gene and pET21-a vectors ready for ligation reaction were obtained.

2.4.3. Ligation of the HIV-1 CA NTD and HIV-2 CA NTD Genes and pET-21a Plasmid

DNA concentrations of the obtained inserts and vectors were measured by Nanodrop Spectrophotometer device and samples prepared for ligation reaction. T4 DNA Ligase Kit (Invitrogen, 15224017) was used for ligation reactions. Kit protocol was followed. Ligation reactions was performed in 20 µl volume. HIV-1 CA NTD ligation reaction conditions and HIV-2 CA NTD ligation reaction conditions are given Table 2.8 and Table 2.9, respectively. Also, negative control reactions were prepared without insert for both ligation reactions. Each ligation reactions were incubated at 23˚C for 16 hours.

Table 2.8. HIV-2 CA NTD ligation reaction conditions.

Components	Amount in 20 µl reaction	Final Concentrations	Amount in 20 µl negative control reaction
5x Buffer	4 µl	1x	4 µl
Insert	0.78 µl	45 fmol	-
Vector	13 µl	15 fmol	13 µl
T4 DNA Ligase	1 µl	1 U	1 µl
dH2O	1.22	-	2 µl

Table 2.9. HIV-2 CA NTD ligation reaction conditions.

Components	Amount in 20 µl reaction	Final Concentrations	Amount in 20 µl negative control reaction
5x Buffer	4 µl	1x	4 µl
Insert	2 µl	72 fmol	-
Vector	13 µl	24 fmol	13 µl
T4 DNA Ligase	1 µl	1 U	1 µl
dH2O	-	-	2 µl

After ligation process, each ligated samples and each negative controls were transformed to E. *coli* DH5α competent cells with 5 µl DNA sample. Each culture was spread to LB agar plate with 0.1 mg/ml ampicillin and incubated at 37˚C for overnight. Next day, a single colony was randomly selected from the overnight grown colonies on the plate and inoculated into falcon tube that containing 4 ml LB media with 0.1 mg/ml ampicillin for plasmid isolation. They were incubated at 37˚C, 220 RPM, for overnight. Next morning, plasmid isolation was done using the Presto™ Mini Plasmid Kit (PDH300). Also, glycerol stocks were prepared by adding 500 µl of these cultures into 500 µl 50% sterile glycerol and stored at -80˚C for next experiments. Isolated HIV-1 CA NTD and HIV-2 CA NTD plasmids were analyzed on 1% agarose gel before sequencing analysis. After gene sizes were confirmed in the gel, sequence analysis was performed by Sanger sequencing. Results of sequences were analyzed by SnapGene Viewer Program.

2.5. Production of HIV Capsid NTD Proteins

2.5.1. Expression Tests of HIV-1 CA NTD and HIV-2 CA NTD Proteins

pET-21a plasmids that containing the HIV-1 CA NTD and HIV-2 CA NTD genes whose sequence was confirmed were transformed into E. *coli* BL21(DE3) pLysS competent cells for expression. Both cultures were spread to TB (Terrific Broth) agar plate with 0.1 mg/ml ampicillin and 0.025 mg/ml chloramphenicol and then, incubated at 37˚C for overnight. Next day, a single colony was randomly selected from the overnight grown colonies on the plate and inoculated into falcon tube that containing 5 ml TB media with 0.1 mg/ml ampicillin and 0.025 mg/ml chloramphenicol. Then, cultures were incubated at 37˚C for overnight by shaking at 220 RPM. Next morning, glycerol stocks were prepared by adding 500 µl of these overnight cultures into 500 µl 50% sterile glycerol and stored at -80˚C for next protein expression experiments. Then, 500 µl of overnight culture (2% of media volume) was inoculated to fresh 25 ml TB media with 0.1 mg/ml ampicillin and 0.025 mg/ml chloramphenicol for both cultures. Optical density (OD) of cultures was followed at 600 nm. These cultures were grown at 37˚C and 220 RPM, until OD_{600nm} reached ~0.8. When the OD value reached around 0.8, the production of HIV CA NTD proteins in bacteria was induced by adding 0.5 mM IPTG (Isopropyl ß-D-1-thiogalactopyranoside) into the cultures. Expression tests were carried out by testing IPTG induction under different temperatures (25˚C and 37˚C). Afterwards, protein expression level was examined by Sodium Dodecyl Sulfate-Polyacrylamide Gel Electrophoresis (SDS-PAGE). Thus, optimum conditions for HIV-1 CA NTD and HIV-2 CA NTD protein production were decided.

2.5.2. Large-Scale Production of HIV-1 CA NTD and HIV-2 CA NTD Proteins

Streak plate was prepared from the glycerol stocks of E. *coli* BL21(DE3) pLysS competent cells, containing pET-21a plasmids with HIV-1 CA NTD and HIV-2 CA NTD, onto TB agar plates with 0.1 mg/ml ampicillin and 0.025 mg/ml chloramphenicol. The same production conditions were applied for HIV-1 CA NTD and HIV-2 CA NTD

proteins. Plates were incubated for overnight at 37˚C. Next morning, a single colony was selected and inoculated into 10 ml TB media with 0.1 mg/ml ampicillin and 0.025 mg/ml chloramphenicol. Culture was grown at 37˚C for overnight by shaking at 220 RPM. Next morning, 4 ml of overnight culture (2% of media volume) was inoculated to fresh 200 ml TB media with 0.1 mg/ml ampicillin and 0.025 mg/ml chloramphenicol for large scale expression and grown at 37˚C and 220 RPM, until OD_{600nm} reached ~0.8. When the OD value reached around 0.8, 0.5 mM IPTG (Isopropyl ß-D-1-thiogalactopyranoside) was added into the culture for induction of expression. After IPTG addition, culture was incubated at 37˚C and 220 RPM for 2 hours. Then, culture was centrifuged at 3200 RPM, 4˚C for 40 min for harvesting and cell pellets were stored at -20˚C. In addition, productions were also performed in 250 ml and 1000 ml culture volumes. Protein expression level was examined by SDS-PAGE with samples taken from the culture.

2.6. Isolation and Purification of HIV-1 CA NTD and HIV-2 CA NTD Proteins

HIV-1 CA NTD and HIV-2 CA NTD proteins were expressed and purified as in the study of Miyazaki et al. (Miyazaki et al., 2017). Same purification protocol was applied to both proteins. All purification processes were carried out at +4°C.

The harvested cell pellet that was stored at -20˚C was dissolved in Lysis Buffer (50 mM Tris pH 8.0, 50 mM NaCl, 0.2% Deoxycholate, 20 mM BME). Additionally, PMSF (1mM), a protease inhibitor, was added to the solution to stop bacterial protease enzymes from working. Cells were lysed by sonication. Sonication was applied through 30 sec at six times with 30 sec intervals. After sonication, centrifugation was applied at 5000 RPM, 4˚C for 90 min to get rid of the cell debris. At this step, HIV-1 CA NTD and HIV-2 CA NTD proteins are soluble in the supernatant. Supernatant were transferred to new falcon and filtered with 0.45 µm syringe filter.

HIV-1 CA NTD and HIV-2 CA NTD proteins were first purified using the immobilized metal ion affinity chromatography (IMAC) and then the ion exchange chromatography. So, filtered sample was loaded to HisTrap FF column (Cytiva, GE17525501) in the GE Healthcare AKTA Prime Plus FPLC (Fast Protein Liquid Chromatography) system. Samples were collected in two stages during the process. To prepare the device for use, the system was washed with IMAC-Binding Buffer (20 mM

Sodium Phosphate pH 8.0, 0.3 M NaCl, 10 mM Imidazole). Then the HisTrap FF column was placed in the system. Filtered sample containing the protein of interest was injected into the system and washed with Binding Buffer. At this step, the relevant protein binds to the column and other molecules that do not bind to the column are separated from the system. The fractions were collected at this step for control in case the relevant protein did not bind to the column either. These fractions are flowthrough samples. Then, the IMAC-Elution Buffer (20 mM Sodium Phosphate pH 8.0, 0.3 M NaCl, 500 mM Imidazole) was given to the system by increasing its concentration in a gradient manner. The high imidazole concentration in the Elution Buffer allows the protein of interest to be separated from the column. At this stage, called gradient washing, the second group of fractions were collected, these fractions are gradient samples.

These gradients samples were put together and dialyzed against to Q-Binding Buffer (20 mM Tris pH 8.0, 40 mM NaCl, 10 mM βME) at 4˚C for overnight by using 3.5 kDa MWCO dialysis membrane to exchange the buffer system. Next morning, dialyzed solution was filtered again with 0.45 µm membrane filter. Then filtered sample was loaded to Q (Quaternary Ammonium) Sepharose anion exchange column (GE Healthcare) in the GE Healthcare AKTA Prime Plus FPLC system. In the process, the procedures applied for the HIV CA proteins by using Q anion exchange column were applied for HIV CA NTD proteins with Q-Binding Buffer (20 mM Tris pH 8.0, 40 mM NaCl, 10 mM βME) and Q-Elution Buffer (20 mM Tris pH 8.0, 1 M NaCl, 10 mM βME). Fractions containing the purified protein were put together. Protein was concentrated with Pall Macrosep Advance Centrifugal Device 3 kDa MWCO and stored at -80˚C. Absorbance signal of concentrated sample was measured at 280 nm. Protein concentration was measured based on extinction coefficient of protein. Samples taken at certain steps during the purification process, were taken for examination in SDS-PAGE gel. Then, the presence of relevant protein and the degree of purity were examined on the SDS gel.

2.7. HPLC Analysis of HIV Capsid NTD Proteins

Purified HIV-1 CA NTD and HIV-2 CA NTD proteins were analyzed with Reversed-Phase HPLC (High Performance Liquid Chromatography). Agilent Technologies 1200 Series HPLC System in İYTE TAM BİYOMER was used for this

analyze. NUCLEOSIL 300-5 C4 column that belonging to İYTE TAM BİYOMER was used. First of all, HPLC system was washed with Binding Buffer (100% Ultrapure water, 0.1% HCl) to change the mobile phase. Then column was placed to system and column conditioning was done by slowly increasing the flowrate from 0.1 ml/min to 1 ml/min. After column conditioning, sample run was started. 20 µl sample was injected from each protein. The concentrations of HIV-1 CA NTD and HIV-2 CA NTD samples loaded into the column were 32 µM and 48 µM, respectively. Run conditions are given at Table 2.10. After sample injection, stationary phase (column) was washed with 100% Binding Buffer for 5 min. Then, the Elution Buffer (90% Acetonitrile, 10% Ultrapure water, 0.1% HCl) was given to the system by increasing its concentration in a gradient manner for 60 min. In this step, the hydrophobic interactions of the sample between the stationary phase change with increasing acetonitrile concentration in the mobile phase. Therefore, the peak of pure protein is expected to be seen at this step. Then stationary phase was washed with 100% Elution Buffer for 10 min. Lastly, 100% Binding Buffer was given to the system for 10 min to remove the acetonitrile. Then HPLC chromatograms were analyzed.

Table 2.10. Reversed-Phase HPLC run conditions

Washing Time	**Concentration Percent of Buffers**
5 min	100% Binding Buffer
60 min	0% to 100% Elution Buffer (in gradient manner)
10 min	100% Elution Buffer
10 min	100% Binding Buffer

2.8. Nanobody Protein

The nanobody protein which is produced in our laboratory was used in the experiments. The protein was produced in the E. *coli* BL21(DE3) pLysS cell strain with pET-22b plasmid containing the nanobody gene. Protein was purified by the immobilized metal ion affinity chromatography (IMAC) method. The molecular weight of the protein is 14,5 kDa.

2.9. Characterization of Proteins

2.9.1. Differential Scanning Fluorimetry

The thermal denaturation of the HIV-1 CA protein was investigated by differential scanning fluorimetry (DSF) assay. First, the appropriate protein concentration for the experiment was tested. Then the experiment was performed at the selected protein concentration with three identical samples.

First, the buffer to be used in the experiment, the final concentration of fluorescent dye (SYPRO Orange) and the protein concentrations to be tested were decided (Huynh & Partch, 2015; Niesen et al., 2007). HIV-1 CA protein was used in the experiment at final concentrations of 2.5 µM, 5 µM, 10 µM and 20 µM. Also, the sample that has no protein was used as a negative control. The final concentration of SYPRO Orange was decided to be 1X and 50 mM Sodium Phosphate pH 8.0 was used as a buffer. Reaction volume was 20 µl. Buffer was prepared at a concentration of 5X (250 mM Sodium Phosphate pH 8.0) in 5 ml. The SYPRO Orange fluorescent dye concentration was diluted with dH2O from 5000X to 10X. The final concentrations of the reagents used in the experiment are given in Table 2.11. The required amounts of reagents for the samples are given in Table 2.12.

Table 2.11. The final concentrations of the DSF assay reagents

Reagent	Final Concentration
HIV-1 CA Protein	2.5 µM, 5 µM, 10 µM, 20 µM
5X Buffer (250 mM Sodium Phosphate pH 8.0)	1X (50 mM Sodium Phosphate pH 8.0)
10X SYPRO Orange Dye	1X

Table 2.12. The required amounts of reagents for the DSF assay with different protein concentrations.

Reagent/ Sample	**20 µM**	**10 µM**	**5 µM**	**2.5 µM**	**Negative Control**
5x Buffer	4 µl	4 µl	4 µl	4 µl	4 µl
Protein	4 µl	2 µl	1 µl	0.5 µl	-
10x SYPRO Orange	2 µl	2 µl	2 µl	2 µl	2 µl
dH2O	14 µl	12 µl	13 µl	13.5 µl	14 µl

Samples were prepared in 96 well plate. Buffer, protein and dH2O amounts calculated for each sample were added to the sample well. Finally, SYPRO Orange fluorescent dye was added to each well and the plate was sealed and placed in the Roche LightCycler® 480 Real-Time PCR device. Since the SYPRO Orange excitation maximum [Ex] and the emission maximum [Em] values are 472 nm and 570 nm, respectively (Simpson, 2010); combination filters were selected as [Ex] 465 nm, [Em] 580 nm from the filter selection panel. Next, in the analysis mode "Melting Curve" was selected. In the “Temperature Targets Section” conditions were selected as Target: 20˚C, Acquisition Mode: none, Hold: 00:00:01, Ramp rate: 4.4. And the other line conditions were selected as Target: 90˚C, Acquisition mode: continuous, Acquisition (per ˚C): 12, Ramp rate: 0.05. Template was saved and assay was started. When run was completed to export the data, in the panel "Analysis" was clicked and next, "Tm Calling" was selected. Thus, two graph results were output, "Melting Curve" and "Derivative of the Melting Curve" of the samples. Then these graphs were examined.

Due to the clear signal at 10 µM protein concentration, DSF assay was repeated with 10 µM protein concentration. The assay was performed with the same samples three times to calculate the Tm value of the protein with the standard deviation. Final concentrations of buffer and SYPRO Orange dye were the same as in the first assay. A sample with no protein was used as a negative control.

Table 2.13. The required amounts of reagents for DSF assay reaction mix.

Reagent / Sample	**10 µM Protein Sample**
5X Buffer	4 µl
Protein	2 µl
10X SYPRO Orange	2 µl
dH2O	12 µl

Samples were prepared in a final volume of 20 µl according to the values in the Table 2.13. Then samples were added to three different well in the 96 well plate. Then 96 well plate was sealed and placed in the Roche LightCycler® 480 Real-Time PCR device. Same assay protocol was applied. "Melting Curve" and "Derivative of the Melting Curve" graphs of the samples, that emerged when the run was completed were analyzed.

2.9.2. Fluorescence Spectroscopy

The chemical denaturation process of the HIV-1 CA protein was investigated by fluorescence spectroscopy in the presence of urea as a denaturant agent. First, the protein was examined in the presence and absence of 8 M urea at four different concentrations to determine the appropriate protein concentration for the experiments. Then protein was examined at increasing urea concentrations as a gradient to observe the denaturation process with two experiments.

First, the buffer content and denaturing agent to be used in the experiment were decided as a result of the literature review (Mateu, 2002; Misselwitz et al., 1995). Two different buffers were prepared to examine the protein in the presence and absence of urea. Native Buffer was urea free, 20 mM sodium phosphate pH 7.0 and, 40 mM sodium chloride. Denatured Buffer was, 20 mM sodium phosphate pH 7.0 and, 40 mM sodium chloride, 8M urea. Protein was used in the experiment at final concentrations of 0.25 µM, 0.5 µM, 1 µM and 2.5 µM. Each sample were prepared in both native and denatured conditions in 700 µl reaction volume. In addition, a blank sample was prepared with own buffers for each sample. Q-Binding Buffer, which is buffer that is stock solution of protein, was added to blanks, instead of protein in the samples. Required protein and buffer amounts for each sample are given in the Table 2.14. The samples were prepared

in the fluorescence-based assays 96-well plate according to the values in the table and the 96-well plate was placed in the Thermo Scientific Varioskan LUX Multimode Microplate Reader device that belongs to İYTE TAM BİYOMER. Plate was scanned between 305-450 nm wavelengths with 2 nm interval, at 25˚C. The excitation wavelength was set to 295 nm.

Table 2.14. Reagents and amounts of the chemical protein denaturation with different protein concentrations experiment.

	Amounts of reagents in 700 µl reaction		
Sample	Protein (µl)	Native Buffer (µl)	Denatured Buffer (µl)
0.25 µM Native Sample	2.30	697.70	-
0.25 µM Denatured Sample	2.30	-	697.70
0.5 µM Native Sample	4.60	695.40	-
0.5 µM Denatured Sample	4.60	-	695.40
1 µM Native Sample	9.21	690.79	-
1 µM Denatured Sample	9.21	-	690.79
2.5 µM Native Sample	23.02	676.98	-
2.5 µM Denatured Sample	23.02	-	676.98

After variation of protein concentration experiment, two experiment were performed with increasing urea concentration at constant protein concentration (3 µM). Native Buffer was urea free, 50 mM sodium phosphate pH 8.0. Denatured Buffer was 50 mM sodium phosphate pH 8.0, 8 M urea. For Experiment 1, 29 samples were prepared with 0.3 M increments from 0 M to 3 M urea, 0.2 M increments from 3 M to 5 M urea, and 0.3 M increments from 5 M to 7.3 M. Experiment 1 samples were prepared in 250 µl reaction volume. For Experiment 2, 31 samples were prepared with 0.3 M increments from 0 M to 3 M urea, 0.2 M increments from 3 M to 5 M urea, and 0.3 M increments from 5 M to 7.9 M. Experiment 2 samples were prepared in 700 µl reaction volume. In addition, blank samples were prepared with own buffers for each sample. Required protein and buffer amounts for each sample are given in the Table 2.15 and Table 2.16 for Experiment 1 and Experiment 2, respectively. The samples were prepared in the

fluorescence-based assays 96-well plate according to the values in the table and the 96-well plate was placed in the Thermo Scientific Varioskan LUX Multimode Microplate Reader device that belongs to İYTE TAM BİYOMER. Plates were scanned between 310-450 nm wavelengths with 1 nm interval in 2 repetitions at 25˚C. The excitation wavelength was set to 295 nm.

Table 2.15. Reagents and amounts for the Experiment 1.

Urea Concentration (M)	Protein (µl)	Native Buffer (µl)	Denatured Buffer (µl)
0.0	21.5	228.50	0.00
0.3	21.5	219.13	9.38
0.6	21.5	209.75	18.75
0.9	21.5	200.38	28.13
1.2	21.5	191.00	37.50
1.5	21.5	181.63	46.88
1.8	21.5	172.25	56.25
2.1	21.5	162.88	65.63
2.4	21.5	153.50	75.00
2.7	21.5	144.13	84.38
3.0	21.5	134.75	93.75
3.2	21.5	128.50	100.00
3.4	21.5	122.25	106.25
3.6	21.5	116.00	112.50
3.8	21.5	109.75	118.75
4.0	21.5	103.50	125.00
4.2	21.5	97.25	131.25
4.4	21.5	91.00	137.50
4.6	21.5	84.75	143.75
4.8	21.5	78.50	150.00
5.0	21.5	72.25	156.25
5.3	21.5	62.88	165.63
5.6	21.5	53.50	175.00
5.9	21.5	44.13	184.38
6.2	21.5	34.75	193.75
6.5	21.5	25.38	203.13
6.8	21.5	16.00	212.50
7.1	21.5	6.63	221.88
7.3	21.5	0.00	228.50

Table 2.16. Reagents and amounts for the Experiment 2.

Urea Concentration (M)	Protein (µl)	Native Buffer (µl)	Denatured Buffer (µl)
0.0	16.9	683.91	0.00
0.3	16.9	657.66	26.25
0.6	16.9	631.41	52.50
0.9	16.9	605.16	78.75
1.2	16.9	578.91	105.00
1.5	16.9	552.66	131.25
1.8	16.9	526.41	157.50
2.1	16.9	500.16	183.75
2.4	16.9	473.91	210.00
2.7	16.9	447.66	236.25
3.0	16.9	421.41	262.50
3.2	16.9	403.91	280.00
3.4	16.9	386.41	297.50
3.6	16.9	368.91	315.00
3.8	16.9	351.41	332.50
4.0	16.9	333.91	350.00
4.2	16.9	316.41	367.50
4.4	16.9	298.91	385.00
4.6	16.9	281.41	402.50
4.8	16.9	263.91	420.00
5.0	16.9	246.41	437.50
5.3	16.9	220.16	463.75
5.6	16.9	193.91	490.00
5.9	16.9	167.66	516.25
6.2	16.9	141.41	542.50
6.5	16.9	115.16	568.75
6.8	16.9	88.91	595.00
7.1	16.9	62.66	621.25
7.4	16.9	36.41	647.50
7.7	16.9	10.16	673.75
7.9	16.9	0.00	683.91

2.9.3. Secondary Structure Analysis with Circular Dichroism Spectroscopy

CD measurements were performed by UNAM (Ankara, Turkey) with Jasco J-815 CD spectrometer. Far-UV spectra of the NB, HIV-1 CA, HIV-1 CA NTD were measured with a cuvette of 0.1 cm pathlength, at 25°C in the 200-260 nm wavelength range with 0.1 nm interval. Scanning speed was 100 nm/min. Nanobody, HIV-1 CA and HIV-1 CA NTD protein samples were used at 5.5 µM, 15.4 µM and 19.1 µM final concentrations in the 20 mM sodium phosphate pH 8.0, 10 mM βME.

Obtained CD spectra were normalized according to the following equation:

Equation (2.1):

$$[\theta] = (\theta 100 M_w)/(clN_A)$$

The recorded CD spectra in millidegrees of ellipticity (θ) were converted to mean residue ellipticity $[\theta]$ in $\mathrm{deg.cm^2.dmol^{-1}}$ by the Eq. (2.4), where c is the protein concentration (mg/ml), l is the pathlength (cm), M_w is the protein molecular weight, and N_A is the number of amino acids in the protein (Douglas et al., 2004).

2.10. Oligomerization of HIV-1 CA Protein

In vitro HIV-1 CA oligomerization was monitored spectrophotometrically at absorbance at 350 nm by light scattering caused by the polymerized tubular structure formed in the presence of high salt concentration. First, two different protein concentrations were tested. Then the experiment was repeated at the determined protein concentration.

First, the buffers to be used and the protein concentrations to be applied were decided with the literature review (del Álamo et al., 2005; Hung et al., 2013; Tsiang et al., 2012; Yant et al., 2019). Two buffers were prepared and filtered with 0.45 µm syringe filter. Buffer1 was contained 200 ml sodium phosphate pH 7.6 (4X). Buffer2 was contained 50 mM sodium phosphate pH 7.6, 4 M NaCl (1X). In the first step, HIV-1 CA protein at 2X final concentration (60 µM and 80 µM) with and without %1 DMSO were

prepared in a buffer containing 50 mM sodium phosphate pH 7.6 in 50 µl volume from Buffer1. Also, blank sample was prepared without protein. Then samples were loaded into a 96-well plate. In the second step, 50 µl of Buffer2 containing 50 mM sodium phosphate pH 7.6, 4 M NaCl to initiate the oligomerization was added into the wells. The plate was covered with a plate sealer. Then plate was placed into the device. The polymerization process was monitored by measuring the change in sample absorbance throughout 7 hours at 350 nm at 25°C at 30 second intervals on the Thermo Scientific™ Multiskan™ GO Microplate Spectrophotometer. Final concentrations of the protein were 30 µM and 40 µM. Final concentration of the buffer was 50 mM sodium phosphate pH 7.6, 2 M NaCl. The reaction volume was 100 µl. Reagents and amounts of the reaction are given in the Table 2.17.

Table 2.17. Reagents and amounts of in vitro HIV-1 CA oligomerization reaction with different protein concentrations.

Reagents	**Amounts in 100 µl reaction (µl)**					
	30 µM Protein	**30 µM Protein with %1 DMSO**	**40 µM Protein**	**40 µM Protein with %1 DMSO**	**Blank**	**Blank with %1 DMSO**
Protein	20	20	26.6	26.6	-	-
Buffer1 (4X)	12.5	12.5	12.5	12.5	12.5	12.5
DMSO (100%)	-	1	-	1	-	1
dH2O	17.5	16.5	10.9	9.9	37.5	36.5
Buffer2 (1X)	50	50	50	50	50	50

Also, absorbance of blank samples was measured at 900 nm and 975 nm in the 96-well plate and 10 mm cuvette for pathlength correction. The liquid pathlength of the well was calculated with following Equation (2.2) and Equation (2.3) with blank sample

values. When the liquid pathlength of the well has been determined, the corrected absorbance values of the samples were calculated with Equation (2.4) (Lampinen et al., 2012).

Equation (2.2):

$$\text{Pathlength}^{well} = \frac{A^{975(well)} - A^{900(well)}}{A^{975(cuvette)} - A^{900(cuvette)}} * \text{Pathlength}^{cuvette}$$

Equation (2.3):

$$\text{K-factor} = A^{975(cuvette)} - A^{900(cuvette)}$$

Equation (2.4):

$$A^{corrected} = A^{raw} * \frac{\text{Pathlength}^{cuvette}}{\text{Pathlength}^{well}} = A^{raw} * \frac{\text{K-factor}}{A^{975(well)} - A^{900(well)}}$$

Then, a new experiment was performed by increasing the duration of the experiment with two identical samples at a selected protein concentration. Same buffers were used and same experimental steps was followed. Also, the blank sample, which had the same conditions in the first experiment, was also used for this experiment. In the first step, HIV-1 CA protein at 2X final concentration (60 µM) with %1 DMSO were prepared in a buffer containing 50 mM sodium phosphate pH 7.6 in 50 µl volume from Buffer1. Then samples were loaded into a 96-well plate. In the second step, 50 µl of Buffer2 containing 50 mM sodium phosphate pH 7.6, 4 M NaCl to initiate the oligomerization was added into the wells. The time from this step until the plate was placed in the device was kept. The plate was covered with a plate sealer then, placed into the device. The polymerization process was monitored by measuring the change in sample absorbance throughout 18 hours at 350 nm at 25°C at 1 min 10 sec intervals on the Thermo Scientific™ Multiskan™ GO Microplate Spectrophotometer. Final concentration of the protein was 30 µM. Final concentration of the buffer was 50 mM sodium phosphate pH 7.6, 2 M NaCl. The reaction volume was 100 µl. Reagents and amounts of the reaction are given in the Table 2.18.

Table 2.18. Reagents and amounts of in vitro HIV-1 CA oligomerization reaction at 30 µM protein concentration.

	Amounts in 100 µl reaction (µl)	
Reagents	**Sample 1**	**Sample 2**
Protein	4.61	4.61
Buffer1 (4X)	12.5	12.5
DMSO (100%)	1	1
dH2O	31.89	31.89
Buffer2 (1X)	50	50

2.11. Interaction Analysis of HIV-1 CA and Nanobody Protein with Isothermal Titration Calorimetry

To investigate HIV-1 CA – Nanobody interaction, isothermal titration calorimetry (ITC) method was used. ITC initial experiments were conducted by UNAM (Ankara, Turkey) with MicroCal ITC-200 instrument at 25°C. Three different titrations were performed: (1) 55 µM Nb was titrated into 30.8 µM HIV-1 CA; (2) 55 µM Nb was titrated into 15.4 µM HIV-1 CA; and (3) 55 µM Nb was titrated into 77 µM HIV-1 CA. Each titration consisted of Nb injections of 1 µl, made every 200 sec, into reaction cell that contains 280 µl HIV-1 CA. Both proteins were extensively dialyzed in 20 mM sodium phosphate pH 8.0, 10 mM βME.

CHAPTER 3

RESULTS AND DISCUSSION

3.1. Transformation and Confirmation of HIV Capsid Genes

Both HIV-1 CA DNA and HIV-2 CA DNA were in the pET-11a expression plasmid. pET-11a plasmids containing the HIV-1 CA DNA and HIV-2 CA DNA were transformed to E. *coli* DH5α competent cells, for both plasmid isolation and glycerol stock preparation. After transformation, colonies were grown on the LB agar plates with ampicillin for both cultures (Figure 3.1).

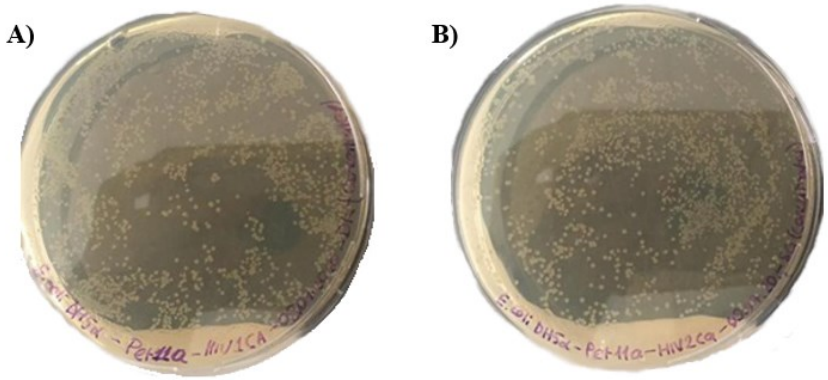

Figure 3.1. Transformation plates of pET-11a-HIV-1 CA and PET-11a-HIV-2 CA plasmids into E. coli DH5α competent cells. A) pET-11a-HIV-1 CA plate. B) pET-11a-HIV-2 CA plate.

pET-11a-HIV-1 CA and pET-11a-HIV-2 CA plasmids were isolated from the overnight grown cultures with a single colony inoculation from the transformation plates. The glycerol stocks for the both cultures were prepared from these overnight grown cultures and stored at -80˚C. Isolated pET-11a-HIV-1 CA and pET-11a-HIV-2 CA plasmids were linearized by single restriction enzyme digesting then, gene sizes were confirmed on 1% agarose gel. Agarose gel result is shown in the Figure 3.2. DNA length of the pET-11a-HIV-1 CA is 693 bp and DNA length of the pET-11a-HIV-2 CA is 687 bp. 1 kb DNA Ladder was used in the agarose gel. All samples except the pET-11a-HIV-

2 CA plasmid sample in lane 4 (Figure 3.2) showed DNA band where expected bp level.

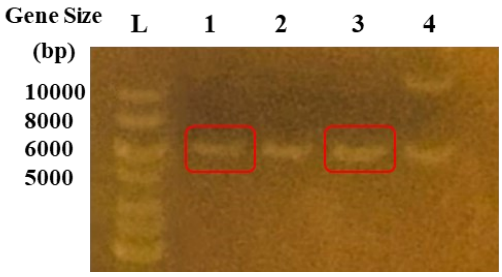

Figure 3.2. Isolated pET-11a-HIV-1 CA and pET-11a-HIV-2 CA plasmids on the 1% agarose gel. L: 1 kb DNA Ladder (Thermo Fisher #SM0311); 1: pET-11a-HIV-1 CA plasmid from colony 1, 2: pET-11a-HIV-1 CA plasmid from colony 2, 3: pET-11a-HIV-2 CA plasmid from colony 1, 4: pET-11a-HIV-2 CA plasmid from colony 2.

Plasmids marked with a red box in the Figure 3.2, were sequenced by Genometri Biyoteknoloji and analyzed by SnapGene Viewer Software. Part of the sequence analysis is presented in the Figure 3.3. Sequence analysis was confirmed the pET-11a vectors contained the HIV-1 CA, and HIV-2 CA genes. The HIV-1 CA and HIV-2 CA gene sequences matched both samples' own templates.

Figure 3.3. Representative image of the sequence analysis result of the plasmids. A) For pET-11a-HIV-1 CA sequence. The selected 693 bases belong to the HIV-1 CA gene. B) For pET-11a-HIV-2 CA sequence. The selected 687 bases belong to the HIV-2 CA gene.

pET-11a-HIV-1 CA and pET-11a-HIV-2 CA plasmids which sequences were confirmed were transformed to E. *coli* BL21(DE3) competent cells and E. *coli* BL21(DE3) competent cells pLysS for expression. After transformation, colonies were grown on the LB agar plates for both cultures. The glycerol stocks for the both cultures were prepared from the overnight grown cultures with a single colony inoculation from the transformation plates, and stored at -80˚C.

3.2. Expression and Purification of HIV-1 CA Protein

Expression test of the HIV-1 CA was carried out in 25 ml LB media with E. *coli* BL21(DE3). Protein expression was induced by the addition of 1 mM IPTG. The HIV-1 CA expression was confirmed by 12% SDS-PAGE gel analysis (Figure 3.4). Protein expression by IPTG induction was observed with a protein band at the molecular weight

level of the protein. HIV-1 CA has a molecular weight of 25.6 kDa. Therefore, the protein band was observed between the 20 kDa and 30 kDa bands in the induced samples shown in the Figure 3.4, belongs to the HIV-1 CA protein.

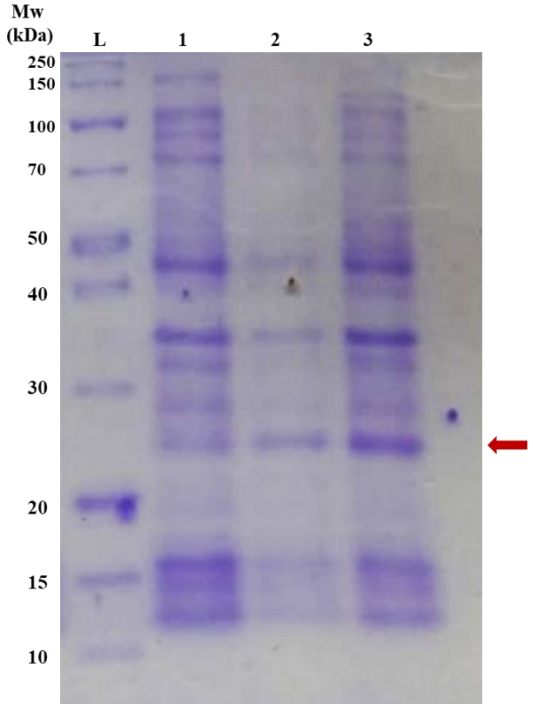

Figure 3.4. HIV-1 CA protein expression test result in 12% SDS-PAGE gel. L: Protein molecular weight ladder (Thermo Fisher #26630). 1: Before IPTG induction. 2: 4h induction after IPTG addition. 3: Overnight induction after IPTG addition.

After successful expression test, large-scale production of HIV-1 CA was performed in 1000 ml TB media with E. *coli* BL21(DE3) pLysS cells. Protein expression was induced by the addition of 0.5 mM IPTG. The cell pellet from the large-scale production culture was isolated and purified. SP cation exchange column chromatography and Q anion exchange column chromatography results of HIV-1 CA are shown in Figure 3.5 and Figure 3.6, respectively. Also, 12% SDS-PAGE analysis is shown in Figure 3.7.

The HIV-1 CA protein binds to the SP column due to ionic interactions. HIV-1 CA protein was eluted in gradient step (Figure 3.5, GR2 fraction). It is seen in the 12% SDS-PAGE gel, HIV-1CA protein was obtained as almost pure (Figure 3.7). Unspecific proteins leave the column in flowthrough step (Figure 3.5, FT fraction). Therefore, the protein band of HIV-1 CA is not seen in the FT fraction (Figure 3.7).

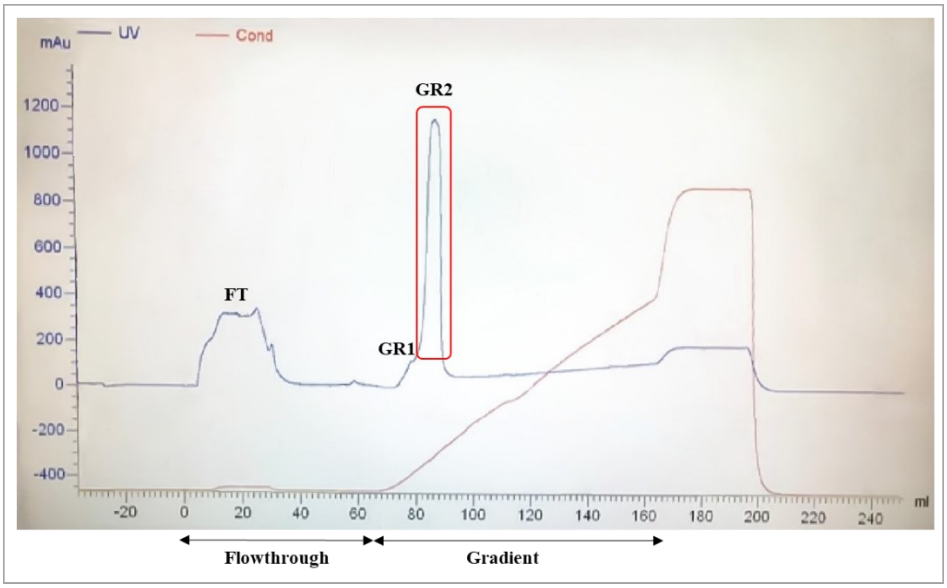

Figure 3.5. Chromatogram of the SP cation exchange column chromatography of the HIV-1 CA. The X-axis is the volume of fluid (ml) passing through the system over time. The y-axis is the absorbance signal (mAu) at 280 nm. In the flowthrough step FT fraction was collected. In the gradient step, G1 and G2 fractions were collected.

As in the study by (Pornillos et al., 2010), the protein sample obtained by SP column chromatography was loaded onto the Q anion exchange column by adding another purification step. HIV-1 CA protein does not bind to the Q anion exchange column due to ionic interactions. Therefore, FT1 and FT2 protein peaks belong to the HIV-2 CA protein (Figure 3.6).

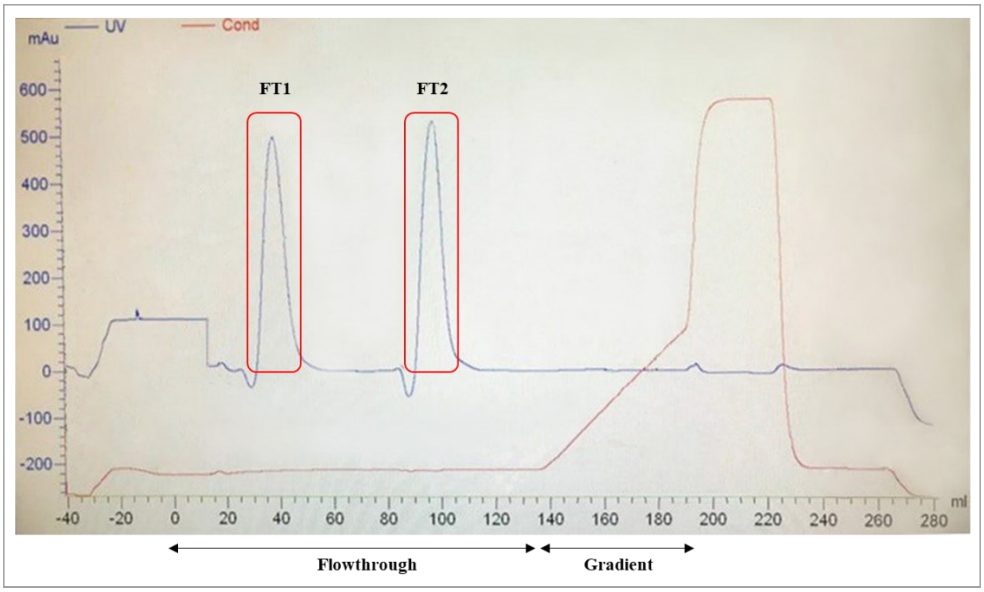

Figure 3.6. Chromatogram of the Q anion exchange column chromatography applied after the SP cation exchange column chromatography of HIV-1 CA. The X-axis is the volume of fluid (ml) passing through the system over time. The y-axis is the absorbance signal (mAu) at 280 nm. The protein sample was loaded into the column with two separate injections, FT1 and FT2 represent the fractions after these two injections, respectively.

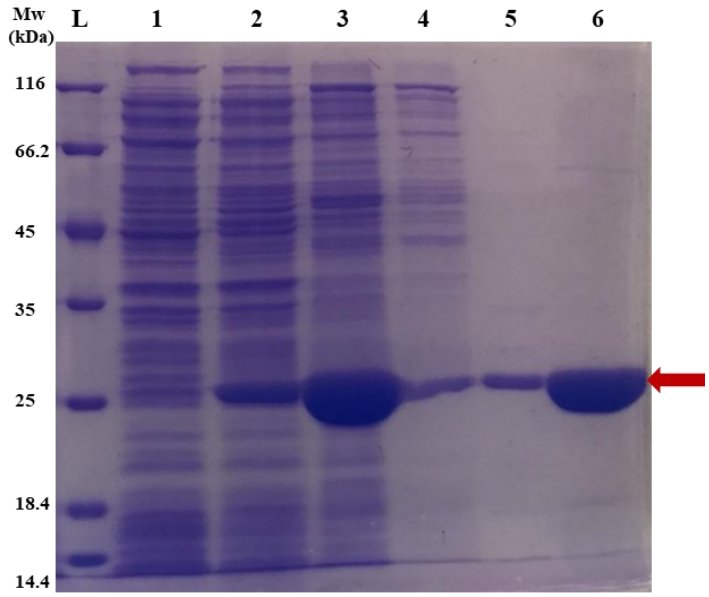

Figure 3.7. 12% SDS-PAGE analysis of the HIV-1 CA purification. L: Protein molecular weight ladder (Thermo Fisher #26610). 1: Before IPTG induction. 2:

Overnight induction after IPTG addition. 3: After pre-purification step. 4: FT fraction from SP cation exchange column chromatography. 5: GR1 fraction from SP cation exchange column chromatography. 6: GR2 fraction from SP cation exchange column chromatography. (HIV-1 CA molecular weight is 25.6 kDa)

HIV-1 CA was produced and purified in three separate batches using LB or TB media in 500 ml or 1000 ml volumes. After purification process, the pure protein was concentrated. Protein concentrations were calculated by the Beer-Lambert equation according to the absorbance value of the concentrated protein measured at 280 nm and the extinction coefficient value of the protein.

Beer-Lambert Equation:

$$A = \varepsilon . c . l$$

In this equation, A is the absorbance at 280 nm of the protein; ε is the molar extinction coefficient of the protein; l is the optical pathlength in cm; c is the molar concentration of the protein. HIV-1 CA protein extinction coefficient is 38960 $M^{-1}cm^{-1}$. Protein absorbance was measured in a 1 cm pathlength cuvette.

As a result of these productions, the final concentrations of purified HIV-1 CA were calculated as 130 µM, 150 µM and 650 µM.

3.3. Expression and Purification of HIV-2 CA Protein

HIV-2 CA expression test was carried out in 25 ml LB media with E. *coli* BL21(DE3). Protein expression was induced by the addition of 0.5 mM IPTG. HIV-2 CA expression was analyzed on the 12% SDS-PAGE gel (Figure 3.8). HIV-2 CA has a molecular weight of 25.7 kDa. Therefore, the protein band was expected between the 20 kDa and 30 kDa bands in the induced samples shown in the Figure 3.8. Faint band was observed in the induced samples (Figure 3.8). It could not be determined exactly which band belongs to the HIV-2 CA protein.

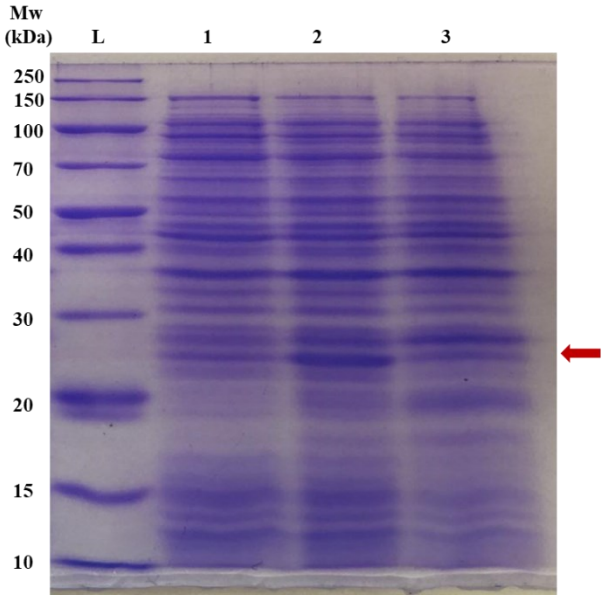

Figure 3.8. HIV-2 CA protein expression test result in 12% SDS-PAGE gel. L: Protein molecular weight ladder (Thermo Fisher #26630). 1: Before IPTG induction. 2: 4h induction after IPTG addition. 3: Overnight induction after IPTG addition.

After expression test, large-scale production of HIV-2 CA was performed in 400 ml LB media with E. *coli* BL21(DE3) cells. Protein expression was induced by the addition of 0.5 mM IPTG. Analysis of the large-scale production of the HIV-2 CA in 12% SDS-PAGE gel is given in the Figure 3.10, A. The protein band was expected between the 20 kDa and 30 kDa bands in the induced samples. However, faint band was observed in the induced samples at the expected molecular weight level (Figure 3.10, A). To ensure the presence of protein expression, the cell pellet obtained from this culture was used in the HIV-2 CA purification experiment. HIV-2 CA purification was performed. The result of SP cation exchange column chromatography is shown in Figure 3.9. Also, 12% SDS-PAGE analysis is given in the Figure 3.10, B. The HIV-2 CA protein should bind to the SP cation exchange column due to ionic interactions. However, chromatography and SDS-PAGE gel results show that HIV-2-CA protein does not bind to the column.

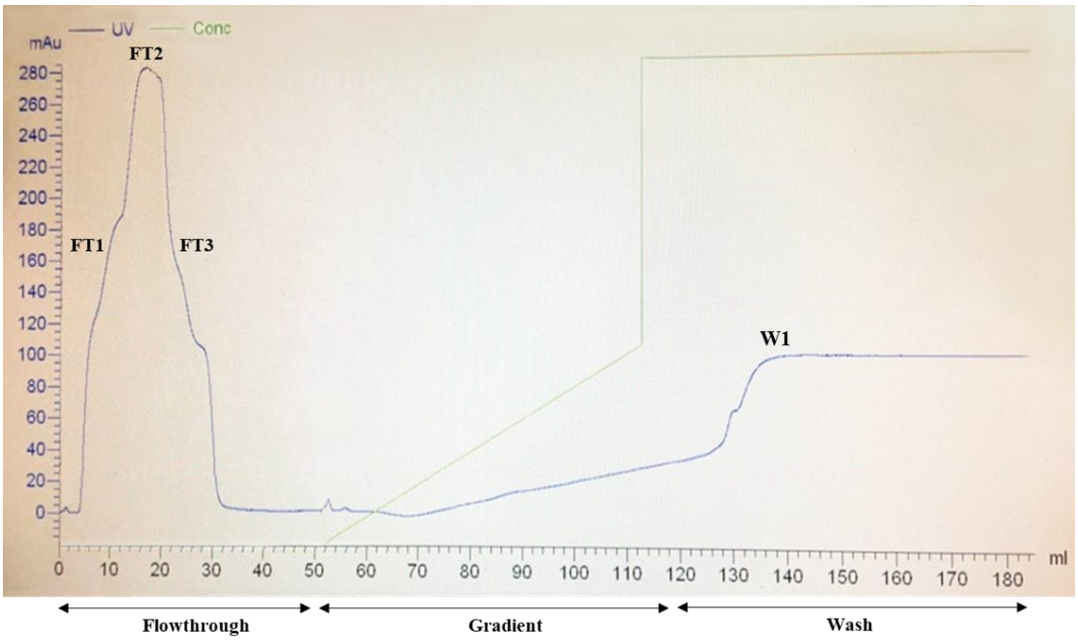

Figure 3.9. Chromatogram of the SP cation exchange column chromatography of HIV-2 CA. The X-axis is the volume of fluid (ml) passing through the system over time. The y-axis is the absorbance signal (mAu) at 280 nm. FT1, FT2 and FT3 fractions were collected in the flowthrough step. W1 fraction was collected in the step of washing with %100 Elution Buffer.

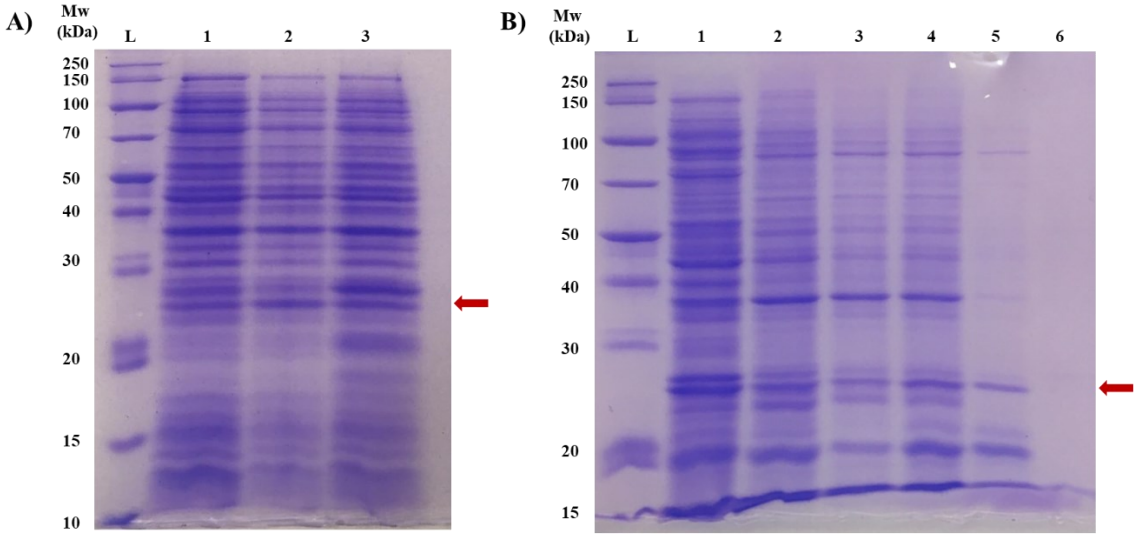

Figure 3.10. L: Protein molecular weight ladder (Thermo Fisher #26630). A) Large-scale production of the HIV-2 CA in 12% SDS-PAGE gel. 1: Before IPTG induction. 2: 2h induction after IPTG addition. 3: Overnight induction after

IPTG addition. B) 12% SDS-PAGE analysis of the HIV-2 CA purification samples 1: Lysis supernatant after sonication step. 2: After pre-purification step. 3: FT1 fraction from SP cation exchange column chromatography. 4: FT2 fraction from SP cation exchange column chromatography. 5: FT3 fraction from SP cation exchange column chromatography. 6: W1 fraction from the SP cation exchange column chromatography. (HIV-2 CA molecular weight is 25.7 kDa.)

When the SDS-PAGE gel was examined (Figure 3.10, B), a band between 20 kDa and 30 kDa was observed, which is thought to belong to HIV-2 CA. However, this protein band is present in flowthrough fractions with many other proteins, because of the protein does not bind to the column. The sample in Lane 5 appears to be a cleaner sample than the others, but there is still a lot of unspecific proteins in the environment and the HIV-2 CA protein is also impure in this sample. Also, the protein band intensity was too low.

HIV-1 and HIV-2 capsid proteins share almost 70% sequence similarity, and their pI values are 6.3 and 5.6, respectively. For this reason, we applied the same production and purification protocol for both proteins. However, we were unable to obtain pure full-length HIV-2 capsid protein. The nanobody protein was determined to bind HIV-1 capsid NTD (Helma et al., 2012). Thus, we decided to produce HIV-1 and HIV-2 capsid NTD to conduct nanobody binding studies.

3.4. Cloning of the HIV Capsid NTD Genes

HIV-1 CA NTD sequence from pET-11a-HIV-1 CA template and HIV-2 CA NTD sequence from pET-11a-HIV-2 CA template were amplified by PCR. The PCR-amplified HIV-CA NTD inserts and pET-21a vector were digested with NdeI and XhoI restriction enzymes and ligated together. Then they were transformed to E. *coli* DH5α competent cells.

3.4.1. HIV Capsid NTDs Amplification

PCR reactions ingredients and conditions for HIV-1 CA NTD and HIV-2 CA NTD are given in the Materials and Methods section. PCR products were confirmed by

1.5% Agarose gel electrophoresis. Agarose gel result of the PCR reactions for both genes are shown in the Figure 3.11.

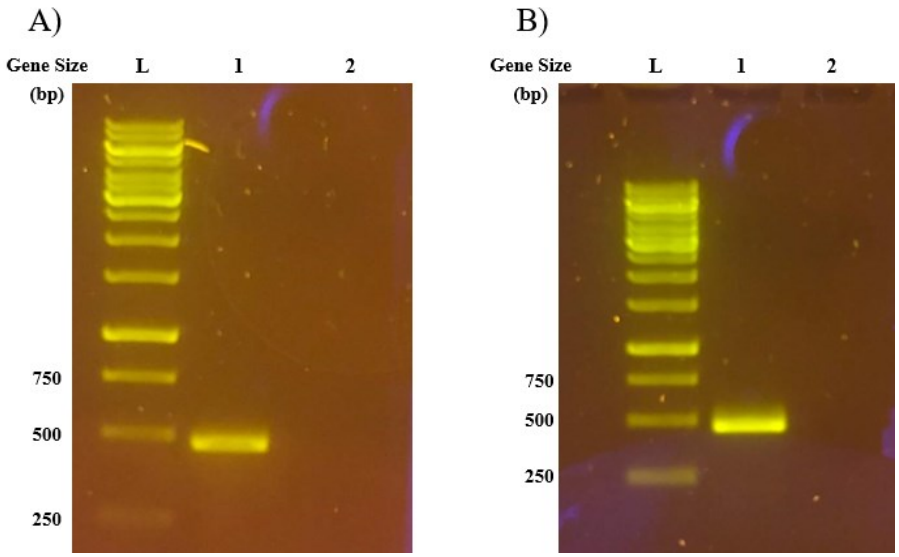

Figure 3.11. 1.5% Agarose gel result of the PCR reactions of HIV-1 CA NTD and HIV-2 CA NTD genes. A) PCR reaction result of HIV-1 CA NTD. L: 1 kb DNA Ladder (Thermo Fisher #SM0311), 1: PCR product with 465 bp, 2: PCR negative control without enzyme. B) PCR reaction result of HIV-2 CA NTD. L: 1 kb DNA Ladder (Thermo Fisher #SM0311), 1: PCR product with 471 bp, 2: PCR negative control without enzyme.

In Figure 3.11 A, PCR product is the HIV-1 CA NTD. The HIV-1 CA NTD gene size is 465 bp. It is expected that the DNA band will appear just under 500bp in the agarose gel, and the band was observed at the expected level. PCR was performed successfully for HIV-1 CA NTD. In Figure 3.11 B, the PCR product is HIV-2 CA NTD with a gene size of 471 bp. The DNA band was observed at the expected level in the agarose gel. PCR was successfully performed for HIV-2 CA NTD.

3.4.2. Digesting of the HIV Capsid NTD Inserts and pET-21a Vector

After, PCR products were confirmed by agarose gel electrophoresis, all PCR products were purified from the agarose gel then, each purified PCR products and empty pET-21a vectors were digested with NdeI and XhoI restriction enzyme. Digested PCR

products and pET-21a plasmids were confirmed by agarose gel electrophoresis (%1.5 for inserts, %1 for vectors). Agarose gel results are shown in the Figure 3.12. Single and double digested DNA samples were examined for HIV-1 CA NTD, HIV-2 CA PCR products and pET-21a vector on agarose gel. For all samples, DNA bands were appeared at the expected DNA length level. The length of the HIV-1 CA NTD PCR product is 465 bp. The length of the HIV-2 CA NTD PCR product is 471 bp. The length of the single digested pET-21a vector is 5443 bp. The length of the empty pET-21a vector (double digested) is 5363 bp. The length between NdeI-XhoI in pET-21a is 80 bp.

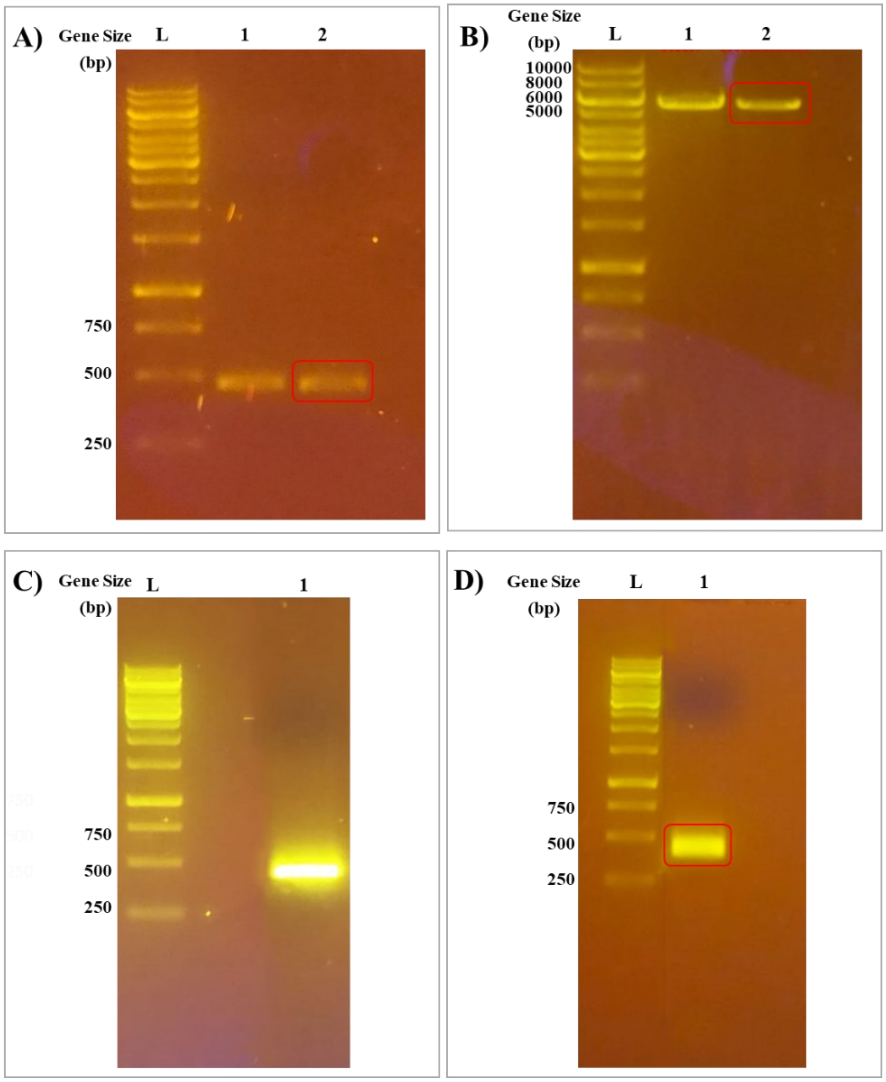

Figure 3.12. Agarose gel results of NdeI and XhoI digesting reactions of PCR products and pET-21a vector. The length of the pET-21a vector is 5363 bp. The length between NdeI-XhoI in pET-21a is 80 bp. L: 1 kb DNA Ladder (Thermo Fisher #SM0311) for all figures. A) 1.5% agarose gel result of NdeI and XhoI digested HIV-1 CA NTD samples. 1: XhoI single digested HIV-1 CA NTD PCR product, 2: XhoI and NdeI double digested HIV-1 CA NTD PCR product. B) 1% agarose gel result of NdeI and XhoI digested pET-21a samples. 1: XhoI single digested pET-21a, 2: XhoI and NdeI double digested pET-21a. C) 1.5% agarose gel result of NdeI digested HIV-2 CA NTD sample. 1: NdeI single digested HIV-2 CA NTD PCR product. D) 1.5% agarose gel result of NdeI and XhoI digested HIV-2 CA NTD sample. 1: XhoI and NdeI double digested HIV-2 CA NTD PCR product.

3.4.3. Ligation of the HIV Capsid NTDs and pET21-a Vector

After double digested PCR products and pET-21a vector were confirmed by agarose gel electrophoresis, all samples were purified from the agarose gel. Then, HIV-1 CA NTD gene and HIV-2 CA NTD gene were ligated into pET-21a vectors. After ligation process, each ligated samples and each negative controls were transformed to E. *coli* DH5α competent cells. Transformation plates after ligation of HIV CA NTD genes into pET-21a vectors are shown in the Figure 3.13. Both HIV-1 CA NTD and HIV-2 CA NTD samples had colonies on the ligation reaction plates. Also, only a few colonies were seen on the plates of the negative control samples. This result indicates that the ligation reactions was successful.

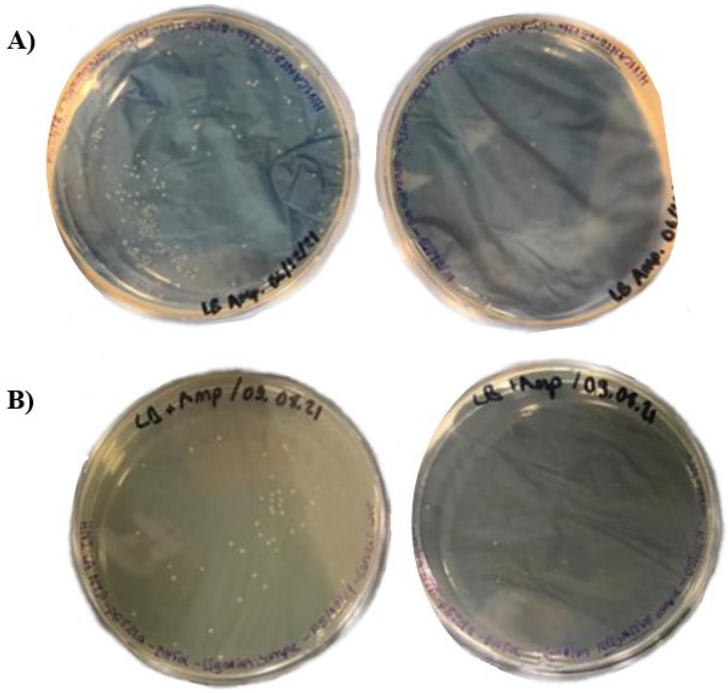

Figure 3.13. Transformation plates after ligation of HIV CA NTD genes into pET-21a vectors. A) E. coli DH5α transformation plates after ligation of HIV-1 CA NTD and pET-21a vector. Plate on the left is belongs the ligation reaction sample. Plate on the right is belongs to the negative control reaction. B) E. coli DH5α transformation plates after ligation of HIV-2 CA NTD and pET-21a vector. Plate on the left is belongs the ligation reaction sample. Plate on the right is belongs the negative control reaction.

pET-21a-HIV-1 CA NTD and pET-21a-HIV-2 CA NTD plasmids were isolated from the overnight grown cultures from the E. *coli* DH5α transformation plates for both. Isolated pET-21a-HIV-1 CA NTD and pET-21a-HIV-2 CA NTD plasmids were analyzed on the 1% agarose gel to confirmation of the gene sizes of the samples then they were sent to sequence analyzing. Sequence analyzing was done by Genometri Biyoteknoloji and results of sequences were analyzed by SnapGene Viewer Program. Part of the sequence analyzing results of the pET-21a-HIV-1 CA NTD and pET-21a-HIV-2 CA NTD are presented in the Figure 3.14. Sequence analysis was confirmed the insertion of both HIV-1 CA NTD and HIV-2 CA NTD genes into the pET-21a vector. The HIV-1 CA NTD and HIV-2 CA NTD gene sequences matched both samples' own templates.

Figure 3.14. Representative image of the sequence analyzing results of the pET-21a-HIV-1 CA NTD and pET-21a-HIV-2 CA NTD plasmids. A) For pET-21a-HIV-1 CA NTD sequence. The selected 477 bases belong to the HIV-1 CA gene+XhoI+His-Tag. B) For pET-21a-HIV-2 CA NTD sequence. The selected 477 bases belong to the HIV-2 CA gene+XhoI+His-Tag.

3.5. Expression and Purification of HIV-1 CA NTD Protein

Expression test of HIV-1 CA NTD was carried out in 25 ml TB media with E. *coli* BL21(DE3) pLysS cells. Protein expression was induced by the addition of 0.5 mM IPTG under two different temperatures (25˚C and 37˚C). The HIV-1 CA NTD expression was confirmed by 15% SDS-PAGE gel analysis which are shown in the Figure 3.15.

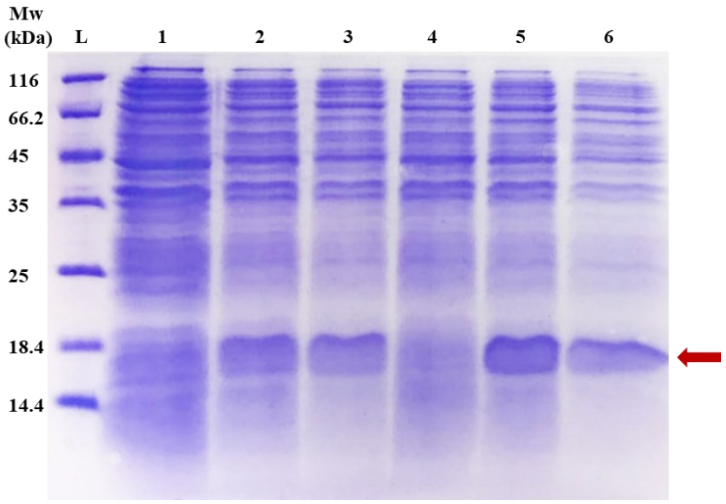

Figure 3.15. 15% SDS-PAGE gel analysis of the HIV-1 CA NTD expression test at 25˚C and 37˚C. L: Protein molecular weight ladder (Thermo Fisher #26610). Lane 1, 2 and 3 are expression test samples at 25˚C. Lane 4, 5 and 6 are expression test samples at 37˚C. 1: Before IPTG induction. 2: 2h induction after IPTG addition. 3: 4h induction after IPTG addition. 4: Before IPTG induction. 5: 2h induction after IPTG addition. 6: 4h induction after IPTG addition.

In the Figure 3.15, it is seen that HIV-1 CA NTD protein expression has been achieved successfully. HIV-1 CA NTD has a molecular weight of 17.7 kDa, therefore the protein band were expected to observe around at 18.4 kDa band in the ladder. Protein band was observed at the expected molecular weight level in the induced samples at both temperatures. Although all samples showed similar results, the protein band of the sample induced at 37˚C for 2h (Lane 5) was observed more intensely. Therefore, it has been decided that the induction conditions to be applied for the large-scale production will be at 37˚C for 2 hours.

Large-scale production of the HIV-1 CA NTD were performed in 200 ml TB

media with E. *coli* BL21(DE3) pLysS cells. Protein expression was induced by the addition of 0.5 mM IPTG. The cell pellet from the large-scale production culture was isolated and purified. HIV-1 CA NTD protein was purified by immobilized metal ion affinity chromatography (IMAC). Then ion exchange chromatography was used as an additional step. Chromatography results are shown in the Figure 3.16 and Figure 3.17, respectively. Also, 15% SDS-PAGE analysis is shown in Figure 3.18.

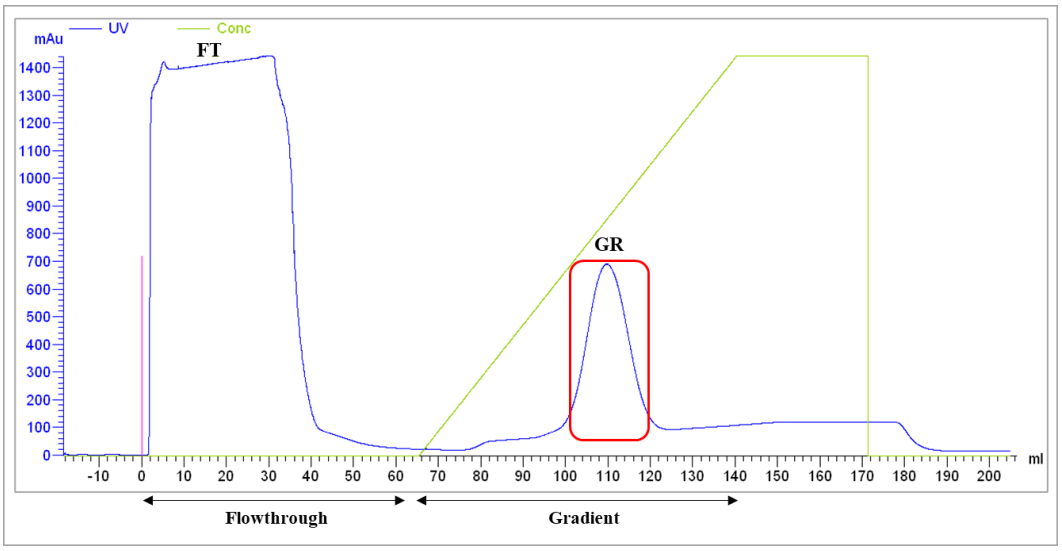

Figure 3.16. IMAC chromatogram of the HIV-1 CA NTD protein. IMAC chromatogram of the HIV-1 CA NTD. The X-axis is the volume of fluid (ml) passing through the system over time. The y-axis is the absorbance signal (mAu) at 280 nm. In the flowthrough step, FT fraction was collected. In gradient step, the GR fraction was collected.

HIV-1 CA NTD protein bind strongly to the nickel ion charged IMAC column due to histidine residues (His-Tag) it contains. Therefore, during washing the column with buffer that contains low concentration of imidazole, the histidine-labeled protein binds to the column and unspecific proteins that do not bind to the column are separated from the column (Figure 3.16, FT fraction). During washing the column with buffer containing high concentration of imidazole, the HIV-1 CA NTD protein is eluted from the column (Figure 3.16, GR fraction) thanks to the competition of imidazole with histidine residues to bind to the nickel ion charged column. HIV-1 CA NTD protein sample obtained by IMAC was loaded to onto the Q anion exchange column.

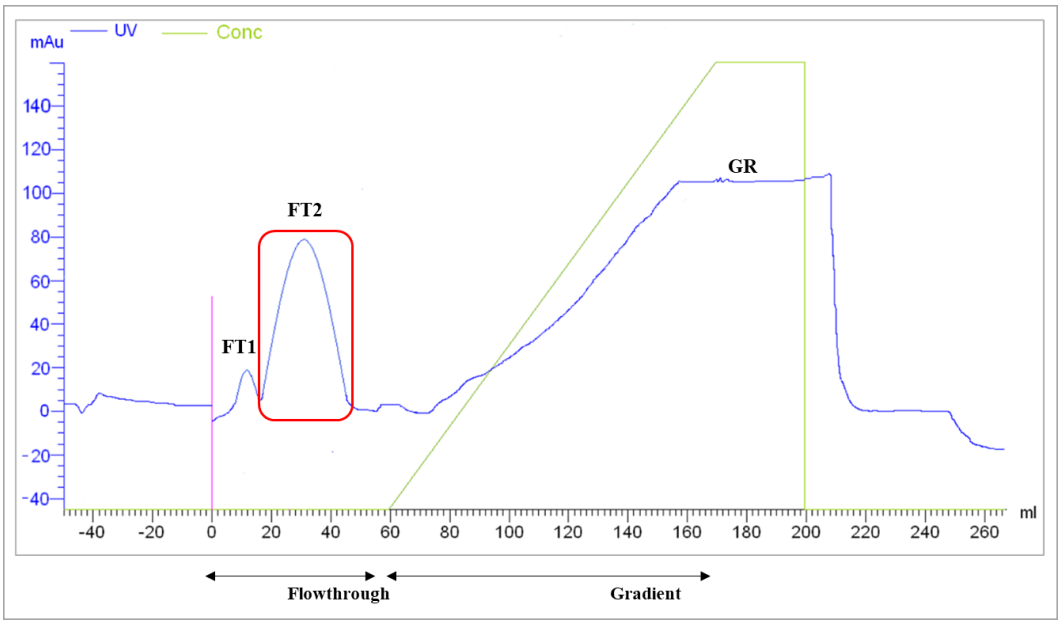

Figure 3.17. Chromatogram of the Q anion exchange column chromatography applied after the IMAC for HIV-1 CA NTD. The X-axis is the volume of fluid (ml) passing through the system over time. The y-axis is the absorbance signal (mAu) at 280 nm. In the flowthrough step, FT1 and FT2 fractions collected separately. In gradient step, the GR fraction was collected during the increasing absorbance signal.

HIV-1 CA NTD protein does not bind to the Q anion exchange column due to ionic interactions. Therefore, Flowthrough2 absorbance peak belongs to the pure HIV-1 CA NTD protein (Figure 3.17). This is also seen in the 15% SDS-PAGE gel (Figure 3.18, B). In addition, when the fractions collected in the gradient step were examined, no protein band was observed (Figure 3.18, B). This proves that all HIV-1 CA NTD protein is obtained as purely in the flowthrough step.

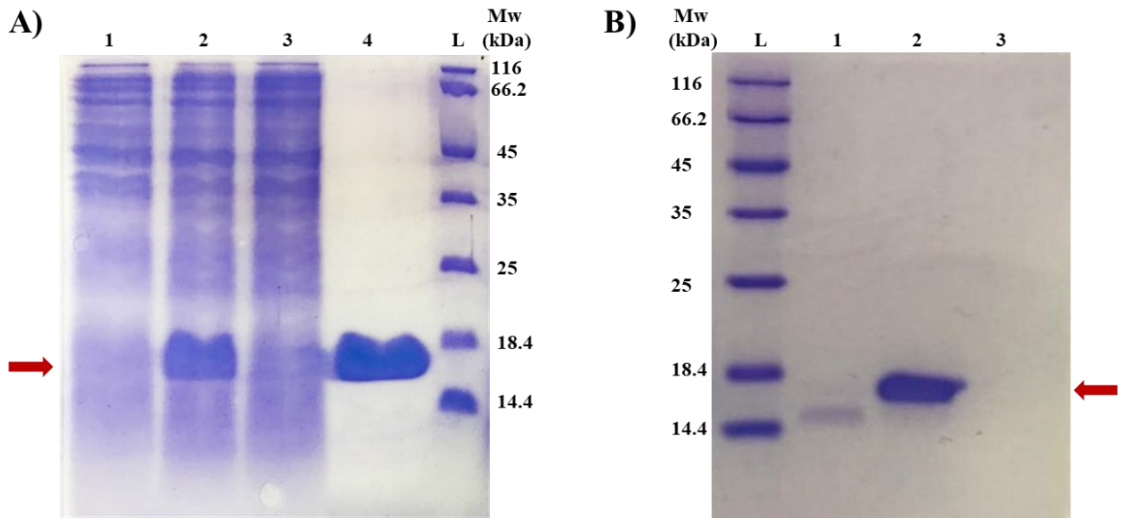

Figure 3.18. 15% SDS-PAGE gel analysis of the samples from large-scale production and purification steps for HIV-1 CA NTD. L: Protein molecular weight ladder (Thermo Fisher #26610). A) 1: Before IPTG induction, 2: After pre-purification step, 3: FT fraction from the IMAC, 4: GR fraction from the IMAC. B) 1: FT1 fraction from the Q column anion exchange chromatography, 2: FT2 fraction from the Q anion exchange column chromatography, 3: GR fraction from the Q anion exchange column chromatography. (HIV-1 CA NTD molecular weight is 17.7 kDa.)

HIV-1 CA NTD was produced and purified in separate two batches using TB media in 200 ml and 1000 ml volume. After purification process, the pure protein was concentrated. Protein concentrations were calculated by the Beer-Lambert equation according to the absorbance value of the concentrated protein measured at 280 nm and the extinction coefficient value of the protein.

Beer-Lambert Equation:

$$A = \varepsilon . c . l$$

In this equation, A is the absorbance at 280 nm of the protein; ε is the molar extinction coefficient of the protein; l is the optical pathlength in cm; c is the molar concentration of the protein. HIV-1 CA NTD protein extinction coefficient is 24980 $M^{-1}cm^{-1}$. Protein absorbance was measured in a 1 cm pathlength cuvette.

As a result of these productions, the final concentrations of purified HIV-1 CA NTD were calculated as 146 µM, 317 µM.

3.6. Expression and Purification of HIV-2 CA NTD Protein

Expression test of HIV-2 CA NTD was carried out in 25 ml TB media with E. *coli* BL21(DE3) pLysS cells. Protein expression was induced by the addition of 0.5 mM IPTG under two different temperatures (25˚C and 37˚C). The HIV-2 CA NTD expression was confirmed by 15% SDS-PAGE gel analysis which are shown in the Figure 3.19.

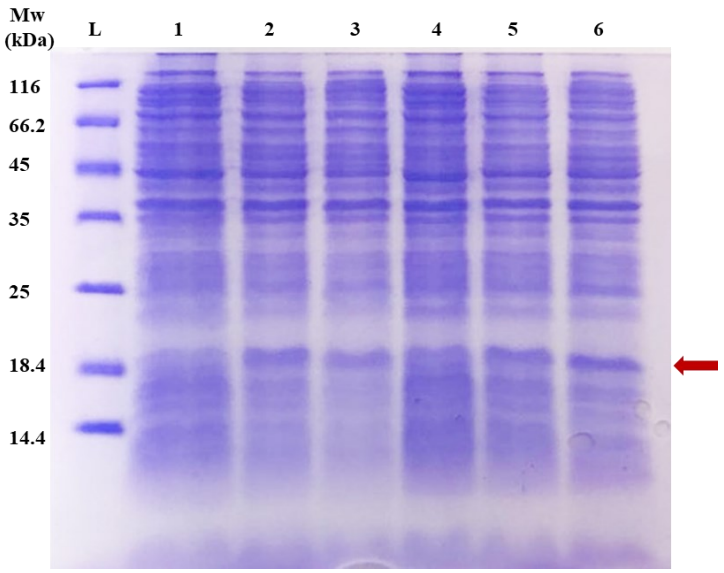

Figure 3.19. 15% SDS-PAGE gel analysis of the HIV-2 CA NTD expression test at 25˚C and 37˚C. L: Protein molecular weight ladder (Thermo Fisher #26610). Lane 1, 2 and 3 are expression test samples at 37˚C. Lane 4, 5 and 6 are expression test samples at 25˚C. 1: Before IPTG induction. 2: 2h induction after IPTG addition. 3: 4h induction after IPTG addition. 4: Before IPTG induction. 5: 2h induction after IPTG addition. 6: 4h induction after IPTG addition.

Figure 3.19 shows that HIV-2 CA NTD protein was successfully expressed. As HIV-2 CA NTD has a molecular weight of 17.9 kDa, therefore, the protein band was expected to be observed in the induced samples in the band of about 18.4 kDa. Protein band was observed at the expected molecular weight level in the induced samples at both temperatures. Due to the more distinct difference in the protein band between the induced and uninduced samples as a result of the test performed at 37˚C, it was decided to perform the large production experiment at this temperature. It was decided that 2 hour was sufficient for the induction time.

Large-scale production of the HIV-2 CA NTD were performed in 200 ml TB media with E. *coli* BL21(DE3) pLysS cells. Protein expression was induced by the addition of 0.5 mM IPTG. The cell pellet from the large-scale production culture was isolated and purified. Immobilized metal ion affinity chromatography (IMAC) and Q-Sepharose anion exchange column chromatography results are shown in Figures 3.20 and Figure 3.21, respectively. Also, 15% SDS-PAGE analysis is shown in Figure 3.22.

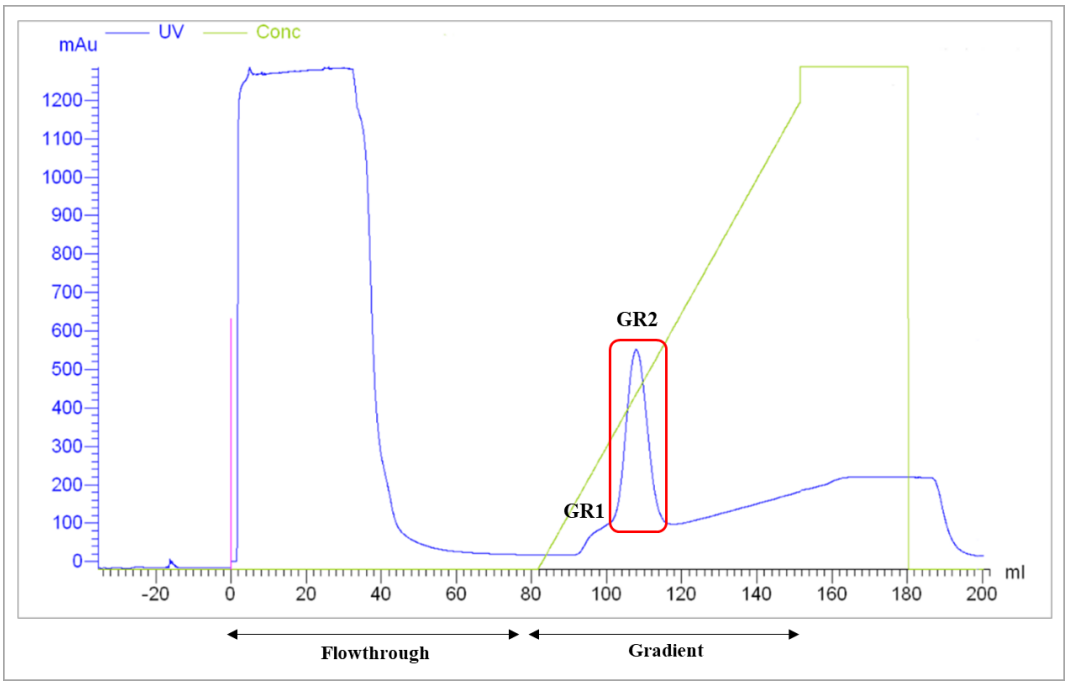

Figure 3.20. IMAC chromatogram of the HIV-2 CA NTD. The X-axis is the volume of fluid (ml) passing through the system over time. The y-axis is the absorbance signal (mAu) at 280 nm. In the gradient step, GR1 and GR2 fractions were collected.

The HIV-2 CA NTD protein binds to the IMAC column because it has His-Tag. Therefore, unspecific proteins are expected to separate from the column in the flowthrough step (Figure 3.20, FT fraction) and elute of the HIV-2 CA NTD protein in the gradient step (Figure 3.20, GR2 fraction) 15% SDS-PAGE gel analysis confirmed that the absorbance peak seen at the gradient step in Figure 3.22 belonged to the HIV-2 CA NTD (Figure 3.22, B). The HIV-2 CA NTD sample collected from IMAC was loaded onto the Q column.

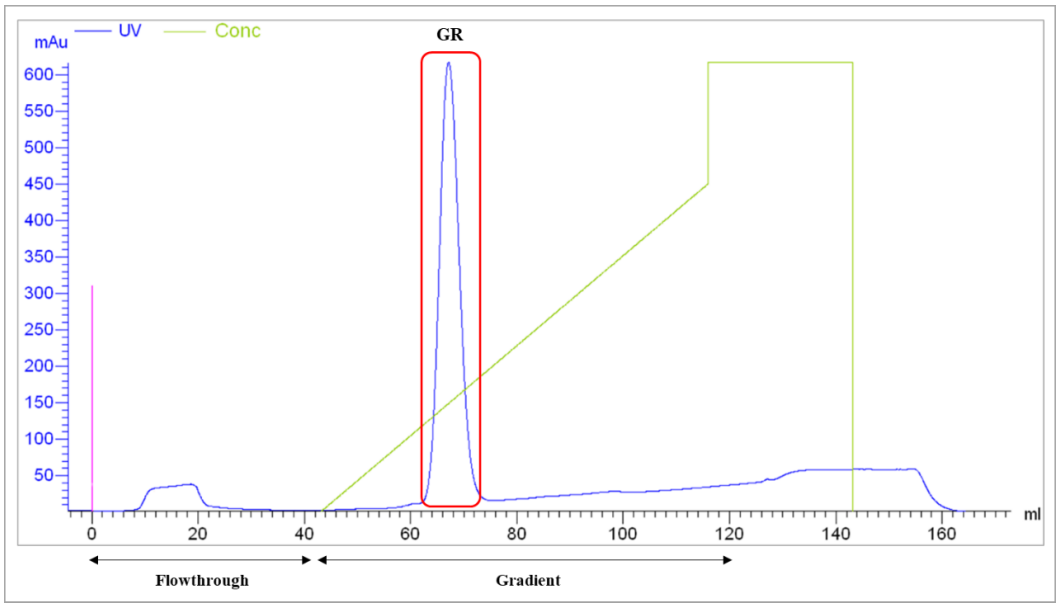

Figure 3.21. Chromatogram of the Q anion exchange column chromatography applied after the IMAC for HIV-2 CA NTD. The X-axis is the volume of fluid (ml) passing through the system over time. The y-axis is the absorbance signal (mAu) at 280 nm. In the gradient step, GR fraction collected.

The HIV-2 CA NTD protein binds to the Q anion exchange column due to ionic interactions. Therefore, the protein was eluted in the gradient step and the protein peak is clearly seen in the Figure 3.21. When this sample was examined on the 15% SDS-PAGE gel, the HIV-2 CA NTD protein band was purely observed around 18.4 kDa band in the ladder (Figure 3.22, B). 15% SDS-PAGE gel also shows the fractions together from the both chromatography. When fractions are examined, it is seen that an additional purification step increases the purity of HIV-2 CA NTD protein.

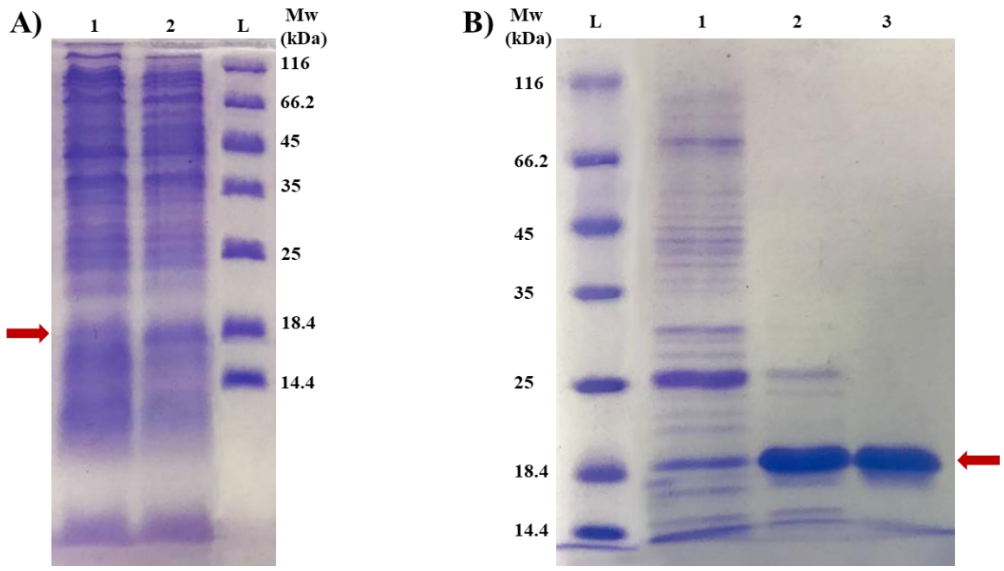

Figure 3.22. 15% SDS-PAGE gel analysis of the samples from large-scale production and purification steps for HIV-2 CA NTD. L: Protein molecular weight ladder (Thermo Fisher #26610) for both images. A) 1: Before IPTG induction, 2: 2h induced after IPTG addition. B) 1: GR1 fraction from the IMAC, 2: GR2 fraction from the IMAC, 3: GR fraction from the Q anion exchange column chromatography. (HIV-2 CA NTD molecular weight is 17.9 kDa.)

After purification process, the pure protein was concentrated. Protein concentration was calculated by the Beer-Lambert equation according to the absorbance value of the concentrated protein measured at 280 nm and the extinction coefficient value of the protein.

Beer-Lambert Equation:

$$A = \varepsilon . c . l$$

In this equation, A is the absorbance at 280 nm of the protein; ε is the molar extinction coefficient of the protein; l is the optical pathlength in cm; c is the molar concentration of the protein. HIV-2 CA NTD protein extinction coefficient is 29450 $M^{-1}cm^{-1}$. Protein absorbance was measured in a 1 cm pathlength cuvette.

The final concentration of purified HIV-2 CA NTD was calculated as 146 µM.

3.7. HPLC Analysis of HIV Capsid NTD Proteins

Purified HIV-1 CA NTD and HIV-2 CA NTD proteins were analyzed with Reversed-Phase HPLC (High Performance Liquid Chromatography) with NUCLEOSIL 300-5 C4 column. The absorbance signal of both proteins was monitored at both 220 nm and 280 nm. 20 µl sample were injected from each protein. The concentrations of injected HIV-1 CA NTD and HIV-2 CA NTD samples were 32 µM and 48 µM, respectively. Chromatograms of HIV-1 CA NTD and HIV-2 CA NTD are shown in Figure 3.23 and Figure 3.24, respectively.

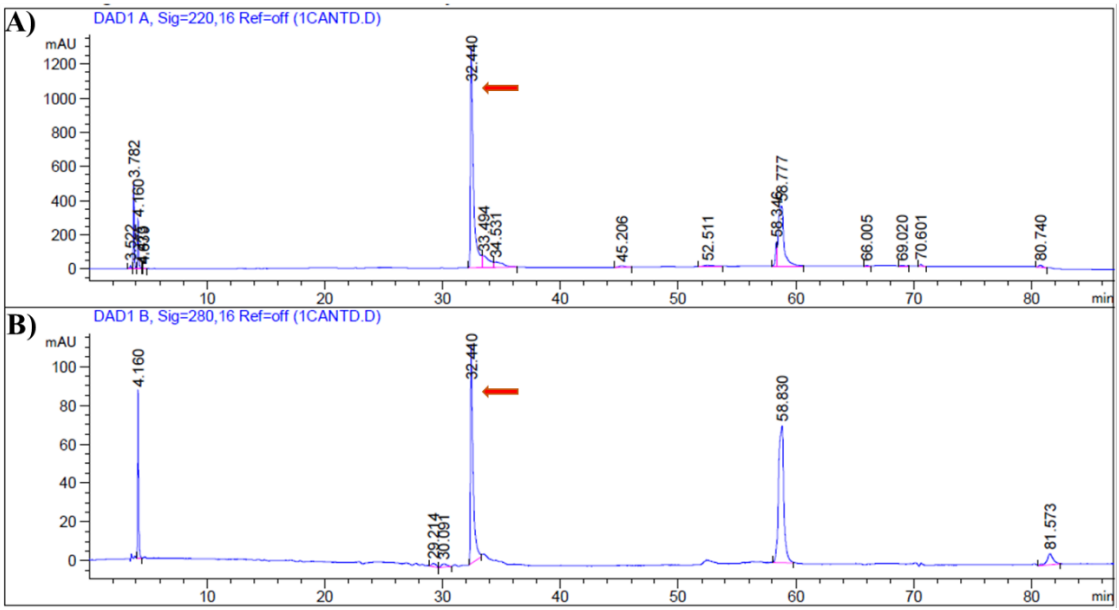

Figure 3.23. HPLC analysis of the HIV-1 CA NTD. A) at 220 nm. B) at 280 nm.

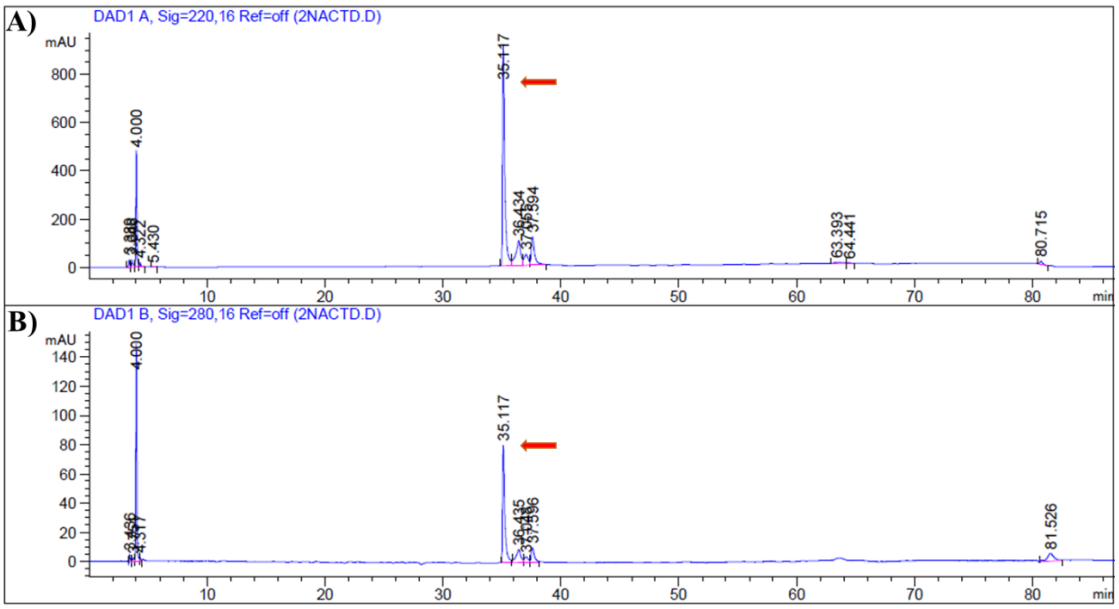

Figure 3.24. HPLC analysis of the HIV-2 CA NTD. A) at 220 nm. B) at 280 nm.

Proteins absorb UV light at 220 nm due to peptide bonds, and absorb UV light at 280 nm due to aromatic amino acids of the protein. Therefore, the absorbance signal received at 220 nm is greater than the signal received at 280 nm.

In both chromatograms, a high peak of the proteins was observed in the elution step (The peak indicated by the arrow in the Figure 3.23 and Figure 3.24). HIV-1 CA NTD and HIV-2 CA NTD proteins appear to be highly pure.

3.8. Characterization of Proteins

The thermal stability of HIV-1 CA protein was investigated by differential scanning fluorimetry (DSF) assay. The melting temperature (Tm) value of the HIV-1 CA protein was determined by the DSF experiment. The chemical denaturation process of the HIV-1 CA protein was investigated by fluorescence spectroscopy method and the unfolding free energy (ΔG) of the protein was determined.

3.8.1. Thermal Denaturation Analysis of HIV-1 CA

Differential scanning fluorimetry (DSF) is a rapid method to investigate protein

stability and conditions that affect stability. The stability of a protein is related to its unfolding free energy (ΔG). ΔG is temperature dependent and the stability of most proteins decreases as temperature increases. The ΔG is in equilibrium at the point where the folded and unfolded protein concentrations are equal and is equal to zero. The temperature at this equilibrium point is expressed as the melting temperature of the protein (Niesen et al., 2007). DSF is also a low-cost initial screening assay to discover new protein-ligand interactions by tracking the change in protein stability with ligand binding (Huynh & Partch, 2015).

DSF is fluorescence-based assay. It follows thermal denaturation of the protein in the presence of SYPRO Orange which is a fluorescent dye. The protein is heated in the presence of SYPRO Orange dye. As the temperature increases, the protein is denatured and its hydrophobic regions are exposed due to denaturation. SYPRO Orange binds to these hydrophobic patches on the target protein and emits light. Denaturation of the protein as a function of temperature is monitored by following the fluorescent emission of the SYPRO Orange dye (Huynh & Partch, 2015).

The thermal denaturation of the HIV-1 CA protein was investigated by differential scanning fluorimetry (DSF) assay. DSF results at four different protein concentrations (2.5 μM, 5 μM, 10 μM and 20 μM) are shown in the Figure 3.25. Proteins were in 50 mM sodium phosphate pH 8.0. The protein-free sample was used as a negative control. In the experiment, protein samples were heated from 20°C to 90°C in a Roche LightCycler® 480 Real-Time PCR instrument. When the experiment was completed, "Melting Curve" and "Derivative of the Melting Curve" graphs were obtained from Roche LightCycler® 480 software.

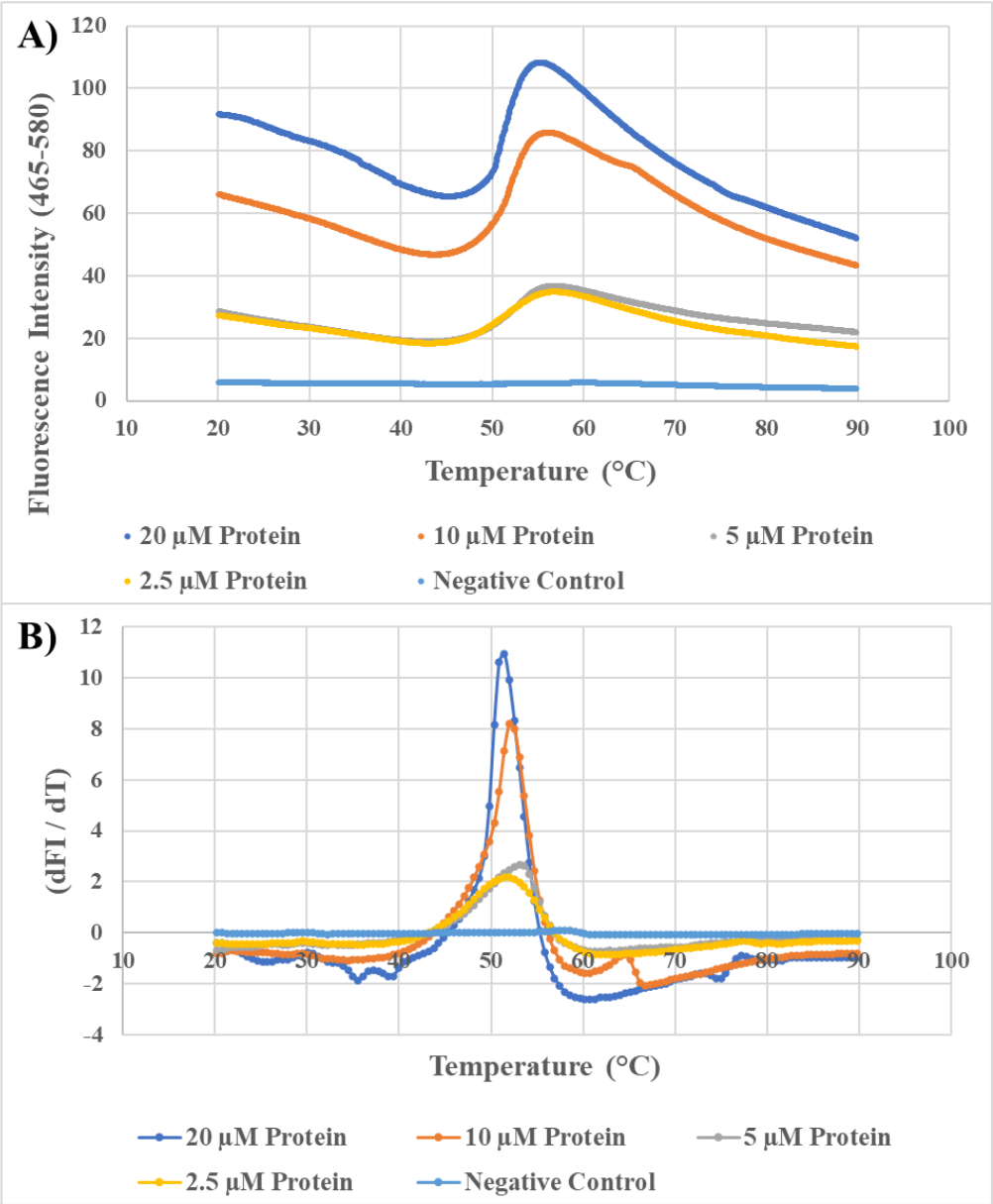

Figure 3.25. Melting Curve and Derivative of the Melting Curve graphs of HIV-1 CA at different concentrations. A) Melting Curve graph, B) Derivative of the Melting Curve graph.

In the "Melting Curve" graph, fluorescence intensity is plotted as a function of temperature. In this graph, the sigmoidal curve generated by the increasing fluorescence intensity with increasing temperature can be described as a two-state transition of protein denaturation. The inflection point of the transition curve represents the (Tm), that is the melting temperature of the protein. At this point, half of the protein in the solution is in the denatured (unfolded) form and the other half is in the native (folded) form (Niesen et

al., 2007). To be able to determine Tm value, the first derivative of the fluorescence intensity as a function of temperature is taken (-dF/dT). To make it easier to read the Tm value from the graph, the y-axis values are converted to (dF/dT) by multiplying by (-). In this graph, Tm is represented as the highest peak of the curve.

The observed Tm values of HIV-1 CA protein at different concentrations are given in the Table 3.1. These values are 51.4˚C, 53.0˚C, 51.9˚C, 51.4˚C at the 2.5 µM, 5 µM, 10 µM and 20 µM HIV-1 CA concentrations, respectively.

Table 3.1. Tm values of the HIV-1 CA at different concentrations.

Sample	**Tm (˚C) of HIV-1 CA at different concentrations**
2.5 µM	51.4
5 µM	53.0
10 µM	51.9
20 µM	51.4

Then DSF experiment was repeated with 3 identical samples at a HIV-1 CA protein concentration of 10 µM. The “Melting Curve” and “Derivative of the Melting Curve” graphs obtained as a result of this experiment are given in the Figure 3.26.

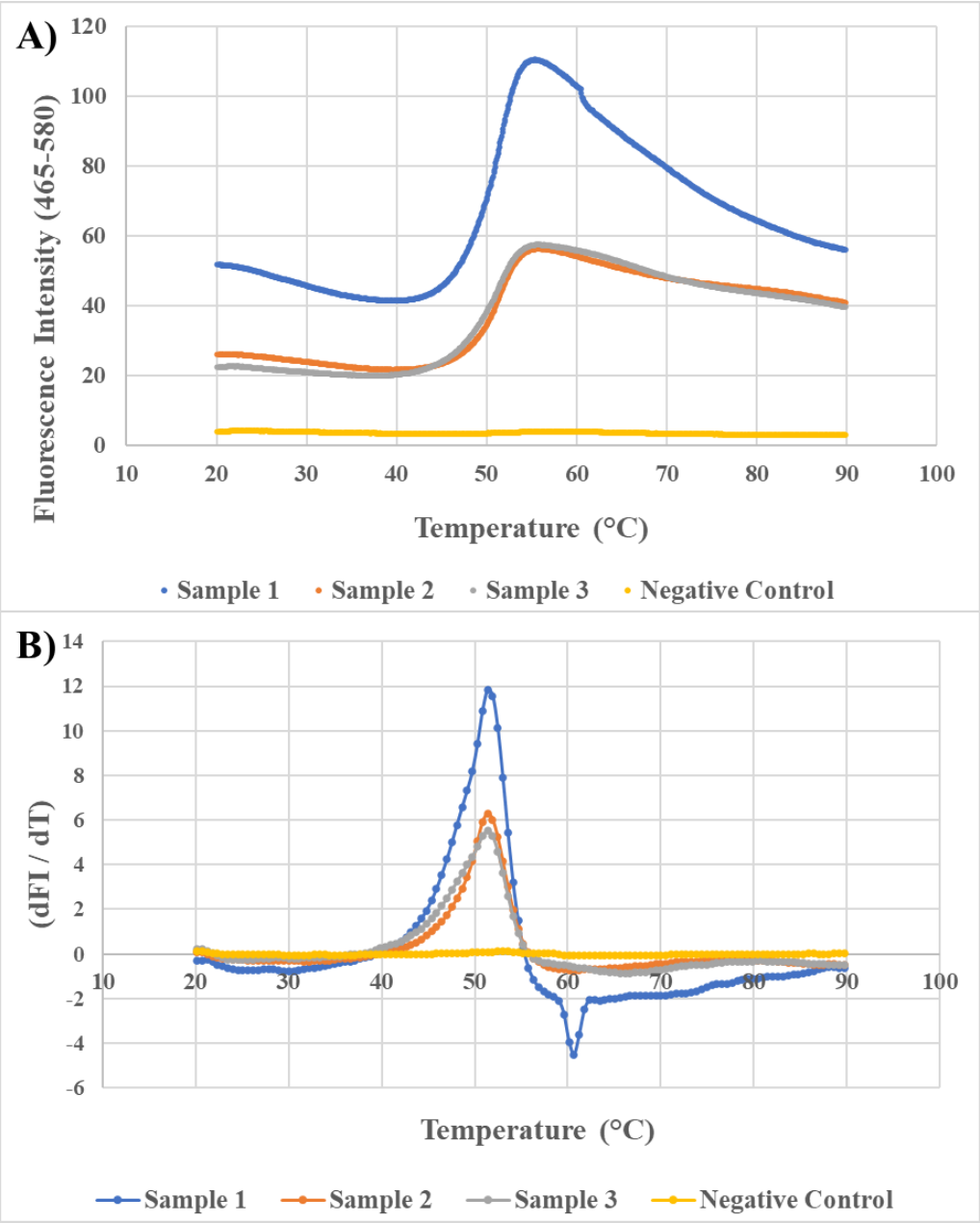

Figure 3.26. Melting Curve and Derivative of the Melting Curve graphs of HIV-1 CA at 10 µM concentration. A) Melting Curve graph, B) Derivative of the Melting Curve graph.

HIV-1 CA Tm values calculated for each sample are given in the Table 3.2. The mean value of Tm at 10 µM HIV-1 CA concentration was calculated with standard deviation as 51.6˚C ± 0.32.

Table 3.2. Tm values of the HIV-1 CA at 10 µM concentration.

Sample	**Tm (˚C) of HIV-1 CA at 10 µM concentration**
Sample 1	51.4
Sample 2	51.4
Sample 3	51.9
Average	51.6 ± 0.32

HIV-1 CA Tm values determined as a result of experiments performed at different concentrations vary in the range of 51.4˚C – 53.0˚C. In the literature the study by Douglas et al., HIV-1 CA Tm value was reported as 54˚C as a result of circular dichroism spectroscopy experiment in 50 mM sodium phosphate pH 8.0 buffer (Douglas et al., 2004). When the mean of all HIV-1 CA Tm values obtained was compared with the literature, similar results were observed with a difference of 2.2˚C. The difference in the Tm value may be due to the monitoring of the protein denaturation by two different methods.

3.8.2. Spectroscopic Analysis of HIV-1 CA Chemical Denaturation

The chemical denaturation of the HIV-1 CA protein was investigated by fluorescence spectroscopy in the presence of urea. First, the protein was examined in the presence and absence of 8 M urea at four different concentrations to determine the appropriate protein concentration for the experiments. The protein was then examined at increasing urea concentrations.

In the fluorescence spectroscopy method, the emission properties of aromatic residues in proteins are utilized. These are phenylalanine, tyrosine, and tryptophan. Among them, tryptophan absorbs the light at the longest wavelength and exhibits the largest extinction coefficient. Therefore, tryptophan emission is monitored when examining proteins by fluorescence spectroscopy. The tryptophan maximum emission occurs around 330 nm, and its absorption at 295 nm or at longest wavelength. The emission of each tryptophan residue in a protein depends on its surrounding environment. When protein was denatured, emission wavelength shift towards higher wavelengths due to the change in protein structure and exposure of tryptophan to solvent (Lakowicz, 2006;

Misselwitz et al., 1995).

In the first experiment, HIV-1 CA protein was used in the experiment at final concentrations of 0.25 µM, 0.5 µM, 1 µM and 2.5 µM. Each sample were prepared in both native and denatured conditions. In addition, a blank sample was prepared with own buffers for each sample. Samples and blanks were analyzed in the 96-well plate. Plate was scanned between 305 nm and 450 nm wavelengths. Experiment was carried out using an excitation wavelength of 295 nm. Fluorescence intensity values obtained for blank samples were subtracted from those of the samples. Then the fluorescent intensity was plotted against the wavelength. A separate graph was prepared for each protein concentration. Data obtained under both native and denatured conditions at the same protein concentration was shown on the same graph (Figure 3.27).

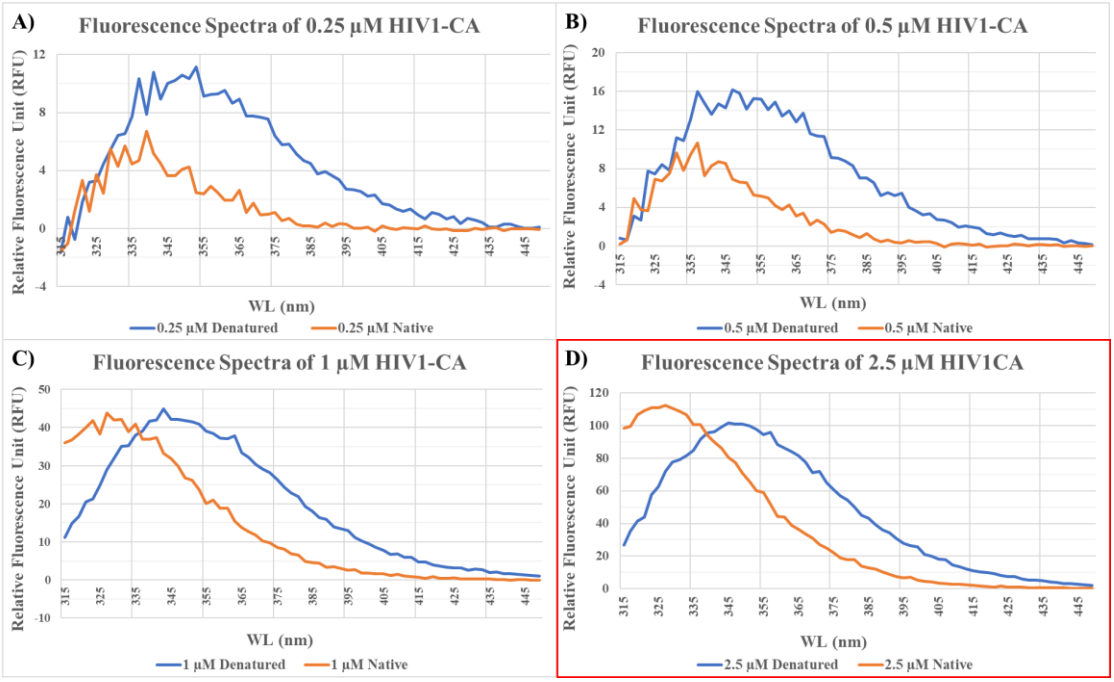

Figure 3.27. Fluorescence emission spectra of HIV-1 CA at different concentrations under native (0 M urea) and denatured (8 M urea) conditions. A) at 0.25 µM HIV-1 CA. B) at 0.5 µM HIV-1 CA. C) at 1 µM HIV-1 CA. D) at 2.5 µM HIV-1 CA.

When the graphs in the Figure 3.27 were examined, it was observed that the protein concentrations of 0.25 µM, 0.5 µM were not sufficient for this experiment. When 1 µM and 2.5 µM protein concentrations were compared, 2.5 µM protein concentration

was enough to get a clear signal. From these data, it was determined that the minimum HIV-1 CA protein concentration limit that can be used for fluorescence spectroscopy experiment is 2.5 μM. When Figure 3.27, D was examined, it was observed that when the protein was in its native (folded) form, it gave a fluorescent signal originating from the emission of tryptophan amino acid around 325 nm. This emission wavelength shows red-shift in the denatured (unfolded) form of the protein when exposed to 8M urea. These results are in agreement with the literature (Misselwitz et al., 1995), and show that the protein was successfully denatured.

After the protein concentration variation experiment, two experiment were performed with increasing urea concentration at constant protein concentration to observe the denaturation. Protein was used in the experiment at final concentration of 3 μM. For Experiment 1, 29 samples were prepared with increasing urea concentrations from 0 M to 7.3 M. For Experiment 2, 31 samples were prepared with increasing urea concentrations from 0 M to 7.9 M. Samples were excited at 295 nm in the fluorescence spectroscopy, and their fluorescence emission spectra was scanned between 310-450 nm wavelengths. The ratio of fluorescence intensity at between 320 nm and 370 nm was plotted against increasing urea concentration after blank subtraction for each data (Figure 3.28). The FI370 / FI320 ratio represents the denaturant-dependent shift of the emission wavelength. The transition curves obtained in the graphs show the chemical denaturation process of the protein (Figure 3.28). The unfolding free energy (ΔG), which is a thermodynamic parameter and related to the structural stability of the protein, can be calculated from this data.

Denaturation data were analyzed according to previous studies and assuming that protein unfolding is two-state transition (Misselwitz et al., 1995; Tang et al., 2016). Data points were fitted according to Eq. (3.1).

Equation (3.1):

$$Y = \frac{(a_N[urea] + b_N) + (a_D[urea] + b_D)(e^{\frac{-\Delta G_{UX} + m[urea]}{RT}})}{1 + e^{\frac{-\Delta G_{UX} + m[urea]}{RT}}}$$

a_N, a_D, b_N, b_D, ΔG_{UX} and m are the fitting parameters. a_N and a_D are the slopes of the linear baselines, and b_N and b_D are the baseline Y-axis intercepts (N: Native, D:

Denatured). ΔG_{UX}, the unfolding free energy of the protein, is the extrapolated value of ΔG_U depending on the urea concentration and is also the main parameter for evaluating protein stability. m is a positive slope of the transition curve. R is the gas constant (8.314 $J.K^{-1}.mol^{-1}$) and T is experimental temperature which was 298 K (25˚C) at this experiment.

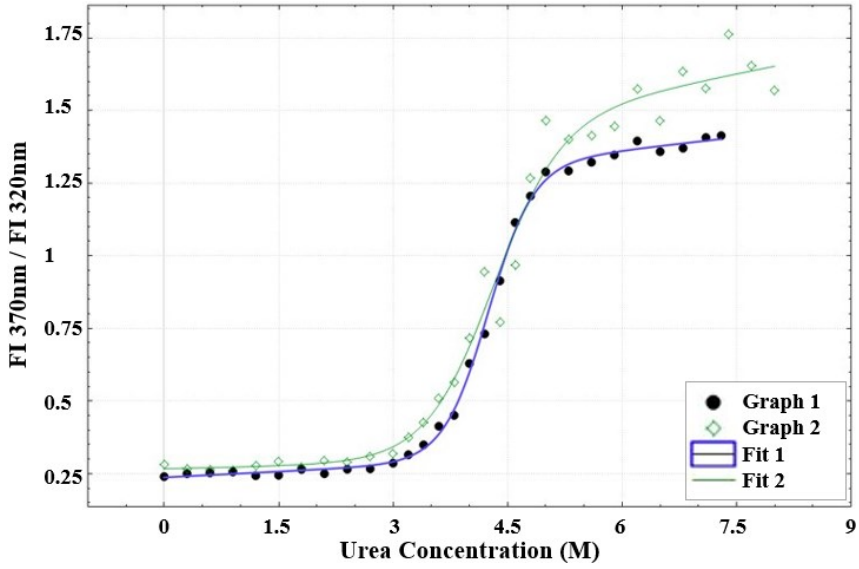

Figure 3.28. Transition curves of chemical HIV-1 CA denaturation with increasing urea concentration. The fluorescence intensity ratio FI 370 nm / FI 320 nm was plotted in dependence on urea. Data was fitted by using Eq. (3.1). (Graph 1 is belonging to the Experiment 1 data. Graph 2 is belonging to the Experiment 2 data.)

Unfolding of the HIV-1 CA started at denaturant concentration of about 3 M urea and reaches plateau values about 5 M urea for both transition curves. Transition-half values ($C_{1/2}$) are 4.20 and 4.29 for Graph 1 and Graph 2, respectively.

Table 3.3. Fitting parameters of HIV-1 CA denaturation transition curves and unfolding free energy ΔG_{UX} of HIV-1 CA protein at 25°C.

	ΔG_{UX} (kJ/mol)	m ($kjmol^{-1}M^{-1}$)	$C_{1/2}$ (M)
Graph 1	35.9 ± 3.3	8.45 ± 0.78	4.20
Graph 2	23.9 ± 5.9	5.59 ± 1.36	4.29

The experiment was repeated two times, the data came out as seen in the graphs (Figure 3.28). Determined ΔG values of the HIV-1 CA are shown in Table 3.3. These ΔG values are different from each other, but the transition-half values ($C_{1/2}$) are almost same. In the literature the study by Misselwitz et al., ΔG value of the HIV-1 CA was determined as 24.1 kJ/mol by following urea denaturation of the protein in 20 mM sodium acetate pH 5.8 buffer by fluorescence spectroscopy (Misselwitz et al., 1995). ΔG value determined from the Graph 2 is very close to the literature value. However, in the circular dichroism scan, this protein showed the typical HIV-1 capsid spectrum (Figure 3.32), it indicates that the protein we obtained is correctly folded HIV-1 CA.

3.8.3. Secondary Structure Analysis of Nb, HIV-1 CA and HIV-1 CA NTD with Circular Dichroism Spectroscopy

The secondary structure of proteins can be studied with the circular dichroism (CD) spectroscopy (Greenfield, 2006). In addition, with this method, thermal or chemical denaturation of proteins can be followed and it provides to determine any conformational change occurring in the protein under different conditions (Martin & Schilstra, 2008). In the circular dichroism spectroscopy, the effects of polarized light on chiral molecules are studied. Chiral molecules absorb right-hand (R) and left-hand (S) circularly polarized light to varying extents. In the experiment, the difference in absorption of right-hand and left-hand circularly polarized light is measured (Greenfield, 2006; Martin & Schilstra, 2008; Ranjbar & Gill, 2009).

With circular dichroism spectroscopy, the secondary structure of proteins (α-helix, β-sheet, β-turn) can be studied in the far-UV spectral region (190-250 nm). At these wavelengths, the chromophore is a peptide bond (Ranjbar & Gill, 2009). In the far-UV spectral region, the α-helical proteins show two negative bands at 208 and 222 nm; and a positive band in the 191-193 nm range. β-sheet proteins show a negative band in the 210-225 nm range and a positive band in the 190-200 nm range (Greenfield, 2006; Martin & Schilstra, 2008; Ranjbar & Gill, 2009).

Nanobody, HIV-1 CA and HIV-1 CA NTD circular dichroism spectra were taken in the 190-270 nm wavelength range, at 25°C with a cuvette of 0.1 cm pathlength. Protein samples were in the 20 mM sodium phosphate pH 8.0, 10 mM βME. Obtained CD spectra were normalized according to the (Eq. 2.1). Normalized CD spectrum of the nanobody is

shown in the Figure 3.31. Normalized CD spectra of the HIV-1 CA and the HIV-1 CA NTD are shown in the Figure 3.32.

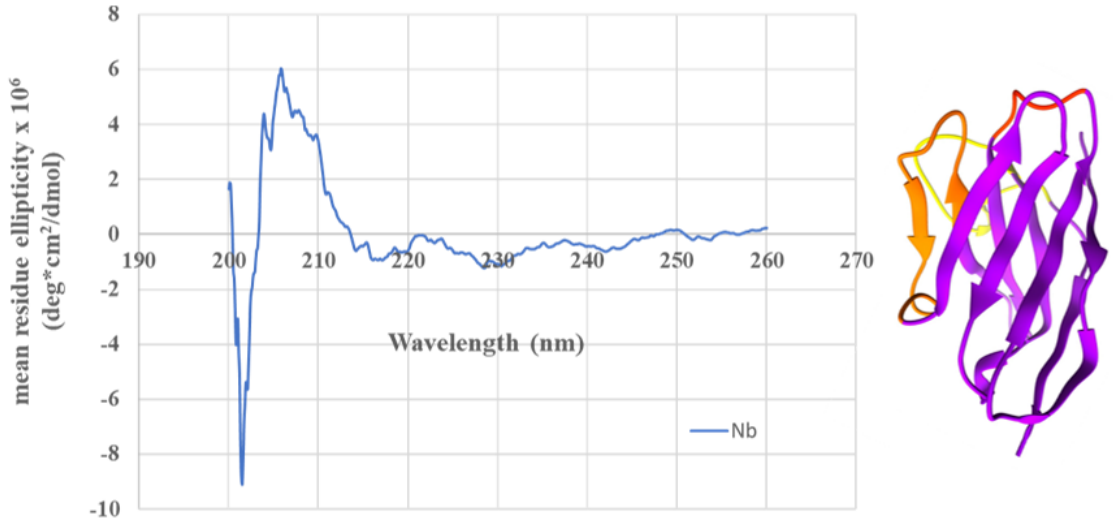

Figure 3.29. CD spectrum of the nanobody protein. Right figure shows hypothetical structure of the nanobody. The three-dimensional structure of this protein is unknown.

Nanobody protein consists of a high proportion of β-sheet, therefore, a negative band in the 210-225 nm range is expected. We did not see the exactly expected signal for this protein, but this is the first time this nanobody protein's CD spectrum is taken. There is no comparable CD data in the literature for this nanobody. The result is acceptable since similar CD spectra were reported for other nanobodies in the literature (Zabetakis et al., 2013) and the nanobody protein remains soluble under the experimental conditions (20 mM sodium phosphate pH 8.0, 10 mM βME).

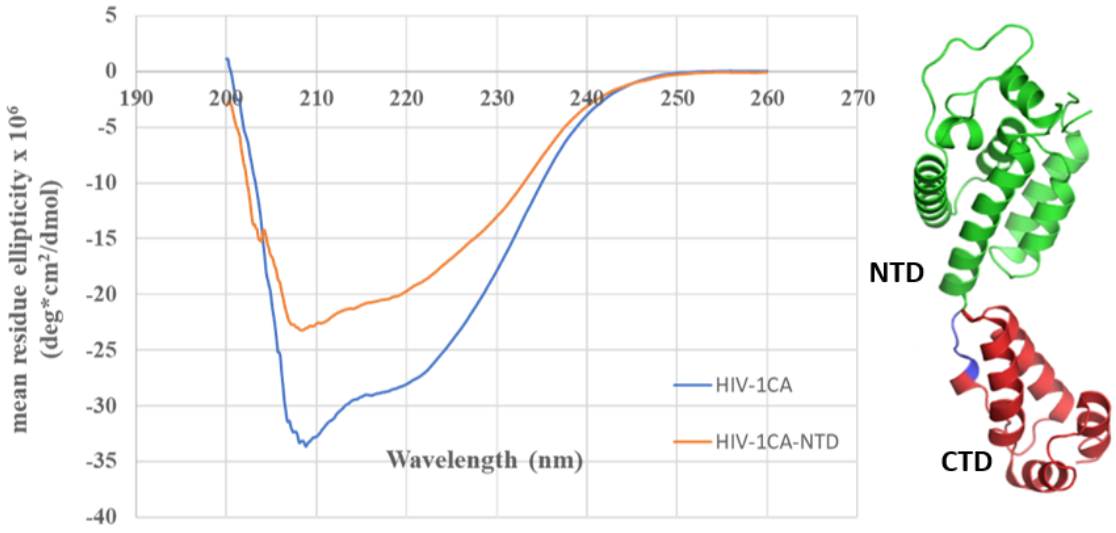

Figure 3.30. CD spectra of HIV-1 CA and HIV-1 CA NTD proteins. Right figure shows the HIV-1 CA structure.

Since HIV capsid proteins contain a high proportion of α-helix, the circular dichroism signal is expected to appear as two negative bands at 208 and 222 nm. HIV-1 CA NTD is a domain belonging to HIV-1 CA, so they are expected to exhibit the same characteristics in their secondary structures. Obtained results for HIV-1 CA and HIV-1 CA NTD reveals a typical HIV-1 CA spectrum with two negative peaks at 208 nm and 222 nm similar to the data in the literature (Douglas et al., 2004; Misselwitz et al., 1995).

3.9. Oligomerization of Recombinant HIV-1 CA

Purified recombinant HIV-1 CA protein can be triggered to self-assemble spontaneously into tube-like structures under high ionic strength conditions in vitro. With the oligomerization assay, information about HIV-1 CA assembly rate and the time it takes to assemble can be obtained (del Álamo et al., 2005; Douglas et al., 2004; Yant et al., 2019).

In vitro HIV-1 CA oligomerization was monitored spectrophotometrically following absorbance signal at 350 nm by light scattering caused by the polymerized tubular structure formed in the presence of high salt concentration. First, two different protein concentrations (30 µM and 40 µM) were tested with and without %1 DMSO. Then the experiment was repeated with two identical sample at the 30 µM protein

concentration with %1 DMSO.

Graphs of the HIV-1 CA oligomerization at different concentration obtained as a result of the first experiment are shown in the Figure 3.29. This experiment was performed at 25°C for 7 hours reading the absorbance at 350 nm with 30 second intervals. Absorbance values in the graphs are values with pathlength correction applied.

In order to evaluate these graphs, two parameters were examined. These are; oligomerization time and oligomerization rate. Oligomerization time was considered as the minute it took for the absorbance signal to reach a plateau. The oligomerization rate was calculated from the slope of the curve where the signal increased linearly.

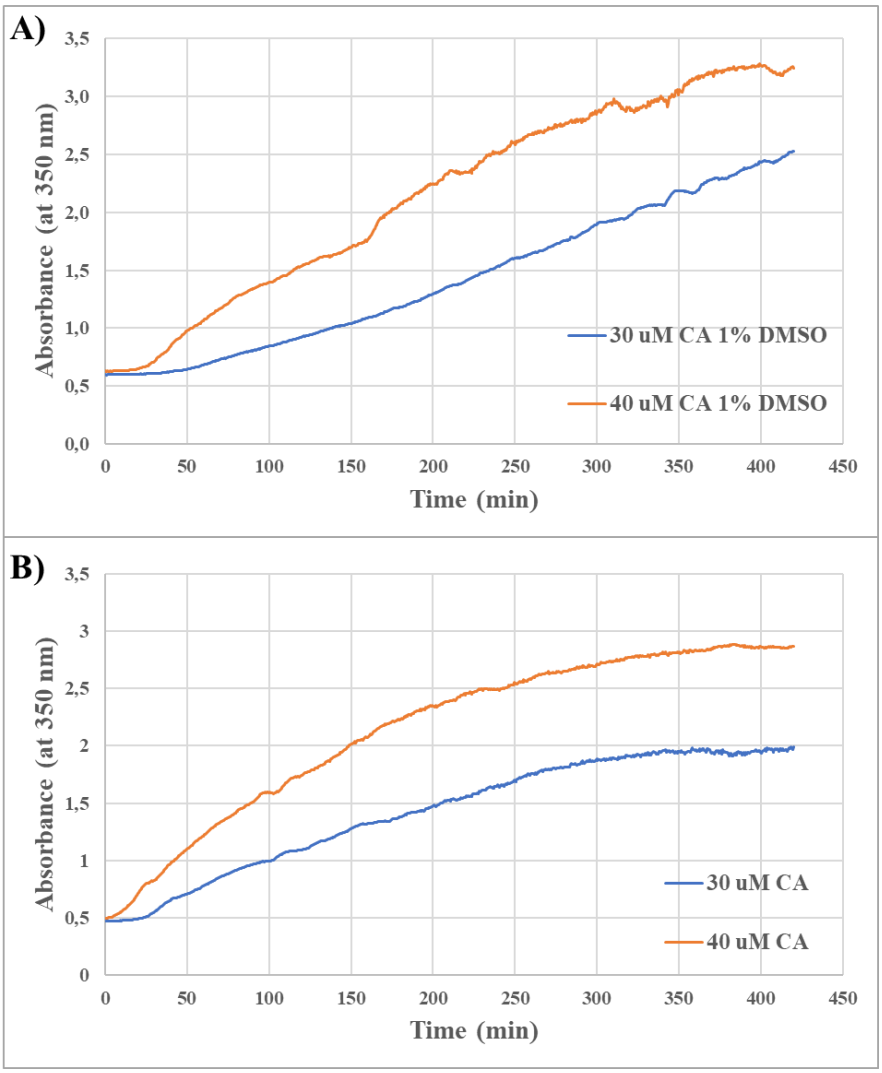

Figure 3.31. HIV-1 CA oligomerization at different concentrations, A) with 1% DMSO, B) without DMSO.

Looking at the increase of the absorbance signal at the graphs in the Figure 3.29, it can be said that HIV-1 CA self-oligomerizes over time. However, the oligomerization process could not be observed completely for these samples. In the graphs, it is not clearly seen that the linear curve reaches a plateau, especially for the sample with 1% DMSO at 30 µM concentration (Figure 3.29, A). Therefore, the oligomerization time and oligomerization rate values could not be determined. Experiment time is not sufficient for the oligomerization of HIV-1 CA protein at these concentrations.

Therefore, in order to observe the oligomerization process in more detail, the experiment duration had to be increased. Thus, a new experiment was performed by increasing the duration of the experiment with two identical samples at a selected concentration. This experiment was performed at 25°C for 18 hours reading the absorbance at 350 nm with 1 min 10 second intervals. Graph of the HIV-1 CA oligomerization at 30 µM concentration is shown in the Figure 3.30. Absorbance values in the graphs are values with pathlength correction applied.

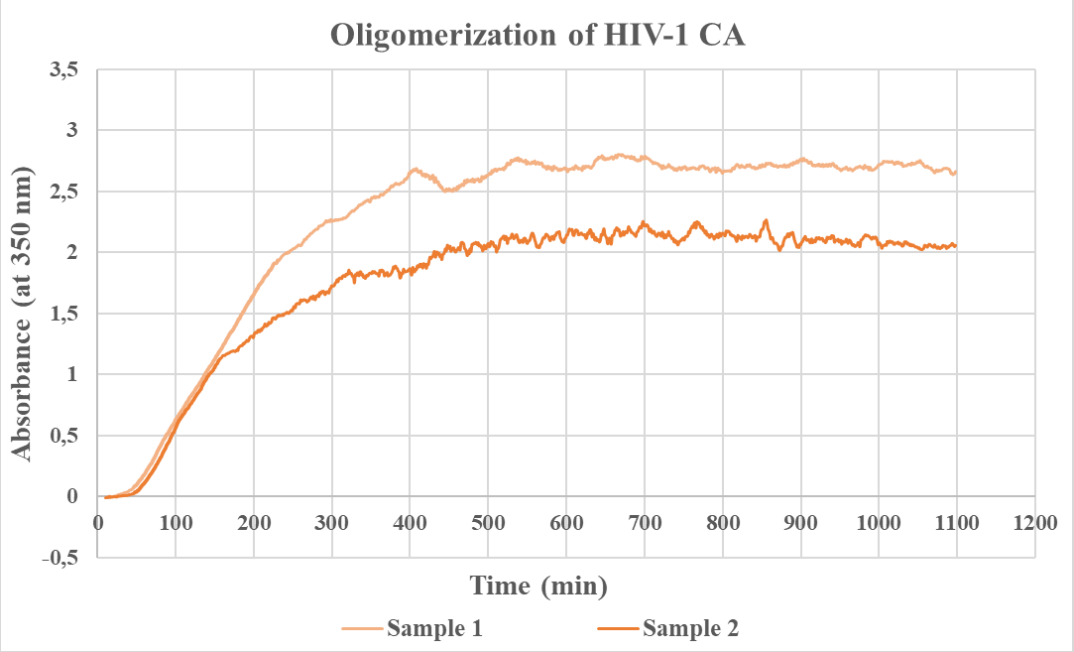

Figure 3.32. HIV-1 CA oligomerization at 30 µM concentration.

Table 3.4. HIV-1 CA oligomerization parameters at 30 μM concentration.

Sample	**Oligomerization Time (min)**	**Oligomerization Rate (Linear Rate, OD/min)**
Sample 1	400	0.0103
Sample 2	350	0.0106
Average	375	0.01045

In the Figure 3.30, increase of the absorbance signal was started approximately 50 minutes after the experiment is started for both samples. During the linear increase, polymerized structures are formed and when it stabilizes, increase of the absorbance signal stops. Oligomerization time and oligomerization rate values were calculated from the graphs for both samples and these values are shown in Table 3.4. Similar results were obtained in the values of oligomerization time and oligomerization rate parameters in both samples. The HIV-1 CA oligomerization time was obtained for the Sample 1 and Sample 2 were 400 min and 350 min, respectively; the HIV-1 CA oligomerization rate was 0.0103 OD/min and 0.0106 OD/min, respectively. The oligomerization of the HIV-1 CA protein observed as a result of the experiment coincides with the HIV-1 capsid self-assembly behavior in the literature (Hung et al., 2013).

3.10. Interaction Analysis of HIV-1 CA and Nanobody Protein with Isothermal Titration Calorimetry

In drug discovery studies, characterization of the interaction between the molecules of interest is required (Velazquez-Campoy et al., 2015). Isothermal titration calorimetry (ITC) technique is ideal for studying protein-protein interactions and protein-ligand interactions (Srivastava & Yadav, 2019). Based on the basic principle of thermodynamics, heat absorbed or released is measured when two components are brought together (Cooper, 1998; Srivastava & Yadav, 2019). Measuring the heat of binding allows determination of thermodynamic parameters such as the binding constant (K), reaction stoichiometry or number of binding sites (n), enthalpy (ΔH), entropy (ΔS), free energy (ΔG) and heat capacity (ΔCp) (Lewis & Murphy, 2005; Liang, 2008).

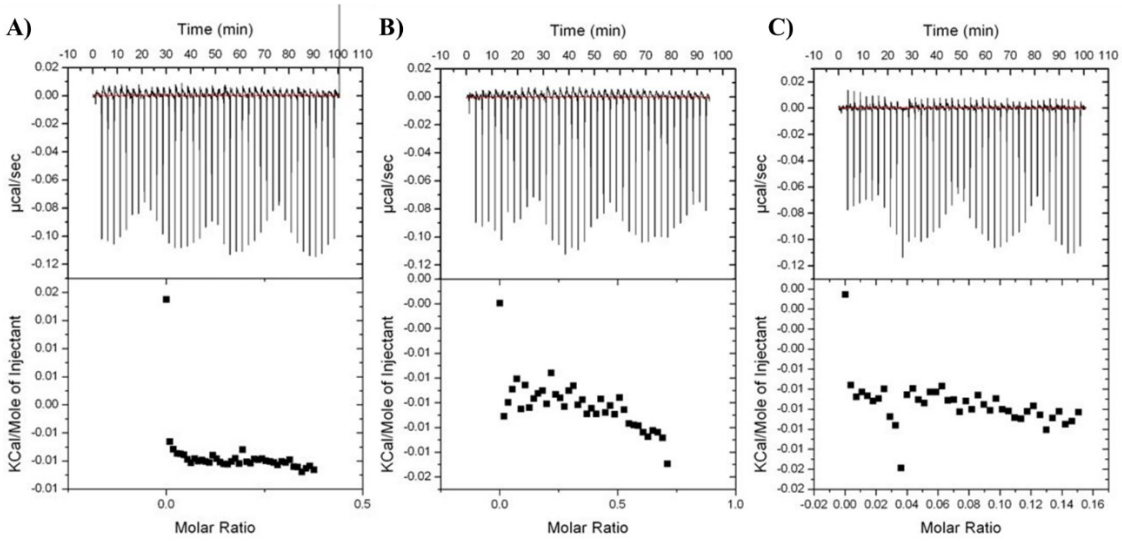

Figure 3.33. ITC binding isotherms of HIV-1 CA titrated into nanobody. Three different titrations were performed: A) 55 µM Nb was titrated into 30.8 µM HIV-1 CA. B) 55 µM Nb was titrated into 15.4 µM HIV-1 CA. (C) 55 µM Nb was titrated into 77 µM HIV-1 CA. Each titration consisted of Nb injections of 1 µl, made every 200 sec, into reaction cell that contains 280 µl HIV-1 CA.

Initial ITC experiments results with three different titrations are shown in the Figure 3.33. The raw signal in isothermal titration calorimetry is the measured power (µcal/sec) after each nanobody injection as a function of time. Temperature changes occur when the nanobody is injected into the sample cell that contains HIV-1 CA. Each injection produces peaks that are recorded as a heat pulse. The titration thermogram is obtained by plotting power versus time (Figure 3.33 top panel). This is represented as energy per unit of time released after each injection of the nanobody into the HIV-1 CA. Binding isotherm is obtained by plotting integration of the area of each peak against the molar ratio of the nanobody and HIV-1 CA (Figure 3.33 bottom panel).

We were able to prepare enough Nb protein for the initial tests of ITC. In the initial experiments, it was observed that the energy was released, indicating that the binding reaction is exothermic. However, the energy released from Nb injections were small. Signal oscillation was observed and it is a problem. We did not observe good binding between the HIV-1 capsid protein and the nanobody protein. Future work requires producing more Nb protein and repeating ITC in a buffer containing additional 50mM NaCl.

CHAPTER 4

CONCLUSION

The HIV capsid protein has a high potential as a drug target for HIV infection with important roles in the early and late stages of the virus life cycle. The high sequence conservation of the capsid protein and its sensitivity to mutations reduce the possibility of resistance to capsid-targeted drugs. In many studies, capsid has been studied as a target molecule and capsid binding inhibitor molecules have been reported. Nanobodies, which are used in many areas in diagnosis and therapy, are suitable agents for target molecules, thanks to their small size and advantages. The aim of this study was to investigate the potential of the nanobody protein, which has been reported to bind to HIV-1 capsid protein in the literature, as a biotechnological drug candidate for HIV-1 and HIV-2 capsid proteins. For this purpose, expression and purification studies of HIV-1 CA and HIV-2 CA proteins were performed. The biophysical characterization of HIV-1 CA protein was completed and similar results were obtained with the literature. Thermal denaturation of HIV-1 CA protein at different concentrations was examined by DSF assay and HIV-1 CA Tm values were determined in the range of 51.4˚C – 53.0˚C. These values are close to the HIV-1 CA Tm value reported in the literature. The chemical denaturation of the HIV-1 CA protein was followed by fluorescence spectroscopy in two experiments and unfolding free energy (ΔG) was determined as 35.9 ± 3.3 kJ/mol and 23.9 ± 5.9 kJ/mol. Overall, the stability of the HIV-1 CA protein was observed similar to the literature value. Also, secondary structure characteristics of the HIV-1 CA protein was examined by CD spectroscopy and the data matched with the typical HIV-1 CA CD spectrum in the literature. It indicates that the protein we obtained is the correctly folded HIV-1 CA. HIV-1 CA in-vitro oligomerization assay was performed and it was seen that the protein self-oligomerized as in the studies in the literature. Pure HIV-2 CA protein could not be produced recombinantly. Therefore, HIV-1 CA NTD and HIV-2 CA NTD proteins were successfully expressed and purified. Secondary structure of HV-1 CA NTD was investigated by CD spectroscopy and the result compatible with the literature. The nanobody protein was produced and purified in our laboratory. The secondary structure characteristics of the nanobody protein was examined by CD spectroscopy. No CD

spectrum has been presented for this protein in the literature, but it showed similar results to the secondary structure properties of other nanobodies in the literature. Therefore, the CD spectrum obtained for the nanobody was interpreted as acceptable. ITC experiment was performed to examine the HIV-1 CA and nanobody interaction. This was the initial experiment. Good binding between the two proteins was not observed. A larger amount of nanobody protein is required for future CA and nanobody interaction experiments.

Future studies require examination of the HIV-2 CA NTD protein by CD and fluorescence spectroscopy. It also requires producing more nanobody protein and repeating ITC in a buffer containing additional 50 mM NaCl with HIV-1 CA, HIV-1 CA NTD and HIV-2 CA NTD. After in vitro protein-protein interaction studies, the effect of the nanobody on the capsid protein in HIV life cycle should be investigated. The nanobody may have the potential to exert an inhibitory effect during the uncoating or maturation stages. After examining the mechanism of action, more detailed research should be done for drug development studies. Further studies for the investigation of nanobody's toxicity, absorption, distribution, excretion and drug delivery system is needed.

Nanobody can also be used for diagnostic purposes for HIV infection. HIV-1 capsid protein (p24) is an antigen that can be detected at the initial stage of the infection. HIV-1 capsid-nanobody pair can also be used to develop a diagnostic test for HIV infection.

REFERENCES

Alfadhli, A., Romanaggi, C. A., Barklis, R. L., Merutka, I., Bates, T. A., Tafesse, F. G., & Barklis, E. (2021). Capsid-specific nanobody effects on HIV-1 assembly and infectivity. *Virology*, *562*, 19–28. https://doi.org/10.1016/j.virol.2021.07.001

Bester, S. M., Wei, G., Zhao, H., Adu-Ampratwum, D., Iqbal, N., Courouble, V. v, Francis, A. C., Annamalai, A. S., Singh, P. K., Shkriabai, N., van Blerkom, P., Morrison, J., Poeschla, E. M., Engelman, A. N., Melikyan, G. B., Griffin, P. R., Fuchs, J. R., Asturias, F. J., & Kvaratskhelia, M. (n.d.). *Structural and mechanistic bases for a potent HIV-1 capsid inhibitor*. http://science.sciencemag.org/

Bhattacharya, A., Alam, S. L., Fricke, T., Zadrozny, K., Sedzicki, J., Taylor, A. B., Demeler, B., Pornillos, O., Ganser-Pornillos, B. K., Diaz-Griffero, F., Ivanov, D. N., & Yeager, M. (2014). Structural basis of HIV-1 capsid recognition by PF74 and CPSF6. *Proceedings of the National Academy of Sciences of the United States of America*, *111*(52), 18625–18630. https://doi.org/10.1073/PNAS.1419945112

Blair, W. S., Pickford, C., Irving, S. L., Brown, D. G., Anderson, M., Bazin, R., Cao, J., Ciaramella, G., Isaacson, J., Jackson, L., Hunt, R., Kjerrstrom, A., Nieman, J. A., Patick, A. K., Perros, M., Scott, A. D., Whitby, K., Wu, H., & Butler, S. L. (2010). HIV capsid is a tractable target for small molecule therapeutic intervention. *PLoS Pathogens*, *6*(12). https://doi.org/10.1371/journal.ppat.1001220

Carnes, S. K., Sheehan, J. H., & Aiken, C. (2018). Inhibitors of the HIV-1 capsid, a target of opportunity. In *Current Opinion in HIV and AIDS* (Vol. 13, Issue 4, pp. 359–365). Lippincott Williams and Wilkins. https://doi.org/10.1097/COH.0000000000000472

Cooper, A. (1998). Microcalorimetry of protein-protein interactions. In R. A. Clegg (Ed.), *Protein Targeting Protocols* (Vol. 88, pp. 11–22). Humana Press.

Curreli, F., Zhang, H., Zhang, X., Pyatkin, I., Victor, Z., Altieri, A., & Debnath, A. K. (2011). Virtual screening based identification of novel small-molecule inhibitors targeted to the HIV-1 capsid. *Bioorganic and Medicinal Chemistry*, *19*(1), 77–90. https://doi.org/10.1016/j.bmc.2010.11.045

Deeks, S. G., Overbaugh, J., Phillips, A., & Buchbinder, S. (2015). HIV infection. *Nature Reviews Disease Primers 2015 1:1*, *1*(1), 1–22. https://doi.org/10.1038/nrdp.2015.35

del Álamo, M., Rivas, G., & Mateu, M. G. (2005). Effect of Macromolecular Crowding Agents on Human Immunodeficiency Virus Type 1 Capsid Protein Assembly In Vitro. *Journal of Virology*, *79*(22), 14271–14281. https://doi.org/10.1128/jvi.79.22.14271-14281.2005

Deshmukh, L., Schwieters, C. D., Grishaev, A., Ghirlando, R., Baber, J. L., & Clore, G. M. (2013). Structure and dynamics of full-length hiv-1 capsid protein in solution. *Journal of the American Chemical Society*, *135*(43), 16133–16147. https://doi.org/10.1021/ja406246z

Douglas, C. C., Thomas, D., Lanman, J., & Prevelige, P. E. (2004). Investigation of N-terminal domain charged residues on the assembly and stability of HIV-1 CA. *Biochemistry*, *43*(32), 10435–10441. https://doi.org/10.1021/bi049359g

Fanales-Belasio, E., Raimondo, M., Suligoi, B., & Buttò, S. (2010). HIV virology and pathogenetic mechanisms of infection: a brief overview. *Annali Dell'Istituto Superiore Di Sanita*, *46*, 5–14.

Flexner, C., Owen, A., Siccardi, M., & Swindells, S. (2021). Long-acting drugs and formulations for the treatment and prevention of HIV infection. *International Journal of Antimicrobial Agents*, *57*(1). https://doi.org/10.1016/j.ijantimicag.2020.106220

Fricke, T., Buffone, C., Opp, S., Valle-Casuso, J., & Diaz-Griffero, F. (2014). BI-2 destabilizes HIV-1 cores during infection and Prevents Binding of CPSF6 to the HIV-1 Capsid. *Retrovirology*, *11*(1), 1–7. https://doi.org/10.1186/S12977-014-0120-X/FIGURES/4

German Advisory Committee Blood (Arbeitskreis Blut), S. 'Assessment of P. T. by B. (2016). Human Immunodeficiency Virus (HIV). *Transfusion Medicine and Hemotherapy*, *43*(3), 203–222. https://doi.org/10.1159/000445852

Goudreau, N., Lemke, C. T., Faucher, A. M., Grand-Maiître, C., Goulet, S., Lacoste, J. E., Rancourt, J., Malenfant, E., Mercier, J. F., Titolo, S., & Mason, S. W. (2013). Novel inhibitor binding site discovery on HIV-1 capsid N-terminal domain by NMR and X-ray crystallography. *ACS Chemical Biology*, *8*(5), 1074–1082. https://doi.org/10.1021/CB400075F/SUPPL_FILE/CB400075F_SI_001.PDF

Greenfield, N. J. (2006). Using circular dichroism spectra to estimate protein secondary structure. *Nature Protocols*, *1*(6), 2876–2890. https://doi.org/10.1038/nprot.2006.202

Gulick, R. M., & Flexner, C. (2019). Long-Acting HIV Drugs for Treatment and

Prevention. *Annual Review of Medicine*, *70*, 137–150. https://doi.org/10.1146/ANNUREV-MED-041217-013717

Helma, J., Schmidthals, K., Lux, V., Nüske, S., Scholz, A. M., Kräusslich, H. G., Rothbauer, U., & Leonhardt, H. (2012). Direct and Dynamic Detection of HIV-1 in Living Cells. *PLoS ONE*, *7*(11). https://doi.org/10.1371/journal.pone.0050026

HIVinfo. (2020). *FDA-Approved HIV Medicines*. https://hivinfo.nih.gov/understanding-hiv/fact-sheets/fda-approved-hiv-medicines

Hoey, R. J., Eom, H., & Horn, J. R. (2019). Structure and development of single domain antibodies as modules for therapeutics and diagnostics. *Exp Biol Med (Maywood)*, *244*(17), 1568–1576. https://doi.org/10.1177/1535370219881129

https://tabs.craic.com. (n.d.). *Therapeutic Antibody Database*. Retrieved June 24, 2022, from (https://tabs.craic.com)

Hung, M., Niedziela-Majka, A., Jin, D., Wong, M., Leavitt, S., Brendza, K. M., Liu, X., & Sakowicz, R. (2013). Large-Scale Functional Purification of Recombinant HIV-1 Capsid. *PLoS ONE*, *8*(3). https://doi.org/10.1371/journal.pone.0058035

Huynh, K., & Partch, C. L. (2015). Analysis of protein stability and ligand interactions by thermal shift assay. *Current Protocols in Protein Science*, *79*, 28.9.1-28.9.14. https://doi.org/10.1002/0471140864.ps2809s79

James, L. C. (2019). The HIV-1 capsid: more than just a delivery package. In U. F. Greber (Ed.), *Physical Virology* (Vol. 1215, pp. 69–83). Springer.

Jing, Y., & Heine, T. (2020). Long-acting antiretroviral therapy. *Nature Materials*, *19*(8), 826–827. https://doi.org/10.1038/s41563-020-0733-5

Joint United Nations Programme on HIV/AIDS. (2021). *Fact sheet 2021 - Latest global and regional statistics on the status of the AIDS epidemic.*

Kemnic, T. R., & Gulick, P. G. (2018). HIV Antiretroviral Therapy. *StatPearls*. http://europepmc.org/books/NBK513308

Kortagere, S., Madani, N., Mankowski, M. K., Schön, A., Zentner, I., Swaminathan, G., Princiotto, A., Anthony, K., Oza, A., Sierra, L.-J., Passic, S. R., Wang, X., Jones, D. M., Stavale, E., Krebs, F. C., Martín-García, J., Freire, E., Ptak, R. G., Sodroski, J., … Smith, A. B. (2012). Inhibiting Early-Stage Events in HIV-1 Replication by Small-Molecule Targeting of the HIV-1 Capsid. *Journal of Virology*, *86*(16), 8472–8481. https://doi.org/10.1128/jvi.05006-11

Kortagere, S., Xu, J. P., Mankowski, M. K., Ptak, R. G., & Cocklin, S. (2014). Structure-activity relationships of a novel capsid targeted inhibitor of HIV-1

replication. *Journal of Chemical Information and Modeling*, *54*(11), 3080–3090. https://doi.org/10.1021/ci500437r

Lakowicz, J. R. (Ed.). (2006). Principles of Fluorescence Spectroscopy. In *Protein Fluorescence In Principles of Fluorescence Spectroscopy* (pp. 530–573). Springer, Boston, MA. https://doi.org/10.1007/978-0-387-46312-4_2

Lamorte, L., Titolo, S., Lemke, C. T., Goudreau, N., Mercier, J. F., Wardrop, E., Shah, V. B., von Schwedler, U. K., Langelier, C., Banik, S. S. R., Aiken, C., Sundquist, W. I., & Mason, S. W. (2013). Discovery of novel small-molecule HIV-1 replication inhibitors that stabilize capsid complexes. *Antimicrobial Agents and Chemotherapy*, *57*(10), 4622–4631. https://doi.org/10.1128/AAC.00985-13

Lampinen, J., Raitio, M., Perälä, A., Oranen, H., & Harinen, R.-R. (2012). Microplate Based Pathlength Correction Method for Photometric DNA Quantifi cation Assay. *Vantaa: Thermo Fisher Application Note*.

Lemke, C. T., Goudreau, N., Faucher, A.-M., Mason, S. W., & Bonneau, P. (2013). A novel inhibitor-binding site on the HIV-1 capsid N-terminal domain leads to improved crystallization via compound-mediated dimerization. *Acta Crystallographica Section D: Biological Crystallography*, *69*(6), 1115–1123.

Lemke, C. T., Titolo, S., von Schwedler, U., Goudreau, N., Mercier, J.-F., Wardrop, E., Faucher, A.-M., Coulombe, R., Banik, S. S. R., Fader, L., Gagnon, A., Kawai, S. H., Rancourt, J., Tremblay, M., Yoakim, C., Simoneau, B., Archambault, J., Sundquist, W. I., & Mason, S. W. (2012). Distinct Effects of Two HIV-1 Capsid Assembly Inhibitor Families That Bind the Same Site within the N-Terminal Domain of the Viral CA Protein. *Journal of Virology*, *86*(12), 6643. https://doi.org/10.1128/JVI.00493-12

Lewis, E. A., & Murphy, K. P. (2005). Isothermal titration calorimetry. In G. U. Nienhaus (Ed.), *Protein-Ligand Interactions* (Vol. 305, pp. 1–15). Humana Press.

Li, C., Tang, Z., Hu, Z., Wang, Y., Yang, X., Mo, F., & Lu, X. (2018). Natural Single-Domain Antibody-Nanobody: A Novel Concept in the Antibody Field. *J Biomed Nanotechnol*, *14*(1), 1–19. https://doi.org/10.1166/jbn.2018.2463

Liang, Y. (2008). Applications of isothermal titration calorimetry in protein science. *Acta Biochimica et Biophysica Sinica*, *40*(7), 565–576.

Margolis, D. A., & Boffito, M. (2015). Long-acting antiviral agents for HIV treatment. *Current Opinion in HIV and AIDS*, *10*(4), 246. https://doi.org/10.1097/COH.0000000000000169

Martin, S. R., & Schilstra, M. J. (2008). Circular dichroism and its application to the study of biomolecules. *Methods In Cell Biology*, *84*, 263–293.

Mateu, M. G. (2002). Conformational stability of dimeric and monomeric forms of the C-terminal domain of human immunodeficiency virus-1 capsid protein. *Journal of Molecular Biology*, *318*(2), 519–531. https://doi.org/10.1016/S0022-2836(02)00091-8

Mattei, S., Schur, F. K., & Briggs, J. A. (2016). Retrovirus maturation - An extraordinary structural transformation. In *Current Opinion in Virology* (Vol. 18, pp. 27–35). Elsevier B.V. https://doi.org/10.1016/j.coviro.2016.02.008

Mcarthur, C., Gallazzi, F., Quinn, T. P., & Singh, K. (2019). HIV Capsid Inhibitors Beyond PF74. *Diseases*, *7*(4), 56. https://doi.org/10.3390/diseases7040056

Misselwitz, R., Hausdorf, G., Welfle, K., Höhne, W. E., & Welfle, H. (1995). Conformation and stability of recombinant HIV-1 capsid protein p24 (rp24). *Biochimica et Biophysica Acta (BBA) - Protein Structure and Molecular Enzymology*, *1250*(1), 9–18. https://doi.org/https://doi.org/10.1016/0167-4838(95)00041-R

Miyazaki, Y., Miyake, A., Koma, T., Uchiyama, T., Adachi, A., & Nomaguchi, M. (2017). Comparison of biochemical properties of HIV-1 and HIV-2 capsid proteins. *Frontiers In Microbiology*, *8*, 1082.

Musumeci, D., Riccardi, C., & Montesarchio, D. (2015). G-Quadruplex Forming Oligonucleotides as Anti-HIV Agents. *Molecules 2015, Vol. 20, Pages 17511-17532*, *20*(9), 17511–17532. https://doi.org/10.3390/MOLECULES200917511

Muyldermans, S. (2013). Nanobodies: Natural single-domain antibodies. In *Annual Review of Biochemistry* (Vol. 82, pp. 775–797). https://doi.org/10.1146/annurev-biochem-063011-092449

Muyldermans, S., & Lauwereys, M. (n.d.). *Unique single-domain antigen binding fragments derived from naturally occurring camel heavy-chain antibodies*.

Niesen, F. H., Berglund, H., & Vedadi, M. (2007). The use of differential scanning fluorimetry to detect ligand interactions that promote protein stability. *Nature Protocols*, *2*(9), 2212–2221. https://doi.org/10.1038/nprot.2007.321

Novikova, M., Zhang, Y., Freed, E. O., & Peng, K. (2019). Multiple Roles of HIV-1 Capsid during the Virus Replication Cycle. *Virologica Sinica*, *34*(2), 119–134. https://doi.org/10.1007/S12250-019-00095-3

Pawar, S., Waghmare, S., Gawde, B., Kale, P., & Johri, Y. (2019). Anti-HIV/AIDS

Drugs: An Overview. *Journal of Drug Delivery and Therapeutics*, *9*(3), 599–608.

Pornillos, O., Ganser-Pornillos, B. K., Banumathi, S., Hua, Y., & Yeager, M. (2010). Disulfide bond stabilization of the hexameric capsomer of human immunodeficiency virus. *Journal of Molecular Biology*, *401*(5), 985–995.

Prevelige, P. E. (2011). New approaches for antiviral targeting of HIV assembly. In *Journal of Molecular Biology* (Vol. 410, Issue 4, pp. 634–640). Academic Press. https://doi.org/10.1016/j.jmb.2011.03.074

Price, A. J., Jacques, D. A., McEwan, W. A., Fletcher, A. J., Essig, S., Chin, J. W., Halambage, U. D., Aiken, C., & James, L. C. (2014). Host Cofactors and Pharmacologic Ligands Share an Essential Interface in HIV-1 Capsid That Is Lost upon Disassembly. *PLOS Pathogens*, *10*(10), e1004459. https://doi.org/10.1371/JOURNAL.PPAT.1004459

Ranjbar, B., & Gill, P. (2009). Circular dichroism techniques: biomolecular and nanostructural analyses-a review. *Chemical Biology & Drug Design*, *74*(2), 101–120.

Rihn, S. J., Wilson, S. J., Loman, N. J., Alim, M., Bakker, S. E., Bhella, D., Gifford, R. J., Rixon, F. J., & Bieniasz, P. D. (2013). Extreme Genetic Fragility of the HIV-1 Capsid. *PLoS Pathogens*, *9*(6). https://doi.org/10.1371/journal.ppat.1003461

Salvador, J. P., Vilaplana, L., & Marco, M. P. (2019). Nanobody: outstanding features for diagnostic and therapeutic applications. *Anal Bioanal Chem*, *411*(9), 1703–1713. https://doi.org/10.1007/s00216-019-01633-4

Schumacher, D., Helma, J., Schneider, A. F. L., Leonhardt, H., & Hackenberger, C. P. R. (2018). Nanobodies: Chemical Functionalization Strategies and Intracellular Applications. *Angew Chem Int Ed Engl*, *57*(9), 2314–2333. https://doi.org/10.1002/anie.201708459

Shi, J., Zhou, J., Shah, V. B., Aiken, C., & Whitby, K. (2011). Small-Molecule Inhibition of Human Immunodeficiency Virus Type 1 Infection by Virus Capsid Destabilization. *Journal of Virology*, *85*(1), 542–549. https://doi.org/10.1128/JVI.01406-10/ASSET/57EA0410-160F-474B-8CC9-68E84F2FA4B3/ASSETS/GRAPHIC/ZJV9990940450005.JPEG

Simpson, R. J. (2010). SYPRO Orange fluorescent staining of protein gels. *Cold Spring Harbor Protocols*, *5*(4). https://doi.org/10.1101/pdb.prot5414

Singh, K., Gallazzi, F., Hill, K. J., Burke, D. H., Lange, M. J., Quinn, T. P., Neogi, U., & Sönnerborg, A. (2019). GS-CA compounds: First-in-class HIV-1 capsid

inhibitors covering multiple grounds. *Frontiers in Microbiology*, *10*(JUN). https://doi.org/10.3389/fmicb.2019.01227

Srivastava, V. K., & Yadav, R. (2019). Isothermal titration calorimetry. In G. Misra (Ed.), *Data Processing Handbook for Complex Biological Data Sources* (pp. 125–137). Elsevier.

Tang, C., Lew, S., & He, D. (2016). Using a second-order differential model to fit data without baselines in protein isothermal chemical denaturation. *Protein Science*, *25*(4), 898–904. https://doi.org/10.1002/pro.2878

Tang, C., Loeliger, E., Kinde, I., Kyere, S., Mayo, K., Barklis, E., Sun, Y., Huang, M., & Summers, M. F. (2003). Antiviral Inhibition of the HIV-1 capsid protein. *Journal of Molecular Biology*, *327*(5), 1013–1020. https://doi.org/10.1016/S0022-2836(03)00289-4

T.C. Sağlık Bakanlığı Halk Sağlığı Genel Müdürlüğü. (2018). HIV/AIDS Tanı Kılavuzu. *Ankara: Halk Sağlığı Genel Müdürlüğü Yayınları*.

Ternois, F., Sticht, J., Duquerroy, S., Kräusslich, H. G., & Rey, F. A. (2005). The HIV-1 capsid protein C-terminal domain in complex with a virus assembly inhibitor. *Nature Structural and Molecular Biology*, *12*(8), 678–682. https://doi.org/10.1038/nsmb967

Tillib, S. v. (2020). Prospective Applications of Single-Domain Antibodies in Biomedicine. *Molecular Biology*, *54*(3), 317–326. https://doi.org/10.1134/S0026893320030164

Tsiang, M., Niedziela-Majka, A., Hung, M., Jin, D., Hu, E., Yant, S., Samuel, D., Liu, X., & Sakowicz, R. (2012). A trimer of dimers is the basic building block for human immunodeficiency virus-1 capsid assembly. *Biochemistry*, *51*(22), 4416–4428. https://doi.org/10.1021/bi300052h

Turner, B. G., & Summers, M. F. (n.d.). *Structural Biology of HIV*. http://www.idealibrary.com

Velazquez-Campoy, A., Leavitt, S. A., & Freire, E. (2015). Characterization of protein-protein interactions by isothermal titration calorimetry. In C. L. Meyerkord & H. Fu (Eds.), *Protein-Protein Interactions* (pp. 183–204). Humana Press.

Wang, Y., Fan, Z., Shao, L., Kong, X., Hou, X., Tian, D., Sun, Y., Xiao, Y., & Yu, L. (2016). Nanobody-derived nanobiotechnology tool kits for diverse biomedical and biotechnology applications. In *International Journal of Nanomedicine* (Vol. 11, pp. 3287–3303). Dove Medical Press Ltd. https://doi.org/10.2147/IJN.S107194

World Health Organization. (2020). *HIV/AIDS*. https://www.who.int/health-topics/hiv-aids/#tab=tab_1

Yant, S. R., Mulato, A., Hansen, D., Tse, W. C., Niedziela-Majka, A., Zhang, J. R., Stepan, G. J., Jin, D., Wong, M. H., Perreira, J. M., Singer, E., Papalia, G. A., Hu, E. Y., Zheng, J., Lu, B., Schroeder, S. D., Chou, K., Ahmadyar, S., Liclican, A., … Link, J. O. (2019). A highly potent long-acting small-molecule HIV-1 capsid inhibitor with efficacy in a humanized mouse model. *Nature Medicine*, *25*(9), 1377–1384. https://doi.org/10.1038/s41591-019-0560-x

Zabetakis, D., Anderson, G. P., Bayya, N., & Goldman, E. R. (2013). Contributions of the Complementarity Determining Regions to the Thermal Stability of a Single-Domain Antibody. *PLOS ONE*, *8*(10), e77678. https://doi.org/10.1371/JOURNAL.PONE.0077678